

INFORMATION TO USERS

The most advanced technology has been used to photograph and reproduce this manuscript from the microfilm master. UMI films the text directly from the original or copy submitted. Thus, some thesis and dissertation copies are in typewriter face, while others may be from any type of computer printer.

The quality of this reproduction is dependent upon the quality of the copy submitted. Broken or indistinct print, colored or poor quality illustrations and photographs, print bleedthrough, substandard margins, and improper alignment can adversely affect reproduction.

In the unlikely event that the author did not send UMI a complete manuscript and there are missing pages, these will be noted. Also, if unauthorized copyright material had to be removed, a note will indicate the deletion.

Oversize materials (e.g., maps, drawings, charts) are reproduced by sectioning the original, beginning at the upper left-hand corner and continuing from left to right in equal sections with small overlaps. Each original is also photographed in one exposure and is included in reduced form at the back of the book. These are also available as one exposure on a standard 35mm slide or as a 17" x 23" black and white photographic print for an additional charge.

Photographs included in the original manuscript have been reproduced xerographically in this copy. Higher quality 6" x 9" black and white photographic prints are available for any photographs or illustrations appearing in this copy for an additional charge. Contact UMI directly to order.

U·M·I

University Microfilms International
A Bell & Howell Information Company
300 North Zeeb Road, Ann Arbor, MI 48106-1346 USA
313/761-4700 800/521-0600

Order Number 8913403

**The effects of frost growth on finned tube heat exchangers under
laminar flow**

Kondepudi, Sekhar Narayana, Ph.D.

Texas A&M University, 1988

U·M·I
300 N. Zeeb Rd.
Ann Arbor, MI 48106

THE EFFECTS OF FROST GROWTH ON FINNED
TUBE HEAT EXCHANGERS UNDER LAMINAR FLOW

A Dissertation

by

SEKHAR NARAYANA KONDEPUDI

Submitted to the Graduate College of
Texas A&M University
in partial fulfillment of the requirement for the degree of
DOCTOR OF PHILOSOPHY

December 1988

Major Subject: Mechanical Engineering

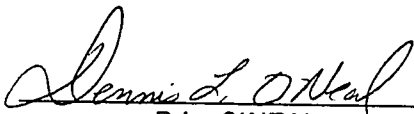
THE EFFECTS OF FROST GROWTH ON FINNED
TUBE HEAT EXCHANGERS UNDER LAMINAR FLOW

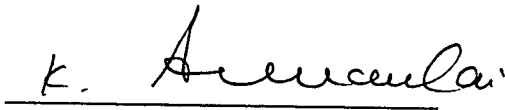
A Dissertation

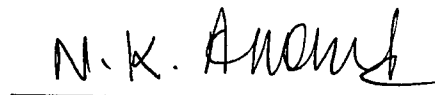
by

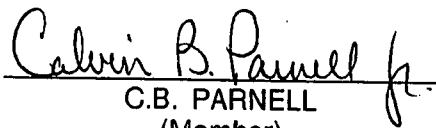
SEKHAR NARAYANA KONDEPUDI


Approved as to style and content by:


D.L. O'NEAL
(Chairman of Committee)


K. ANNAMALAI
(Member)


N.K. ANAND
(Member)


C.B. PARNELL
(Member)


for M. J. RABINS
(Head of Department)

DECEMBER 1988

ABSTRACT

The Effects of Frost Growth on Finned
Tube Heat Exchangers under Laminar Flow. (December 1988)

Sekhar Narayana Kondepudi

B.Tech, Indian Institute of Technology

M.S., Colorado State University

Chairman of Advisory Committee: Dennis L. O'Neal

A study on the effects of frost growth on the performance of finned tube heat exchangers under laminar flow has been conducted. The study was both experimental and analytical.

The experimental part of the investigation dealt with different fin geometries: louvered, corrugated, wavy, flat plate fins and also spine fin types. The parameters which were varied include the air humidity, air and refrigerant temperature, air flow rate and fin density. A new term called the *energy transfer coefficient* has been defined to account for the combined heat and mass transfer processes occurring during frosting. The variables measured were the amount of frost growth, the energy transfer coefficient, the pressure drop across the coils, the enthalpy drop, and the effectiveness of the coils. The general trends were found to be consistent with the literature. It was found that the frost growth increases with humidity, air temperature, velocity and fin density due to an increase in the mass transfer. The dominant factor was the humidity content of the air. When the relative humidity was increased from 74 % to 80 % at an air temperature of

32 ° F, the frost growth increased by approximately 22 %. The energy transfer coefficient initially increases by 10 to 15 % with the onset of frost formation due to increased surface area and surface roughness but then drops off due to the insulating layer of frost. The louvered fin type had the highest energy transfer coefficient in the neighborhood of 50 Btu/hr-F-ft² as compared to the flat fin type which was in the neighborhood of 38 Btu/hr-ft². However, when these results were normalized with respect to dry conditions, it was found that the flat fin type performed better than the louvered fin type.

A mathematical model was developed to simulate the experiments, based on fundamental heat and mass transfer principles. Due to the complexity of the problem, the model in its present form can handle flat plate fin types only. In addition to being able to predict energy transfer and frost growth, the model also performs a non-dimensional analysis on the heat exchanger performance in terms of NTU – Effectiveness, and Fin Performance. Comparisons were made between the experimental results and those predicted by the model for the frost growth, energy transfer coefficient, pressure drop and heat exchanger effectiveness. The results from the model were within 15 to 20 % of the experimental values

To my parents

ACKNOWLEDGMENTS

I am very deeply indebted to my advisor, Dr. Dennis L. O'Neal, who not only propelled me in the right direction and gave me all the support and guidance I needed, but was there constantly to help me out in almost all sorts of situations. My committee members have been constantly in touch with my work and have been very good about giving me the right advice at the appropriate time.

My parents who have taught me the value and necessity of a higher education constantly have been a source of encouragement and will always hold a special place in my heart. Without their support, I am sure that I would have never come to graduate school in the first place and they deserve a special thanks.

My wife, Anupama, needs to be thanked for her constant encouragement and cheerful attitude towards my work. I can still remember the times when I would hesitate to work in the laboratory and she would come with me to make sure that I worked.

TABLE OF CONTENTS

CHAPTER	Page
I	INTRODUCTION 1
	A. CONTRIBUTORY NATURE OF THIS STUDY 2
	B. PURPOSES AND SCOPE OF INVESTIGATION 3
II	LITERATURE REVIEW 6
	A. FROST PROPERTIES 7
	B. FROST GROWTH 9
	C. HEAT AND MASS TRANSFER 13
	D. FINNED TUBE HEAT EXCHANGERS 16
	E. CONCLUSIONS 47
III	EXPERIMENTAL FACILITY 50
	A. DESIGN BACKGROUND 50
	B. TEST FACILITY COMPONENTS 52
IV	ANALYTICAL MODEL 67
	A. ASSUMPTIONS 67
	B. GOVERNING EQUATIONS 68
	C. NON-DIMENSIONAL DESIGN PARAMETERS 82
	D. MODEL APPLICATION AND EXPECTED RESULTS 87
	E. CONCLUSIONS 115
V	EXPERIMENTAL RESULTS AND DISCUSSION 117
	A. DESIGN METHODOLOGY / TEST MATRIX 117
	B. EXPERIMENTAL CONDITIONS AND LIMITATIONS 119
	C. RESULTS 123
	D. CONCLUSIONS 176
VI	COMPARISON OF EXPERIMENTAL RESULTS WITH MODEL 181
	A. FROST GROWTH 182
	B. PRESSURE DROP ACROSS THE COILS 182
	C. ENERGY TRANSFER COEFFICIENT 185
	D. OTHER RESULTS 186
	E. SUGGESTED IMPROVEMENTS 190

TABLE OF CONTENTS (Continued)

CHAPTER		Page
VII	CONCLUSIONS AND RECOMMENDATIONS	192
	A. CONCLUSIONS	192
	B. RECOMMENDATIONS FOR FUTURE WORK	197
	REFERENCES	200
	NOMENCLATURE	205
	APPENDIX A	207
	APPENDIX B	209
	APPENDIX C	212
	APPENDIX D	216
	APPENDIX E	220
	VITA	224

LIST OF FIGURES

Figure	Page
2.1 Schematic of Fin with Frost	18
2.2 Fin Efficiency Ratio vs. Frost Height	21
2.3 Fin Temperature Distribution vs. Frost Height	22
2.4 Variation of U_o with Frost Accumulation - Stoecker [31,32]	26
2.5 Variation of U_o with Frost Growth - Hosoda and Uzanashi [33]	29
2.6 Variation of U_o with Frost - Sanders [29]	31
2.7 Variation of U_o with Relative Humidity - Gatchilov and Ivanova [35]	33
2.8 Heat Transfer vs. Mass Transfer - Gates <i>et al</i> [36,37]	37
2.9 Effect of Frost Growth on Pressure Drop - Stoecker [31,32]	39
2.10 Pressure Parameter vs. Time - Gates <i>et al</i> [36,37]	43
2.11 Effect of Relative Humidity on Pressure Drop - Gatchilov and Ivanova [35]	44
3.1 Experimental Schematic	51
3.2 Psychrometric Process in Test Loop	53
3.3 Schematic of Test Coil Configuration	55
3.4 Schematic of Saturation Spray	61
3.5 Resistance Heater Coils	63
4.1 Convergence of Frost Densities	89
4.2 Frost Growth Patterns for Different Initial Frost Densities	90
4.3 Effect of Humidity on Frost Accumulate	92
4.4 Effect of Humidity on Frost Height	93
4.5 Effect of Humidity on Pressure Drop Across the Coils	94
4.6 Effect of Humidity on Energy Transfer Coefficient	95
4.7 Effect of Humidity on Enthalpy Drop	97
4.8 Effect of Fin Density on Frost Height	99
4.9 Effect of Fin Density on Energy Transfer Coefficient	100

LIST OF FIGURES (Continued)

Figure	Page
4.10 Effect of Fin Density on Pressure Drop Across the Coils . . .	101
4.11 Effect of Face Velocity on Frost Height	103
4.12 Effect of Face Velocity on Energy Transfer Coefficient	104
4.13 Effect of Face Velocity on Pressure Drop Across the Coils .	105
4.14 Effect of Refrigerant Temperature on Frost Height	107
4.15 Effect of Refrigerant Temperature on Enthalpy Drop	108
4.16 Effectiveness as a Function of Fin Density	109
4.17 Number of Transferred Units as a Function of Face Velocity .	110
4.18 Dimensionless Heat Transfer for Individual Fin	112
4.19 Frost Growth as a Function of Location	113
4.20 Air Enthalpy as a Function of Location	114
4.21 Frost Surface Temperature as a Function of Location	116
5.1 Variation of Air Temperatures in a Typical Test	120
5.2 Variation of Air Flow Rates in a Typical Test	122
5.3 Variation of Air Relative Humidity in a Typical Test	124
5.4 Effect of Humidity on Frost Accumulation	126
5.5 Effect of Fin Spacing on Frost Accumulation	128
5.6 Effect of Face Velocity on Frost Accumulation	129
5.7 Effect of Air Temperature on Frost Accumulation	131
5.8 Effect of Refrigerant Temperature on Frost Accumulation . . .	132
5.9 Frost Accumulation for Different Fin Geometries	133
5.10 Frost Accumulation for Spine Fin Geometries	135
5.11 Effect of Humidity on Pressure Drop Across Coil	137
5.12 Effect of Fin Spacing on Pressure Drop Across Coil	138
5.13 Effect of Face Velocity on Pressure Drop Across Coil	139
5.14 Effect of Refrigerant Temperature on Pressure Drop Across Coil	140

LIST OF FIGURES (Continued)

Figure	Page
5.15 Pressure Drop Across Coil for Different Fin Geometries	141
5.16 Effect of Humidity on Energy Transfer Coefficient	145
5.17 Effect of Face Velocity on Energy Transfer Coefficient	146
5.18 Effect of Air Temperature on Energy Transfer Coefficient . . .	148
5.19 Effect of Refrigerant Temperature on Energy Transfer Coefficient	149
5.20 Effect of Fin Spacing on Energy Transfer Coefficient	150
5.21 Energy Transfer Coefficient for Different Fin Geometries . . .	151
5.22 Energy Transfer Coefficient for Spine Fin Geometries	153
5.23 Sensible and Latent Energy Transfer Coefficients	155
5.24 Effect of Humidity on Dimensionless Energy Transfer Coefficient	157
5.25 Effect of Refrigerant Temperature on Dimensionless Energy Transfer Coefficient	158
5.26 Effect of Air Temperature on Dimensionless Energy Transfer Coefficient	159
5.27 Dimensionless Energy Transfer Coefficient for Different Fin Geometries	160
5.28 Dimensionless Energy Transfer Coefficient for Spine Fin Geometries	161
5.29 Effect of Humidity on Dimensionless Sensible Heat Transfer Coefficient	164
5.30 Effect of Air Temperature on Dimensionless Sensible Heat Transfer Coefficient	165
5.31 Effect of Refrigerant Temperature on Dimensionless Sensible Heat Transfer Coefficient	167
5.32 Dimensionless Sensible Heat Transfer Coefficient for Different Fin Geometries	168
5.33 Dimensionless Sensible Heat Transfer Coefficient for Spine Fin Geometries	169
5.34 Effect of Humidity on Effectiveness	172

LIST OF FIGURES (Continued)

Figure	Page
5.35 Effect of Air Temperature on Effectiveness	173
5.36 Effect of Refrigerant Temperature on Effectiveness	174
5.37 Effect of Air Face Velocity on Effectiveness	175
5.38 Effect of Fin Spacing on Effectiveness	177
5.39 Effectiveness for Different Fin Geometries	178
5.40 Effectiveness for Spine Fin Geometries	179
6.1 Frost Growth : Comparison between Model and Experiment .	183
6.2 Pressure Drop : Comparison between Model and Experiment .	184
6.3 Energy Transfer Coefficient : Comparison between Model and Experiment	187
6.4 Enthalpy Drop : Comparison between Model and Experiment .	188
6.5 Effectiveness : Comparison between Model and Experiment .	189

LIST OF TABLES

Table	Page
2.1 Heat Exchanger Configurations Used by Gates <i>et al</i>	35
2.2 Effect of Fin Spacing on Airflow – Niederer	45
5.1 Test Matrix	118

LIST OF PHOTOGRAPHS

Photograph	Page
3.1 Test Coil	56
3.2 Tube in Tube Heat Exchanger	57
3.3 Cooling Coil Configuration	59
3.4 Residential Heat Pump connected to Cooling Coil	60
3.5 Humidity Sensors	65
3.6 Datalogger and Computer	66

CHAPTER I

INTRODUCTION

A major problem occurring with refrigeration and heat pump equipment is the deposition and progressive buildup of frost on the cold surface of the heat exchanger coil. The frost accumulation is a direct result of the combined heat and mass transfer between the moist air flowing across the heat exchanger and the cold refrigerant flowing inside the coil.

Whenever moist air passes over the cold heat exchanger coils and the temperature of the coils is below the dewpoint of the air, then the moisture in the air condenses on the coils. If the surface temperature of the coils is below freezing, then frost can begin to form on the surface of the coil.

The presence of frost on the heat exchanger surface affects the heat transfer performance of the coil. Initially, it roughens the surface of the coil resulting in new air flow patterns and enhanced heat and mass transfer characteristics. As the frost grows, it decreases the air flow area and insulates the cold heat exchanger surface from the warmer air. As a result, the heat transfer rate between the air and refrigerant is reduced. The blockage of the air flow area further results in a higher pressure drop across the coil and hence affects the system characteristics of the blower. The higher pressure drop across the blower results in a drop in air flow through the heat exchanger. Under such conditions, to ensure a reasonably good performance from the unit, a periodic defrost is required. This defrost extracts an additional penalty in energy consumption.

Journal model is the Journal of Heat Recovery Systems.

Considerable work has been done on frost formation and properties in simple geometries. The literature available on finned tube heat exchangers with regards to frosting is limited. An increased knowledge and a better understanding of the mechanism of frost formation and growth and its impact on the performance of the heat exchangers could be useful in the designing of heat exchangers.

A. CONTRIBUTORY NATURE OF THIS STUDY

Only a few investigations, to date, have been devoted to studying the effects of frosting on heat exchanger performance. Almost all the studies have been experimental in nature and limited to rectangular plate fins. There is also no comprehensive mathematical model of the entire problem. This study develops such an analytical model from fundamental heat and mass transfer principles, which considers the growth of the frost, the heat exchanger geometry and characteristics and the pressure characteristics of the blower present in the system. Fin types such as louvered, wavy and spine are also common in heat pump industry in addition to rectangular plate type. This study focusses on evaluating the effect of frost growth on the above set of finned tube heat exchangers under laminar flow conditions. Typical air flow face velocities are in the range of 130 to 200 feet per minute.

There is little design information on the effects of frost growth on performance, which can be of direct use to designers and manufacturers of heat transfer equipment. Information presented in the form of standardized design charts such as NTU-Effectiveness charts as a function of frost growth for various geometries, or percentage blockage as a function of time and heat exchanger geometry

could prove to be very useful to the designer. This study provides analytical and experimental information which can be a starting point for the development of design aids and / or tools.

B. PURPOSES AND SCOPE OF INVESTIGATION

The primary purpose of this study is to determine the effects of frost formation on the performance of finned tube heat exchangers with different fin types. This investigation is both experimental and analytical.

The experimental part of the investigation quantifies the effects of frost growth on heat exchanger performance for different geometries and environmental conditions. The parameters of interest include approaching air temperatures, humidity, air flow rates and refrigerant temperatures. Fin types studied include louvered, flat plate, wavy, corrugated and spine fins.

The results obtained from the experiments include frost growth, pressure drops and dimensional and non-dimensional heat and mass transfer coefficients. These are presented as functions of the above mentioned environmental conditions and geometrical configurations.

The mathematical model serves to simulate the frosting process on finned tube heat exchangers with plate fins. It is based on fundamental heat and mass transfer concepts. The effects of frost growth are presented in terms of fin performance, overall heat and mass transfer, pressure drop across the coil, and NTU-Effectiveness charts.

The model allows for a variety of environmental input conditions. It also

considers the special properties of the frost, such as varying thermal properties and porosity. However, the complex nature of the fin geometry restricts the model in its present form to a flat plate fin type. Comparisons with experimental results are made wherever possible.

This investigation should provide a better understanding into the effects of frost formation and growth on finned tube heat exchangers with varying fin types. To date, a comprehensive frosting model as applied to finned tube heat exchangers is not available and this model should prove to be a step forward towards that goal.

Chapter II provides a comprehensive literature survey on frost properties, frost growth, heat and mass transfer processes in frost layers and the overall impact frost on the performance of finned tube heat exchangers. More discussion is devoted towards the performance of heat exchangers under frosting conditions since that is of primary concern in the present study.

A detailed description of the experimental facility constructed for the purposes of this study is presented in Chapter III. Schematic diagrams and photographs of the facility and a systematic explanation of the individual components which comprise the test loop are included.

The mathematical model of the frosting process on heat exchangers is discussed in Chapter IV. This includes the details of the frost growth model, the heat exchanger characteristics and system parameters describing the blower and other pressure losses. A flow chart describing the simulation program is also presented. The trends predicted by the model are also presented and discussed.

Results are presented in dimensionless form, such as NTU-Effectiveness charts as a function of frost growth.

Details from the experimental work are presented in Chapter V : a detailed description of the various tests conducted, the exact physical characteristics of the heat exchangers (fin types, fin and tube row spacing), the conditions of the air (humidity and temperature) and the refrigerant temperature. In addition, plots of relevant experimental results, such as frost growth, pressure drops, and heat transfer data both in dimensional and non-dimensional form are presented in the form of graphs.

In Chapter VI, the experimental results of frost growth, the pressure drop across the coils and heat and mass transfer characteristics of the heat exchangers are discussed and compared relevant to the proposed model and results presented by other investigators.

In Chapter VII, appropriate and relevant conclusions from this investigation and other studies are discussed. The contribution of this study is also presented and discussed relevant to the present status of the problem. The limitations of this investigation and recommendations for future work are also presented.

CHAPTER II

LITERATURE REVIEW

There is a wealth of information available on the general topic of frost formation and growth. Most of this information relates to the thermophysical properties of the frost and its growth on simple geometries such as cylindrical surfaces, flat plates and parallel plates. The available information on the effects of frost growth in more complex geometries, such as finned tube heat exchangers, is very limited.

The available literature was divided into four main sections :

- a. Frost Properties – The importance lies in the need to have input for the modelling of the frost heat and mass transfer and growth.
- b. Frost Growth – This is important since it allows the investigator to develop and model basic relationships between frost growth and the heat and mass transfer processes in the frost.
- c. Heat and Mass Transfer under frosting conditions – The limitations and applicability of previously reported results is of invaluable importance to the investigator.
- d. Finned Tube Heat Exchangers – This is of particular importance to the designer in terms of the effect of frosting on the performance of various heat transfer equipment such as heat pumps, air coolers, and condensers.

The section on finned tube heat exchangers has been discussed more in

detail than the other sections since it is of particular relevance to this investigation. Though the information available is limited, it has proven to be useful.

A. FROST PROPERTIES

Since the properties of frost will be used in the analytical and numerical modelling of frost growth, a better understanding and knowledge of these will aid model development.

Two properties which have a major effect on the heat and mass transfer and growth of frost include the frost conductivity, k_f , and the frost density, ρ_f . There is a general consensus in the literature that there is a relationship between these two properties. Chen and Rosenhow [1], identified a need for correlations between frost density, thermal conductivity and the heat and mass transfer mechanisms which occur in a frosting process. Early investigators such as Beatty [2], Chung and Algren [3,4], Kamei *et al* [5] and Yamakawa *et al* [6] concluded that the frost thermal conductivity not only played a major role in the heat transfer mechanisms, but increased with frost density.

Yonko and Sepsy [7], were the first investigators to attempt an empirical correlation between the frost thermal conductivity and the density for frosting on a horizontal plate :

$$k_f = 0.014 + 0.00668\rho_f + 0.000175\rho_f^2 \quad (2.1)$$

where k_f is in Btu/hr-ft-°F and ρ_f is in lb/ft³. This correlation is only valid for the cold wall temperature ranging between - 22 and 14 °F and for an ambient

temperature range of 68 and 77 °F .

Sanders [8], in a study on the frost formation on air cooled condensers, found that a generalized relation between frost density and thermal conductivity was not possible. He presented his results only as curves. O'Neal [9], reports that the following curve fits Sanders' data quite well :

$$k_f = (1.202 \times 10^{-3}) \rho_f^{0.963} \quad (2.2)$$

where k_f is in W/m-K and ρ_f is in kg/m³. This correlation is applicable for frost densities less than 500 kg/m³.

Biguria and Wenzel [10], Seki *et al* [11], Brian *et al* [12,13] observed that the frost density had no spatial variation in the direction of frost growth. They attempted to correlate the frost thermal conductivity with not only density but also the frost surface temperature, air velocity and humidity.

Dietenberger [14], concluded that no single model accurately reflected the true characteristics of frost thermal conductivity after a study of existing literature. All the correlations presently available are only valid either for small ranges or with specific restrictions. He postulated a generalized correlation, by trying to incorporate the concept of an effective air-ice thermal conductivity, the water-vapor conductivity and density.

Hayashi *et al* [15], classified frost formation into three major categories :

- (i) Crystal Growth
- (i) Frost Layer Formation
- (ii) Frost Layer Growth

They developed correlations for the density of the frost as a function of surface

temperature T , for each category, but the relationship between the thermal conductivity and density of frost was not considered. The restrictions under which their model is valid are unclear.

From the above mentioned literature and other sources, there appears to be no agreement on the form that the relation between thermal conductivity and density of the frost should take. Dietenberger's [12] observation that no reasonable correlation is available must be taken seriously. Therefore, it is suggested that for future use, these correlations be utilized carefully and applied only in cases with conditions close to the experiments from which they were determined.

B. FROST GROWTH

The growth of the frost layer has been studied by many investigators for a variety of geometries including cylindrical, flat plate, annular and parallel plate geometries. Most results presented have been based on experimental work but a few have been purely analytical in nature.

From a general overview of the literature, the major factors affecting the frost growth are :

1. Temperature of the heat transfer surface
2. Humidity of moist air stream
3. Air velocity (or Reynolds Number)
4. Location along heat exchanger surface

There is universal agreement on the first two factors mentioned above. Frost

growth is more rapid with a decrease in the temperature of the heat transfer surface and with an increase in the humidity of the air flowing across the surface.

There is no conclusive evidence on the effect of air velocity (Reynolds number). Schneider [16], did not find that the Reynolds Number, Re had any bearing on frost growth. However, O'Neal [17] found that there was a critical Re of about 15900, above which the Re had no effect on frost growth, but below which there was a strong dependence on Re . Data from other investigators such as Kamei *et al* [5] and Yamakawa *et al* [6] suggests that there is a critical Re after which the velocity (and hence Re) has no effect. This critical value appears to lie between 12000 and 18000.

The variation of the frost thickness along the length of the plate is not fully understood. From general boundary layer theory it would appear that there would be more frost along the leading edge of the plate. Hayashi [15], reports this phenomena, but Beatty [2], reports that there is not much variation in thickness along the plate length. O'Neal [17] observed that for low flow rates, his results agreed with Hayashi's [15] results. For higher flow rates, he observed no significant variation in thickness.

Schneider [16], proposed a simple frost growth model based on the heat and mass transfer in a single needle of frost. He found that the frost thickness was a function of the plate temperature, the ambient temperature, the vapor pressure differences (and hence humidity), time and ice properties. This model shows reasonably good agreement with other studies but is valid only for time periods greater than 1 hour.

O'Neal [17], proposed a model for frost growth which made assumptions on frost properties similar to that suggested by White and Cremer [18], on the dual role of the water vapor diffusing into the frost layer (partly to increase the frost density and partly to increase frost thickness). He further assumed no spatial variation of density within the frost layer, similar to Dietenberger [14]. He concurred with previous investigators that that the frost thickness was a strong function of the plate temperature, the ambient air temperature and the air humidity. As mentioned earlier, he found a strong dependence on frost growth for Reynolds Number less than 15900. His study is restricted to parallel flow geometry. His correlation is similar to that of Schneider for high Re but not so for lower Re. A clear understanding of the effect of the Reynolds number on frost growth does not exist as yet.

White and Cremers [18] suggested that of the total mass of water vapor which diffuses into the frost layer, approximately half of it goes to increase frost density and the other half goes to increase thickness of the frost layer. They found their hypothesis to be in good agreement with previously reported experimental results. Therefore, this hypothesis was useful in helping develop an analytical model for frost formation and growth. This concept has been used by other investigators in the course of their modeling attempts.

Jones and Parker [19] attempted to quantify the frost formation process via the use of molecular diffusion of the water vapor at the frost surface using energy and mass balances. They incorporated the humidity, surface temperature of plate, porosity, mass diffusion of water vapor, density and thermal conductivity into their model. They derived a single expression for the frost surface temperature as a

function of the frost thickness. However, due to the rather complex, interdependent set of simultaneous non-linear equations, a numerical scheme was necessary to utilize the model. When compared with experiments, it had an accuracy of about 20 %. One serious limitation was that the model does not work when the surface temperature reached 0 ° C because the frost melts and refreezes to form ice, which is a non-porous media. Once this occurs, the assumption of molecular diffusivity of the water vapor is no longer valid.

Seki *et al* [11] performed a study on incipient frost formation. They formulated a model very similar to that of Jones and Parker [19], and O'Neal [17,25]. Their results suggest that their model predicts the experimental values well. They concluded that the thickness of the frost is a parabolic function of time (similar to Schneider [16] and O'Neal [17]).

Parish and Sepsy [20], presented a numerical, finite difference formulation to study the frosting process under forced convection. Their method is based on a finite difference scheme with boundary layer momentum, energy and mass balances. The model allows for frost properties to be functions of the frost surface temperature. Chuang [21], presented a simple mathematical model based on basic heat and mass transfer to study the frost formation process. It accounts for humidity, air temperature, plate temperature and frost surface temperature. However, it assumes that the density of the frost is a constant.

Loper [22], performed heat and mass transfer analysis on the frost formation on a thin aluminium tank containing liquid oxygen. Hayashi *et al* [23] developed a theoretical model of the frost layer in order to study frost formation.

Most results available to date are experimentally based. There is still not a comprehensive explanation of the frosting mechanisms, probably because of the large number of variables affecting frost growth. Therefore, conclusive results on the frost formation and growth are not available and are highly dependent on specific environmental and other conditions.

C. HEAT AND MASS TRANSFER

Heat and mass transfer occur simultaneously in the frosting process. There is a general consensus that the Chilton-Colburn analogy relating heat and mass transfer is valid for the frost formation process. This analogy is given by :

$$\frac{St_m}{St_h} = \left(\frac{Pr}{Sc} \right)^{0.66} = Le^{0.66} \quad (2.3)$$

The above analogy has been seen to be applicable by many investigators such as Kamei *et al* [5], and Chung and Algren [3,4]. However, Yamakawa *et al* [6], found that this analogy underpredicted their experimental results. In general, it has been accepted that this analogy is valid for frosting conditions. Therefore, if one is able to determine the heat transfer coefficient, the mass transfer coefficient is known and vice-versa.

Hayashi *et al* [15], report that the surface roughness and air velocity are strong functions of the mass transfer process in frosting. They found that as the frost layer grows, the surface roughness decreases and the mass transfer starts to approach a constant value. They found that for higher air velocities, the mass transfer was higher. They correlated the non-dimensional mass transfer

coefficient, Sherwood Number (Sh) with roughness, ϵ and Re.

Overall Heat Transfer Coefficient (Nu_T and U)

Many investigators including Chung and Algren [3,4], Beatty *et al* [2], and Yonko and Sepsy [7] have reported that the overall heat transfer coefficient, U went through three distinct phases as the frost layer grew in time. First, there was an increase in U which was attributed to the increase in roughness and surface area due to initial frost formation. In the second phase, U remained approximately constant. This was attributed to a compensating effect of increasing thermal conductivity of the frost for an increased frost thickness. In the final phase, U decreased with time.

Chung and Algren [3,4], in experimental work on cylindrical tubes, presented two separate correlations for transient and steady state conditions for external flows. This is because of the transient nature of the frost. Heat transfer keeps varying with the growth of the frost. The relationships are :

For transient conditions :

$$Nu_T(t) = Nu_{T_\infty} (1 + 0.023e^{-t/23.1}) \quad (2.4)$$

For steady state conditions :

$$Nu_{T_\infty} = 0.394 Re^{0.509} \quad (2.5)$$

where t is time in seconds.

O'Neal and Tree [24,25], presents a correlation presenting a relationship between the Nu, Re and Pr. This is valid for parallel plate geometry, for Re less than 16000.

$$Nu_T = 0.038 Re^{0.75} Pr^{0.33} \quad (2.6)$$

Frost Surface to Air Heat Transfer Coefficient (Nu_f)

Kamei *et al* [5], present correlations for the heat transfer coefficient in a round tube and a relation between the local heat transfer coefficient, h and water vapor coefficient, k' . These correlations are based on frosting in internal flows.

For a round tube :

$$Nu_f = 0.018 (Re)^{0.80} \quad (2.7)$$

For the water vapor transfer coefficient :

$$h/k' = Cp \left(\frac{Re}{Pr} \right)^{0.66} \quad (2.8)$$

O'Neal and Tree [25], present a correlation for the local heat transfer coefficient between the air and frost surface. It is valid for flow in parallel plate geometry.

$$Nu_f = 0.034 Re^{0.80} \quad (2.9)$$

It is of interest to note that the coefficient for Re is the same for O'Neal and Tree [24,25], as well as Kamei *et al* [5].

There have been other forms of results quantifying the heat transfer mechanism presented. For example, O'Neal and Tree [25], present a set of heat transfer correlations in terms of the ' j ' factor for frosting in parallel plates. The ' j ' factor is a dimensionless heat transfer parameter and is defined as :

$$j = St_h Pr^{0.66} \quad (2.10)$$

The relationship between j_s , Re and Pr was :

$$j_s = 0.043 Re^{-0.25} Pr^{0.33} \quad (2.11)$$

Almost all the above correlations deal with flows which are non-laminar ($6000 < Re < 30000$) and for air temperatures above freezing . Nothing has been published for laminar flows and for air temperatures below freezing. Since most heat pump heat exchangers operate at laminar flow conditions, such information would be invaluable.

D. FINNED TUBE HEAT EXCHANGERS

A substantial amount of literature is available on frost properties and growth, heat and mass transfer under frosting conditions for simple geometries. O'Neal and Tree [9] have provided a comprehensive review of frosting in those geometries. For more complex geometries such as that of finned heat exchangers, the amount of available literature is limited. The reasons for the limited literature can be attributed to the very large number of variables, the complex surface geometry of the heat exchangers and the thermodynamic properties of humid air. In view of this, the problem becomes very complex and a complete generalization is difficult to formulate.

The available literature on the various aspects of the frosting process with reference to heat exchangers has been divided into four sections :

1. Fin efficiency
2. Overall heat transfer coefficient
3. Pressure drop across the heat exchanger coil
4. Surface roughness.

Fin Efficiency

Fin efficiency, η_f , is defined as the ratio of actual heat transfer from the fin to that if the entire fin was at the base (primary surface) temperature. Incorporating such a concept in extended surface heat transfer allows one to eliminate or overcome the difficulty of locally variable surface temperatures.

Under the conditions of a thin rectangular plate fin with constant thermal and geometric properties and an adiabatic tip having one-dimensional conduction, the following expression for fin efficiency is given by Kays and London [26] :

$$\eta_F = \frac{\tanh(mL)}{(mL)} \quad (2.12)$$

For a fin with no frost, the fin parameter, m , is given by :

$$m = \sqrt{\frac{h_a P}{k_F A_c}} \quad (2.13)$$

Expressions for the equivalent length of the fin, L , are available in literature on extended surface heat transfer such as McQuiston and Parker [27] and Kern and Kraus [28] .

Only a handful of investigators have focused attention on the effect of frost on fin performance. Figure 2.1 is a schematic of the frost layer on a typical fin of uniform cross section.

Sanders [29] was among the first to extend the concept of fin efficiency to the problem of frosting in extended surface heat exchangers. He studied the effect of frosting on air cooler performance. The type of fins in consideration were the

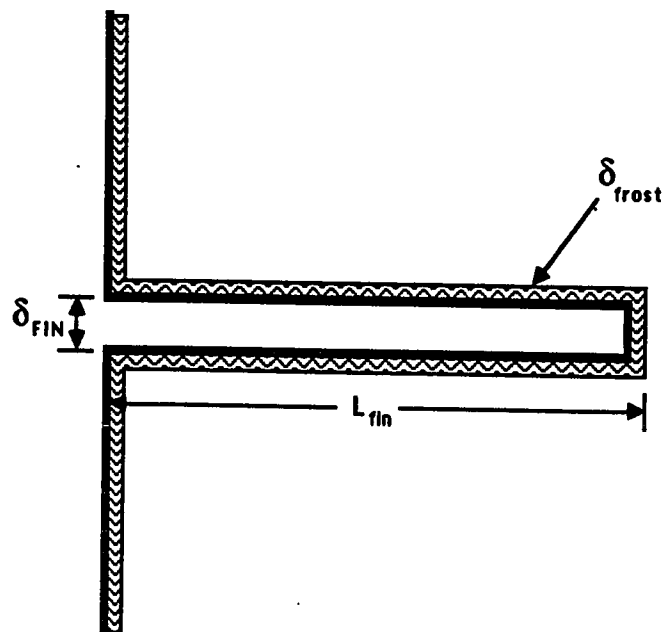


Figure 2.1 Schematic of Fin with Frost

rectangular-plate type. He introduces the concept of a "wet" fin efficiency for the combined heat and mass transfer as follows :

$$m_{wet} = \sqrt{\frac{h_a b}{C_{p_w} k_f \delta_f}} \quad (2.14)$$

where,

C_{p_w} = specific heat of the moist air

However, he does not attempt to explicitly incorporate humidity into his expressions for fin efficiency. He also introduces an average thermal resistance for the frost layer, and incorporates this into the fin parameter to obtain a frosted fin efficiency. This is done by the addition of the thermal resistance of the frost layer and that of the air (the inverse of the effective heat transfer coefficient).

He makes the following assumptions :

1. The heat transfer is one-dimensional along the length of the extended surface.
2. There is no heat transport in the frost layer parallel to the length of the fin.
3. The frost layer on the primary surface is neglected.
4. The heat transfer coefficient, h_a , is uniform all along the length of the fin.
5. The frost layer has a uniform thickness along the fin length.

The resulting expression for fin efficiency with frost, $\eta_{f,F}$, is :

$$\eta_{f,F} = \frac{\tanh(m_{f,F} L)}{(m_{f,F} L)} \quad (2.15)$$

where,

$$m_{f,F} = \sqrt{\left[\frac{1}{\frac{\delta_f}{k_f} + \frac{C_{p_w}}{h_a} \delta_f} \cdot \frac{1}{\delta_F k_F} \right]} \quad (2.16)$$

Sanders [29] demonstrates the influence of the frost layer on the rate of heat transfer by determining the ratio of fin efficiencies with and without frost for varying frost thicknesses (Figure 2.2).

He mentions that the fin efficiency increases with increasing frost thickness as a result of an equalization of fin temperature that is caused by the insulating layer of frost. However, he does not show this in a rigorous fashion. Figure 2.3 illustrates the effect of temperature equalization along the length of the fin with frost growth. The fin temperature distribution tends to values nearer the base temperature as the frost layer increases. When this occurs, the fin efficiency tends to rise (as seen from the definition of fin efficiency).

For the case of a rectangular plate-fin with a constant base temperature, T_b , an adiabatic tip, and the environment at a temperature, T_∞ , the nondimensional temperature distribution, θ , along the non-dimensional length of the fin, x^* , is given by:

$$\theta(x^*) = \frac{\text{Cosh} \left[m^*(1 - x^*) \right]}{\text{Cosh} (m^*)} \quad (2.17)$$

where,

$$\theta(x^*) = \frac{T(x) - T_\infty}{T_b - T_\infty} \quad (2.18)$$

$$x^* = \frac{x}{L} \quad (2.19)$$

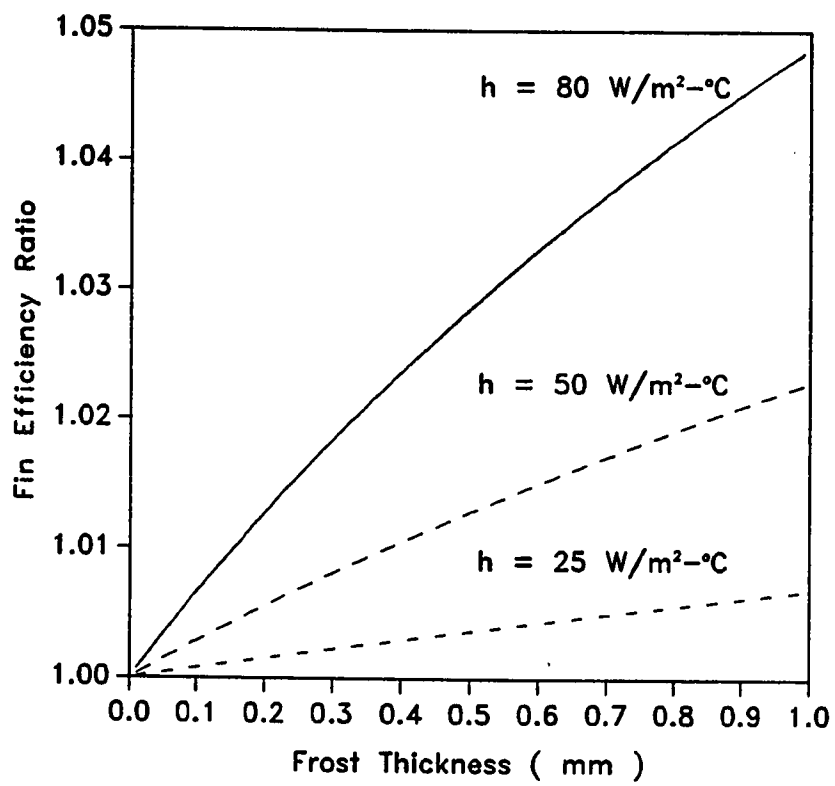


Figure 2.2 Fin Efficiency Ratio vs. Frost Height

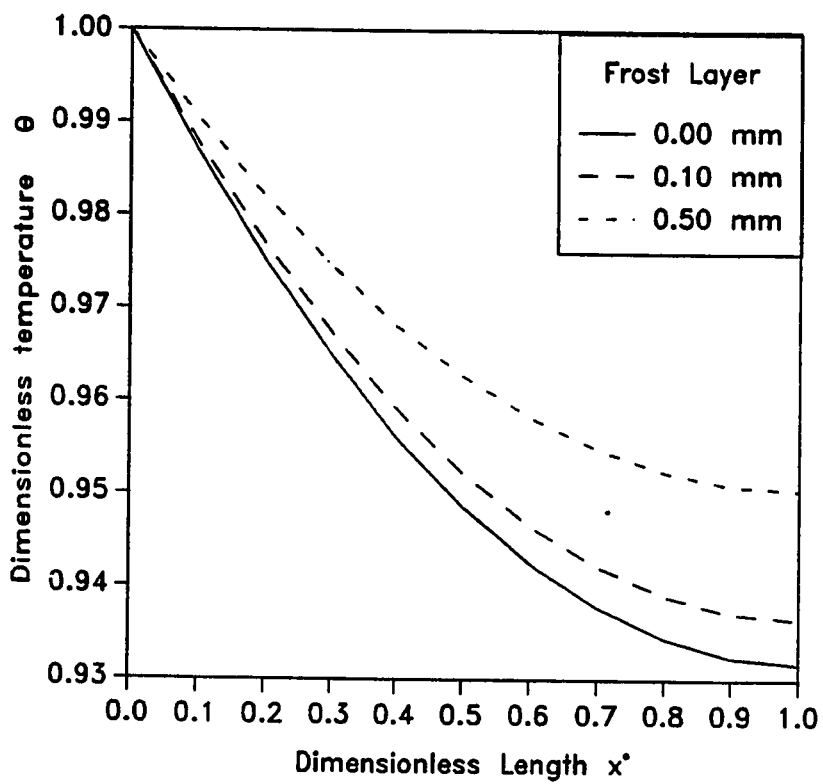


Figure 2.3 Fin Temperature Distribution vs. Frost Height

and m^* , the modified nondimensional fin parameter is given by :

$$m^{*2} = \frac{h_a L}{k_f \delta_f} \quad (2.20)$$

When m^* is replaced with $m_{f,F}^*$, which is the modified nondimensional fin parameter with frost growth, the temperature distribution for the frosted fin is obtained. $m_{f,F}^*$ is given by Equation 2.21

$$m_{f,F}^* = m^* \sqrt{\left[\frac{1}{1 + Bi_{f,F}} \right]} \quad (2.21)$$

where $Bi_{f,F}$ is the Biot number for the frost with δ_f as the characteristic length. Figure 2.3 shows the variation of temperature along the fin length for increasing frost thicknesses.

Barrow [30] presents a simplified analysis on the frosting of heat pump evaporator surfaces. He presents another expression for the frosted fin parameter m_{fr} :

$$m_{fr} = \sqrt{\frac{h_a}{k_{fr} \delta_{fr} + k_f \delta_f}} \quad (2.22)$$

However, there is no derivation of this expression from a basic energy balance on the fin. It is an addition of the terms $(k\delta)$ for the fin and frost replacing that of the fin alone. This does not appear to be physically meaningful. It also does not appear to be consistent with the governing differential equation.

When the above two formulations are compared under the same conditions, there is a considerable difference. m_{fr} varies by less than 1% in the case of Barrow [30] but drops by about 20% in the case of Sanders [29] when the frost layer increases from 0 mm to 1 mm (0 in. to 0.04 in.). This change (or

lack of) in m_{fr} translates into a change (or lack of) in the fin efficiency η_f . m_{fr} does not vary significantly in the case of Barrow [30], since the thermal resistance of the frost is typically several orders of magnitude larger than that of the fin. This has led the researcher to believe that this formulation by Barrow [30] for a frosted fin efficiency is incorrect.

On the other hand, Sanders' [29] expression is consistent with the thermal resistance analogy and can be derived from the basic energy balance. This appears to be more logical and correct.

The existing models of fin efficiency with frost growth are simple modifications of fin efficiency models of dry, unfrosted fins. No investigator has presented empirical results to verify the validity of the expressions discussed above. Since the fin is an important component in the overall heat transfer coefficients for finned-tube heat exchangers, more data should be developed relating the effects of frost growth on fin efficiency.

Overall Heat Transfer Coefficient

The overall heat transfer coefficient, U_o , is an important heat transfer parameter. The thermal resistance of the system is the inverse of the product, $(U_o A)$. Therefore, a knowledge and understanding of its variation and trends under frosting conditions is important. If U_o is low, then it means that the system has a high thermal resistance. As frost grows, the heat transfer coefficient drops as much as by 20% for 3 mm (0.118 in.) frost thickness. The coefficient is not purely a function of the frost thickness but also a function of the geometry, the frost properties and the flow rate of the air flowing across

the coils. As such, the complexity of the problem is apparent.

One of the earliest investigators to report the variations of U_o with frost was Stoecker [31,32]. He tested two finned refrigeration coils with 2 fin pitches – 9 fins per inch and 4 fins per inch under test conditions of 32°F and 72% relative humidity. The airflow rate was maintained constant using dampers. Further details of the test conditions are not available. He reported that :

1. There is an initial increase in U_o with the onset of frosting. This is attributed to an increase in heat transfer area as a result of increasing surface roughness when the frost first forms. The roughness also increases the flow velocity of the air and this results in an increase in U_o .
2. Eventually the value of U_o decreases. This trend is a result of the insulating effect of the frost as the frost layer grows. U_o drops by about 15% for about 2 to 3 lbs (0.909 to 1.363 kg) of frost accumulation on the coils.

When U_o of the two coils with different fin densities are compared, values for the frosted 4 fins per inch coil were higher than that of the 9 fins per inch frosted coil. He further observed that an increased airflow rate led to an increase in U_o . His results are shown in a graphical form in Figure 2.4.

Hosoda and Uzahashi [33] studied the effects of frost on the heat transfer coefficient in a cross-fin heat exchanger. They developed correlations for the heat transfer coefficient for such a configuration with and without frost. Their expression is :

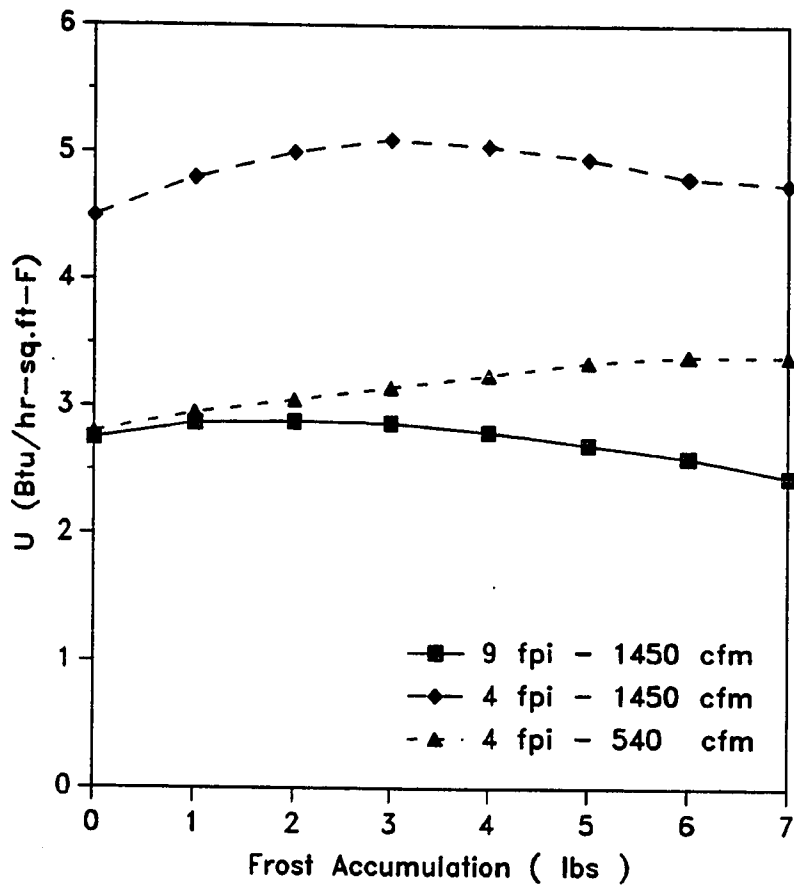


Figure 2.4 Variation of U_o with Frost Accumulation - Stoecker [31,32]

$$U_o = \frac{k_f \left[\frac{31V^{11.578}}{1 + \frac{2L^2}{3k_f S} \sqrt{P/d}} \right]}{k_f + S_f \left[\frac{31V^{11.578}}{1 + \frac{2L^2}{3k_f S} \sqrt{P/d}} \right]} \quad (2.23)$$

where, V_{max} , the maximum velocity between the fins is given by :

$$V_{max} = \frac{P_f P_1 V_f}{\{P_f - (2S_f + S)\} \{P_1 - (2S_f + d)\}} \quad (2.24)$$

where,

- ΔP = pressure drop across the coils in (mm water)
- K_f = frost thermal conductivity (kcal/m· hr °C)
- S_f = frost layer thickness (m)
- S = fin thickness (m)
- P_f = fin pitch (m)
- P_1 = pipe transverse pitch (m)
- P = mean pipe pitch (m)
- V = air velocity downstream of the coil (m/s)
- d = pipe outer diameter (m)

Their experimental results concur with Stoecker's [31] observation that initially the heat transfer coefficient increases when frost begins to form, but decreases after that. U_o drops by about 20% for 3 mm (0.118 in.) layer of frost growth.

Their results present U_o as a function of V_{max} , but do not show any relationship with the fin-plate temperature, air humidity and temperature. The experimental conditions were reported, but the model does not reflect these. The

geometry of the heat exchanger is important as well as the conditions under which frost will form and grow.

Under such restrictions, one would suspect that the applicability of such an expression is probably limited to the conditions (or close to) under which Hosoda and Uzahashi [33] conducted their experiments.

They performed experiments with heat exchangers having two fin spacings: 6 mm and 10 mm (0.236 in. and 0.394 in.). Their results show that the heat exchanger with a larger fin spacing of 10 mm (0.394 in.) has a higher heat transfer coefficient than the coil with a narrow fin spacing. This too concurs with Stoecker's [31,32] observations. Figure 2.5 shows the variation of U_o with frost thickness as adapted from their data.

Sanders [29] was the first to attempt an analytical form for U_o . His study was very extensive and included the effects of frosting on air cooler performance. His method is based on defining a frosted fin efficiency (discussed earlier in this paper), and the various geometrical parameters as well as the frost and heat exchanger properties. He uses an *enthalpy potential* to develop the heat and mass transfer mechanisms in addition to the linearized relationship between saturation enthalpy of the moist air and temperature mentioned earlier. His final expression for U_o is :

$$U_o = \left[\frac{1}{\left[h_a \eta_{fr} + h_p A_{pf} \right]} + \frac{A_{fi} b}{C' p_a h_r} \right]^{-1} \quad (2.25)$$

where,

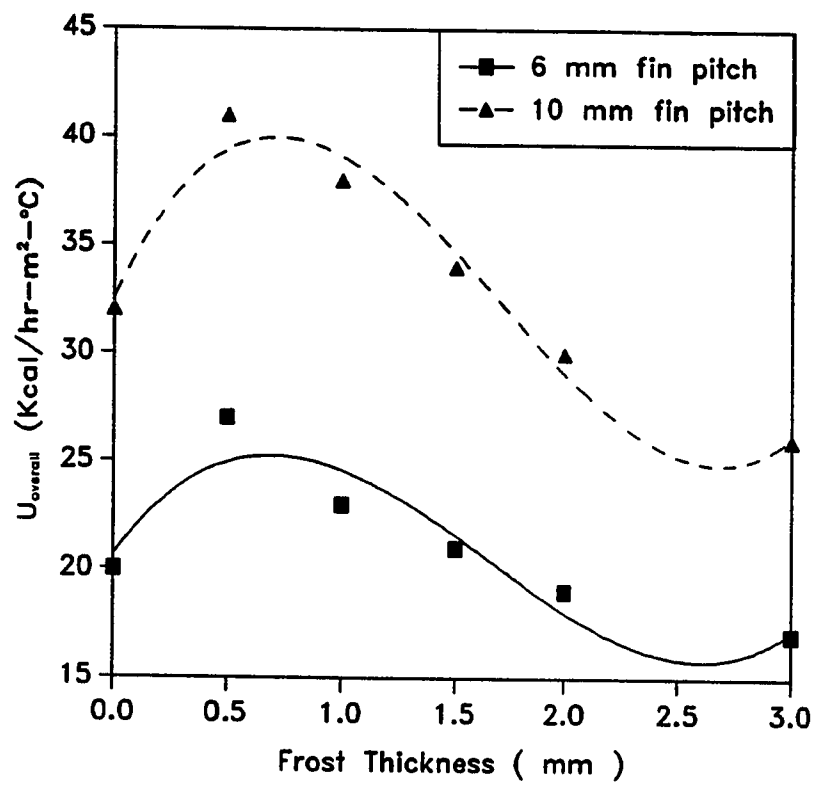


Figure 2.5 Variation of U_o with Frost Growth - Hosoda and Uzahashi [33]

- h_p = heat transfer coefficient at outside surface of pipe
 h_r = heat transfer coefficient of the refrigerant
 A_{fi} = ratio of fin area to inside area of pipe
 A_{pf} = ratio of outside pipe area to fin area

Sanders [29], however, does not explicitly show how U_o varies with increasing frost thickness as predicted by his model. Figure 2.6 reflects the trends as established by adaptation of Sanders' [29] expression.

The model is not able to reflect the initial increase in U_o as reported by Stoecker [31]. However, since the heat transfer coefficient, h_a , also varies with the frost formation, it is possible that if the behavior of h_a is known, then the increase in U_o could be obtained from Sanders' [29] expression. The final effect of decreasing U_o is seen very clearly. U_o drops by about 15% as the frost layer grows to 1 mm (0.039 in.) . It must be remembered that the model developed by Sanders [29] does not consider surface roughness created by the frost. The roughness enhances the heat transfer coefficient and hence the heat transfer. The stochastic nature of the frost formation makes it very difficult to model the roughness. His model is an improvement over Hosoda and Uzahashi's [33] model in that he considers the plate temperature and moistness of the air, but he does not explicitly consider the flow of air across the coils as a factor. The effects of airflow can be probably be absorbed into h_f and h_p . It is not mentioned if the mass flow rate is assumed to be constant or varying. The distinct advantage of his expression is that it can be derived from first principles.

Niederer [34] studied frosting on a variety of finned heat exchanger coils

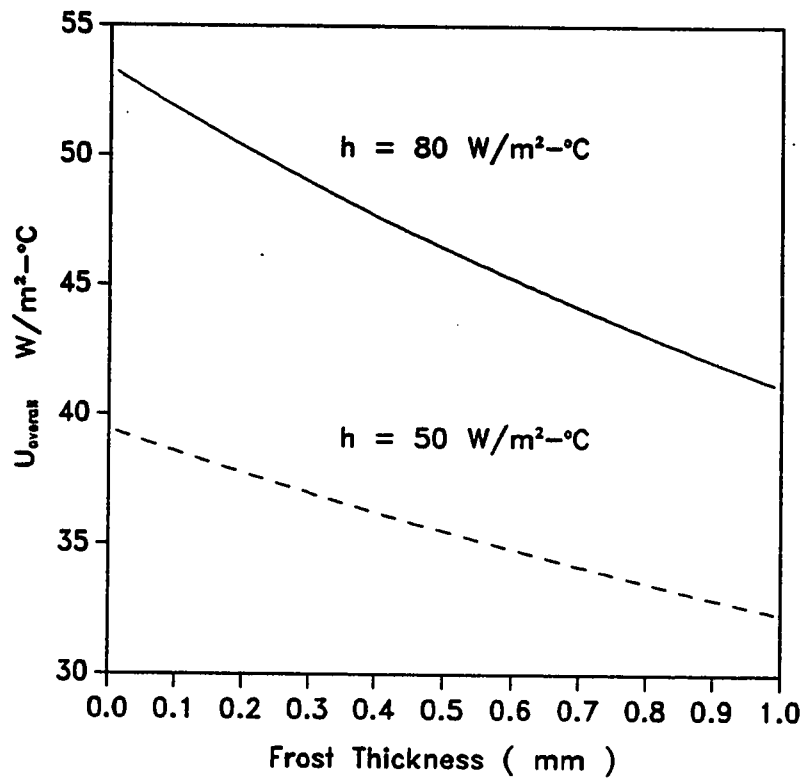


Figure 2.6 Variation of U_o with Frost - Sanders [29]

ranging from 2 to 6 fins per inch including variable fin spacing. He reports that heat exchangers with a wider fin spacing perform better under frosting conditions than narrow finned coils. This concurs with Stoecker's [31,32] observations. He also observes that coils with a variable fin spacing perform the best when compared to the wide or narrow finned coils.

Barrow [30] presents an analysis for a finned heat exchanger, based on a thermal resistance network. The overall heat transfer coefficient, U_o , based on the air side area, A_a can be expressed as :

$$\frac{1}{U_o} = \left[\frac{A_a}{h_r A_r} + \frac{1}{h_a \eta_f \left[\frac{A_f}{A_a} \right] + \left[\frac{h_a k_{fr} / \delta_{fr}}{h_a + k_{fr} / \delta_{fr}} \right] \left[1 - \frac{A_f}{A_a} \right]} \right] \quad (2.26)$$

He reports that the frosting has a negligible influence on U_o in finned heat exchangers. This result differs from those reported by other investigators such as Stoecker [31,32], Hosoda and Uzahashi [33]. The manner in which the fin efficiency, η_f , is defined by Barrow [30] is the primary cause for such a negligible variation in U_o . As mentioned previously, his analysis appears to be incorrect.

Gatchilov and Ivanova [35], performed experiments on frost formation in air coolers. They had three different air coolers with varying fin pitches of 7.5, 10, and 15 mm (0.295, 0.394 and 0.590 in.). They found that U_o is strongly influenced by relative humidity, ϕ , of the air. As in the case of Stoecker [31] and Hosoda and Uzahashi [33], they found that U_o increased initially as frost started to form. A higher ϕ produced a higher U_o . As the frost grew, U_o decreased (Figure 2.7). They further conclude that a coil with variable fin spacing performs

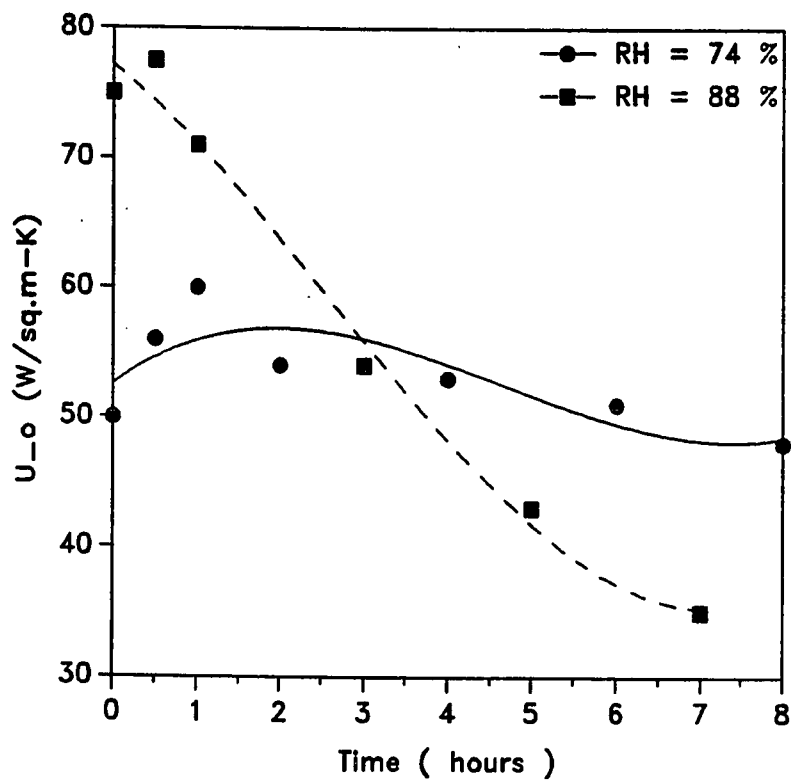


Figure 2.7 Variation of U_o with Relative Humidity - Gatchilov & Ivanova [35]

better than a constant fin spacing. This is in agreement with Niederer [34].

Gates, Huffman, and Sepsy [36,37] studied the effect of frost formation in extended heat transfer surfaces. They used a variety of heat exchanger configurations including varying fin densities, and tube rows (staggered and straight) with different spacings between tubes. All their data were for a constant air flow rate. Table 2.1 shows the configurations they used.

The variables used in correlating data included the dry-bulb temperature difference and the difference in specific humidity (upstream and downstream of the coils). These represent the driving forces for the heat and mass transfer taking place. This differs from the other approach of enthalpy potential which was used by Sanders [29]. Huffman and Sepsy [37] mention a thermal resistance network based expression for U_o but do not present it in an explicit form. They choose to express the heat transfer in a nondimensional heat transfer parameter, H :

$$H = \frac{h'_{avg}}{h'_{int}} \quad (2.27)$$

where,

h'_{int} = initial nondimensional heat transfer coefficient

h'_{avg} = average nondimensional heat transfer coefficient

where h' is defined by :

$$h' = St_a Pr_a^{2/3} \quad (2.28)$$

Such an expression was used since the heat transfer coefficient was

TABLE 2.1 Heat Exchanger Configurations Used by Gates *et al.* [36,37].

Heat Exchanger	Fins Per Inch	Tube Rows	A_c (sq.ft)
1	6	1	0.600
2	6	2	0.600
3	6	3	0.600
4	6	4	0.600
5	6	6	0.600
6	12	1	0.577
7	12	2	0.577
8	12	3	0.577
9	12	4	0.577
10	12	6	0.577
11	2	4	0.614
12	4	4	0.607
13	8	4	0.592
14	16	4	0.562

dependent on the air velocity, the dry-bulb temperatures and the humidity differences. They further correlate the Reynolds Number with $St_a Pr_a^{2/3}$, thereby establishing the relation between the heat transfer coefficient and air velocity.

They present their results as graphs showing the variation of the nondimensional heat transfer parameter, H , against a nondimensional mass transfer parameter, W , defined by the following expression :

$$W = \frac{\Delta\omega}{\omega_{sat}} = \frac{\omega_{up} - \omega_{sat}}{\omega_{sat}} \quad (2.29)$$

A typical curve is shown in Figure 2.8. Their results show the following :

1. Presence of frost on the heat exchanger surfaces resulted in overall lower heat transfer rates.
2. The number of tube rows in the heat exchanger, has little or no effect on the heat transfer under frosting conditions.
3. H decreases as the number of fins per inch increases. This is consistent with Stoecker [31], Hosoda and Uzahashi [33] as well as Niederer [34].
4. The variation in heat transfer coefficient with time was partially dependent on varying frost properties.

They also present a simple numerical example to predict the time dependent behavior of a frosted, finned heat exchanger coil. This information has been used subsequently by Tantakitti and Howell [38] in a simulation of heat pumps operating under frosting conditions.

It is really not possible to directly compare the results of Gates, *et al.* [36,37],

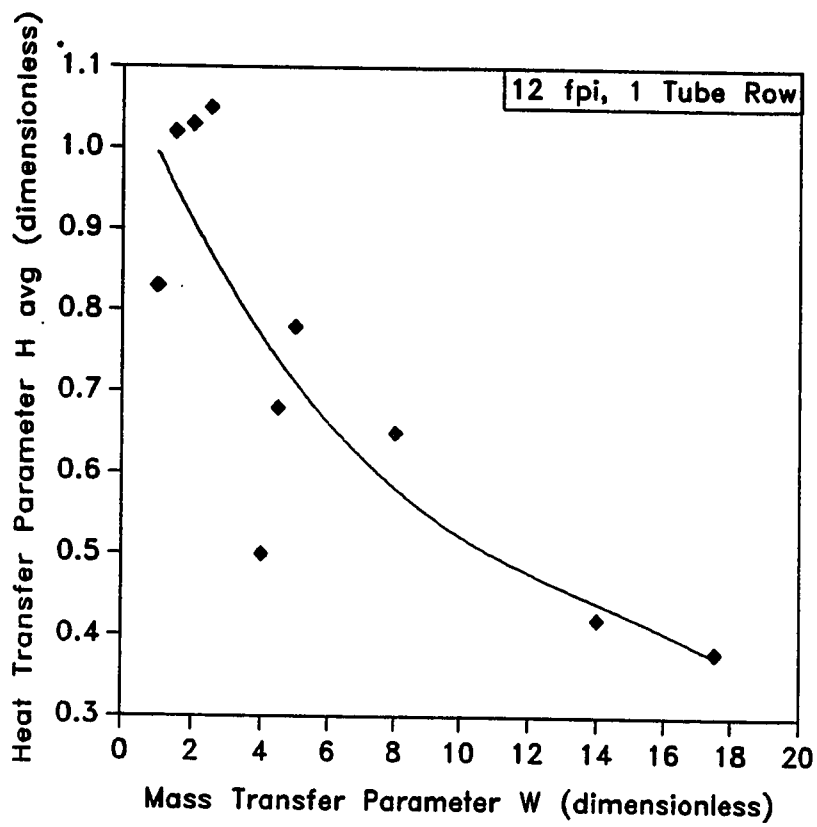


Figure 2.8 Heat Transfer vs. Mass Transfer - Gates et al, [36,37]

with any other investigator's work. They do not present the frost growth as an explicit parameter as the others (Sanders [29], Stoecker [31], Hosoda and Uzahashi [33]) do. The role of humidity in the frosting process is mentioned by all. Only Gates, *et al.* [36,37], use it as an explicit variable. Overall, none of the investigators gives sufficient data and information to compare results.

Pressure Drop

The pressure drop across the coils, ΔP , is an important parameter in the study of heat exchangers. Since centrifugal fans are used to move air across the heat exchanger coils, the pressure drop is a measure of the flow rate of the air across the coils and hence the blockage effect. There is also a change in the air-side heat transfer coefficient as a consequence of the velocity associated with the blockage of the fins by the frost.

Stoecker [31,32] studied the effect of frost growth on the coils on the pressure drop across the coil. He found that there was an increased pressure drop for higher flow rates (CFM) as frost accumulated on the coils. He observed that the airflow had more adverse impact on the overall performance of the heat exchanger coil when compared to that of U_o . Wide finned coils have a lesser ΔP than narrow finned coils.

In his experiments, Stoecker [31] allowed 6.5 lbs (2.95 kg.) of frost to accumulate on the coils. There is a dramatic increase in the pressure drop across the coils and a decrease in U_o . The pressure drop versus frost accumulation for different airflow rates and fin spacings are shown in Figure 2.9.

Hosoda and Uzahashi [33] present an empirical expression for the pressure

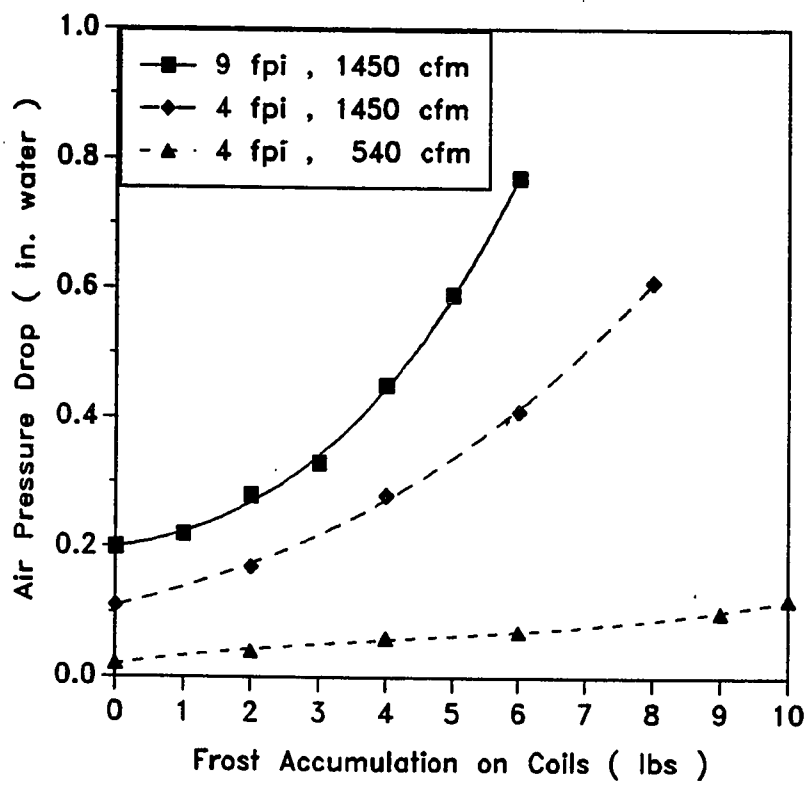


Figure 2.9 Effect of Frost Growth on Pressure Drop - Stoecker [31,32]

drop across the coils for a cross-flow finned tube heat exchanger with frost. Their expression is :

$$\Delta P = 5.88 \times 10^{-4} N_2 \times \frac{\left[2/P_f \left\{ P_2 - \frac{\pi(d+2S_f)^2}{4P_1} \right\} + \frac{\pi(d+2S_f)}{P_1} \right]^{1.3}}{P_2^{0.3}} \times \left[\frac{P_f P_1}{\{P_f - (2S_f + S)\}\{P_1 - (2S_f + d)\}} \right]^3 V_f^{1.7} \quad (2.30)$$

where,

N_2 = the number of tubes

P_2 = pipe longitudinal pitch (m)

The expression is probably applicable only to conditions close to that of the experiment. It was not possible to verify the validity of this expression with the data from other investigators since other investigators did not give sufficient information on the heat exchanger fin and tube geometries.

When geometrical data for a typical heat exchanger coil used in heat pumps is substituted in the above expression, for a fin pitch of 1.25 mm (0.05 in.) the pressure drops were two orders of magnitude greater than when the fin pitch was 6.0 mm (0.236 in.) with all the other parameters remaining unchanged. The pressure drops for the larger fin pitch were comparable to those reported by other investigators. Therefore, it would appear that the above expression by Hosoda and Uzahashi [33] is valid only for large fin spacings greater than 4.0 mm (0.157 in.).

Gates, *et al.*, [36,37] attribute the change in the pressure drop across the

coils to the following reasons :

1. Reduction in free flow area,
2. The change in friction factor resulting from an increased Reynolds Number, and
3. The change in surface roughness.

They chose to work with friction factors to represent the ΔP . The friction factor, f , was determined experimentally by measuring the pressure drop across the coils and applying the following heat transfer equation from Kays and London [26] .

$$f = \rho_m \frac{A_F}{A_a} \left[\frac{2g\Delta P}{\dot{G}_a^2} - \left(1 + \left(\frac{A_F}{A_{fr}} \right) \right) \left(\frac{\rho_d - \rho_u}{\rho_u \rho_d} \right) \right] \quad (2.31)$$

where,

- A_F = free-flow area without frost
 \dot{G}_a^2 = mass velocity
 A_{fr} = free-flow area in the presence of frost
 ρ_m = mean (ρ_u and ρ_d) air density

The nondimensional pressure loss parameter, F , was defined as :

$$F = \frac{f_{avg}}{f_{int}} \quad (2.32)$$

where,

- f_{int} = the initial friction factor (with no frost).

f_{avg} = the average friction factor with frost.

This parameter, F , was empirically correlated as a function of the mass transfer parameter, W , and dimensionless time, θ . These are shown in sets of curves for the various heat exchanger configurations. A typical curve of their results is given in Figure 2.10. The scatter in the data was attributed to the random deposition of the frost.

Their results show the following :

1. F decreases with increasing fin pitch and with decreasing W . This concurs with Stoecker's [31,32] observations.
2. A plot of $Q/\Delta P$ against fin spacing shows that the maximum heat transfer per unit pressure occurs at an intermediate fin spacing of 8 fins per inch.

Niederer [34] shows that the decrease in heat exchanger performance as a result of frosting is mainly due to a drop in airflow rate. He presents his results (for 30 lbs (13.6 kg) of condensate) in a tabular form (Table 2.2). His findings show that there is less airflow rate reduction for wide finned coils. This supports Gates *et al.* [36,37] and Stoecker's [32] findings. Variable fin spacing appears to have the best overall performance.

Gatchilov and Ivanova [35] found that pressure drop across the coils was higher when the air had higher relative humidity. This is probably because there is increased mass transfer with this higher airflow. The higher mass transfer produces more frost and causes the pressure drop to increase. Figure 2.11 shows the trends as measured by them.

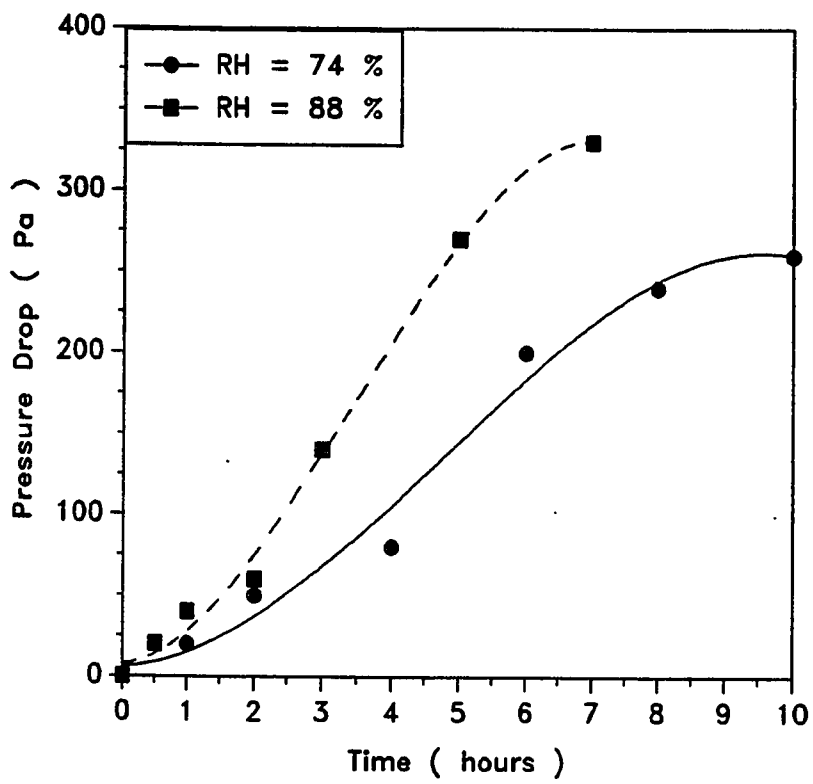


Figure 2.10 Pressure Parameter vs. Time - Gates *et al* [36,37]

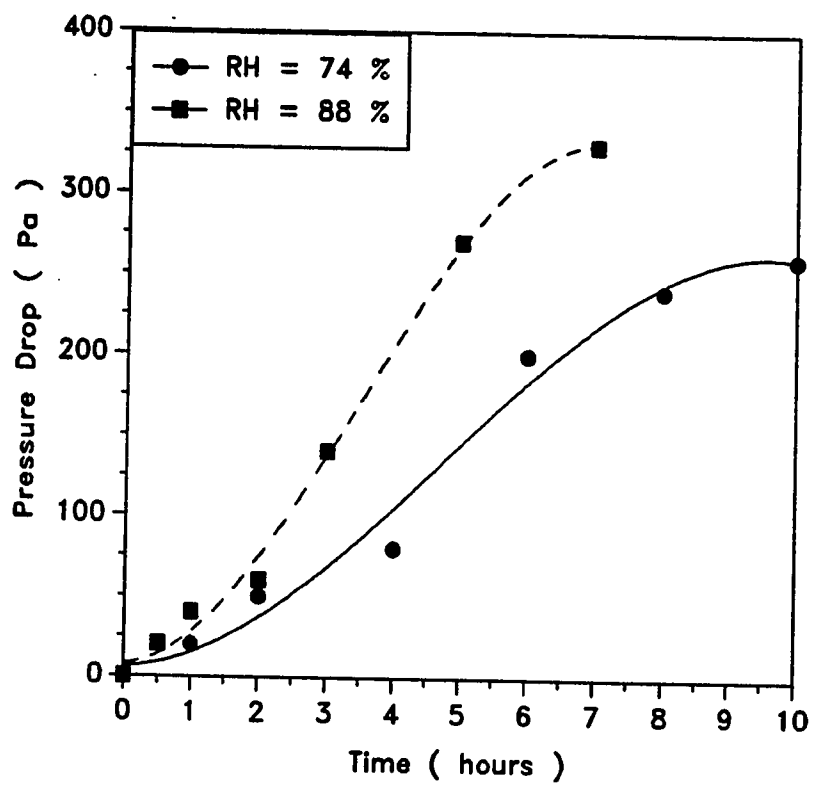


Figure 2.11 Effect of Relative Humidity on Pressure Drop

- Gatchilov and Ivanova [35]

Table 2.2 Effect of Fin Spacing on Airflow – Niederer [34]

Fin Spacing (fpi)	Air Reduction %	Capacity Reduction %
2/4 - Variable Spacing	8.3	5
3/6 - Variable Spacing	16.9	12
4	30.0	22
6	50.0	40

Sanders [29] does not go into detail while discussing the problem of pressure drop but states that the established relations for pressure drop across heat exchanger coils such as those given in Equation 2.33 could be used.

$$\Delta P = \frac{f \dot{G}_a^2 A}{2g\rho_m A_c} \quad (2.33)$$

The area of cross-sectional flow, A_c , is a function of frost growth and keeps decreasing with increased frost accumulation. In addition, the fan characteristic curve (pressure versus flow) is dependent on the airflow rate.

Barrow [30] gives a rough estimate of the air side heat transfer coefficient, h_a , as a function of the square root of the face velocity of air, V_a , flowing across the coils :

$$h_a \propto \sqrt{V_a} \quad (2.34)$$

There is no indication as to origins of this estimate, but it does serve to show that the pressure drop across the coils is an important factor. The velocity V_a is related to the pressure drop by well established relations similar to Equation

2.33. He also mentions that the fan characteristic of the blower in the system plays a role in determining this pressure drop but does not elaborate.

Quantitative comparisons between various investigators are difficult. A general conclusion about the pressure drop across the coils is that it is a more important parameter than the overall heat transfer coefficient in determining the effect of frost on the coil heat transfer. The frost restricts the free flow area through the heat exchanger, reducing airflow which translates into reduced energy transfer.

Surface Roughness

The crystalline structure of the frost results in the frost surface being rough and uneven. The roughness of the frost surface is difficult to predict. However, the roughness of the surface contributes to an enhancement of the heat transfer to the heat exchanger.

As Sanders [29] notes, the surface roughness enhances the heat transfer only in the early stages of frost formation. As frost grows, the insulating nature of the frost becomes the dominant effect. This is reflected in the studies of Stoecker [31,32], Hosoda and Uzahashi [33], and Gatchilov and Ivanova [35].

Gatchilov and Ivanova [35] found that the roughness was also a function of the conditions under which the frost was formed. For a relative humidity, ϕ , of 0.82 and an air mass velocity, $\dot{G}_a = 2 \text{ kg/m}^2 \cdot \text{s}$, the fin surfaces of the coolers were relatively smooth when compared to that of $\phi = 0.88$ and an air mass velocity, $\dot{G}_a = 8 \text{ kg/m}^2 \cdot \text{s}$. For a small (approximately 5 %) increase in ϕ , and a large increase in flow velocity, the roughness increased considerably. This may be related to the type of frost being formed as studied by Hayashi et

al [15]. They further found that the initial rows of fins had increased frost and roughness. Such a claim needs to be validated by further experimentation since such an observation could very well be a result of a non-uniform flow approach of the air across the cooler surfaces.

Considering that the surface roughness is helpful to the performance of the heat exchanger only for the initial part of the frosting process, and that quantification is difficult, it is natural that very few investigators have attempted to study the roughness of frost formation in great detail.

E. CONCLUSIONS

Several major conclusions can be drawn from the above survey of the literature available.

1. Frost growth is generally detrimental to heat transfer in heat exchangers.
2. A large amount of work has been done to quantify the formation and growth of frost and variation of properties in simple geometries. These geometries include flat plates, cylinders, tubes, parallel plates and annuli.
3. There does not appear to be a unique relationship between the frost thermal conductivity and density. Numerous attempts have been made to quantify this relationship, but the data still show much scatter.
4. Frost growth is enhanced by an increase in humidity and decrease in the heat transfer surface temperature.
5. Numerous heat and mass transfer correlations for frosting in simple geome-

tries have also been proposed and can be used. However, the influence of the Reynolds number has not been well established as yet.

6. The amount of literature available on finned tube heat exchangers is limited, but it has been well established that frost formation and growth is detrimental to their performance.
7. Fin efficiency increases initially with frost growth and then tends to approach a constant value. The initial rise is attributed to the equalization of the temperature distribution along the fin length.
8. More work, especially experimental, is needed to determine the exact effect of frost performance on fin performance.
9. The overall heat transfer coefficient has an initial surge upon the onset of frosting as a result of increased surface area and surface roughness. This surge is soon offset by the increase in thermal resistance of the frost layer.
10. The overall heat transfer increases with the relative humidity of the air flowing across the coils.
11. Heat exchangers with wider fin spacing perform better under frosting conditions than those with narrow fin spacing. Variable fin spacing coils appear to perform better.
12. A generalized yet reasonably accurate correlation between the overall heat transfer coefficient, the geometry of the heat exchanger coils, and the varying environmental conditions will be very useful.

13. The pressure drop (and hence the drop in airflow) across the coils appears to be the more influential parameter of frost formation, affecting the heat transfer performance of heat exchanger coils.
14. Further studies are recommended to study the optimum amount of frost accumulation for the defrosting mechanism to activate, thereby maintaining suitable airflow rates and pressure drops.
15. Surface roughness is helpful to coil performance only in the early stages of frost growth. It is a function of the the relative humidity and flow rate of the air flowing across the coils.
16. Most information regarding frosting in finned tube heat exchangers is experimental in nature, and a satisfactory mathematical model to simulate the process is as yet unavailable.
17. There is a growing need to place any information available on this problem in a design oriented format which can easily utilized by designers and manufacturers.

CHAPTER III

EXPERIMENTAL FACILITY

To facilitate the experimental part of this study, a closed and sealed test loop has been built at the Texas A & M University Energy Systems Laboratory. The purpose of this facility is to study the effects of frost growth under different environmental conditions (temperature and humidity) on the performance of finned tube heat exchangers. The test heat exchangers will be of different geometrical configurations including fin spacing, tube row spacing and fin type.

The test loop has been designed to allow for the controlled flow of air at various temperatures and humidities. The loop consists of galvanized sheet metal ductwork, (2 foot sq. in cross section) air cooling and heating equipment, a saturation system, a blower to provide air flow, a conical diffuser and turning vanes to ensure smooth, uniform air flow, various measuring devices, such as thermocouple (Copper-Constantan) grids, manometers for pressure drops and humidity sensors for humidity measurements.

Figure 3.1 shows the layout of the test loop and the location of its constitutive elements. The top covers of the test section, cooling coil section and the saturation section are made of plexiglass. This allows for a visual observation of the frost formation process. The test loop is well insulated by a 2 inch layer of polystyrene foam.

A. DESIGN BACKGROUND

Because the test loop is closed and sealed, air will continuously circulate in

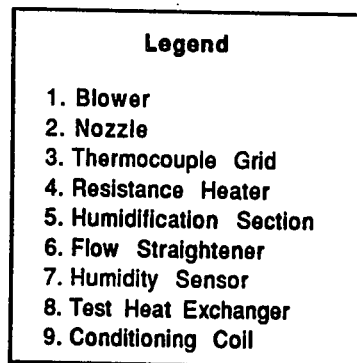
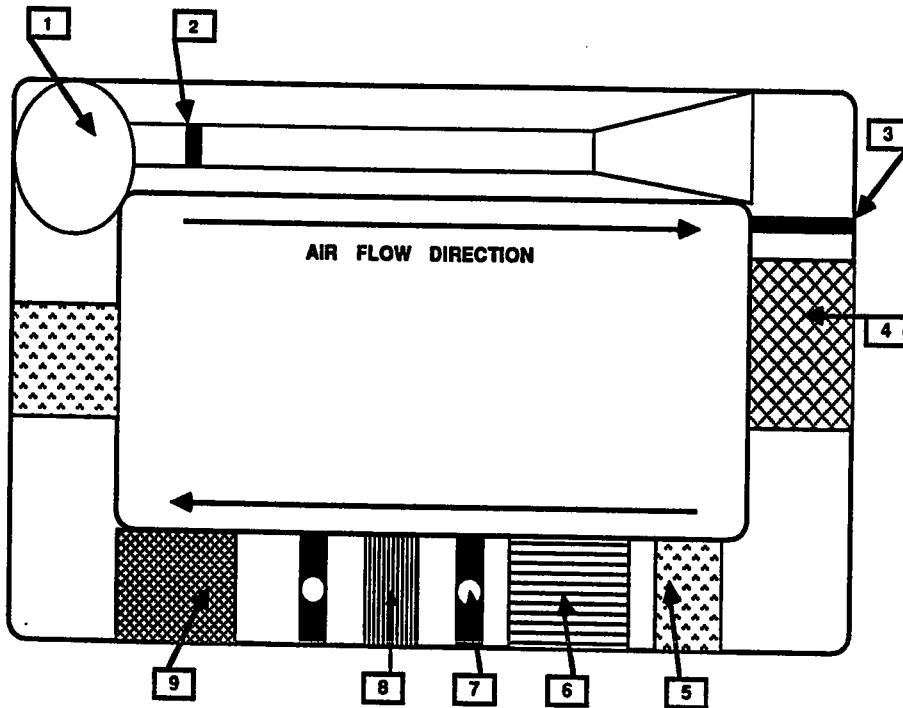


Figure 3.1 Experimental Schematic

the loop. A typical circuit can be described as follows :

When the air leaves the test coil, it will be at a lower temperature and humidity than when it approaches the coil. This temperature and humidity is further reduced as the air passes over the condensing/cooling coil. Then, the humidity is raised by the primary saturation system. The air is now at a higher humidity but the temperature must be increased. Resistance heaters provide the additional sensible heat required. The secondary saturation system is adjusted to achieve desired humidity levels. The process can be represented on a psychrometric chart (Figure 3.2).

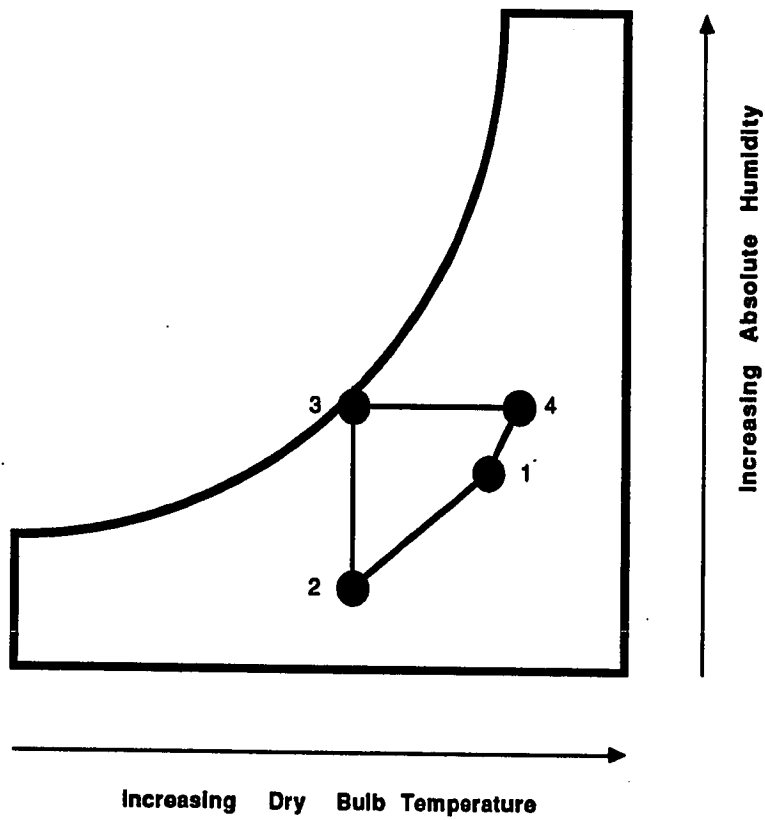
The system needs time to achieve a steady state because initially, the air inside the loop will be at ambient conditions. This is achieved in a few hours after system start-up. The system will be able to provide temperatures in the range of (30 to 40 ° F) and relative humidities in the range of (65 to 85 %).

B. TEST FACILITY COMPONENTS

There are 6 basic elements of the test loop :

1. Test Section
2. Cooling Section
3. Saturation System
4. Air Flow Control
5. Heater Section
6. Monitoring/Instrumentation

Each element of the experimental setup is described below.



LEGEND	
1 - 2	Cooling and Dehumidification (COOLING COIL)
2 - 3	Humidification (SATURATION SPRAY)
3 - 4	Sensible Heating (HEATERS)
4 - 1	Cooling and Dehumidification (TEST COIL)

Figure 3.2 Psychrometric Process in Test Loop

Test Section

Various test heat exchangers are used in the test section. Each is an air to liquid (ethylene glycol - water mixture) heat exchanger with varying fin densities and geometrical configurations (flat, wavy, corrugated, louvered and spine fins).

The cold ethylene glycol - water mixture circulates between the test heat exchanger and a well insulated sump tank. The ethylene glycol - water mixture in the sump tank is maintained at a constant temperature via the use of a tube-in-tube refrigerant to ethylene glycol heat exchanger with R-502* as the other heat transfer working fluid. This second heat exchanger behaves as the evaporator for a 3 ton residential heat pump operating in the heating mode. Typical temperatures of the ethylene glycol required before frost would form were below 10 ° F.

The reason for such a configuration is the ease with which the test heat exchanger can be replaced without having to recharge the heat pump with refrigerant for every new test. R-502 was preferred to the more common and standard R-22 since it has a smaller pressure ratio for a set of given operating conditions.

Figure 3.3 is a schematic of the configuration. Photograph 3.1 shows a typical test heat exchanger undergoing a test and Photograph 3.2 shows the configuration of the tube in tube refrigerant to ethylene - glycol heat exchanger.

Cooling Section

The condensing/cooling coil is a permanent fixture. It is connected to a 3 ton

* R-502 and R-22 designate refrigerant 502 and 22 respectively.

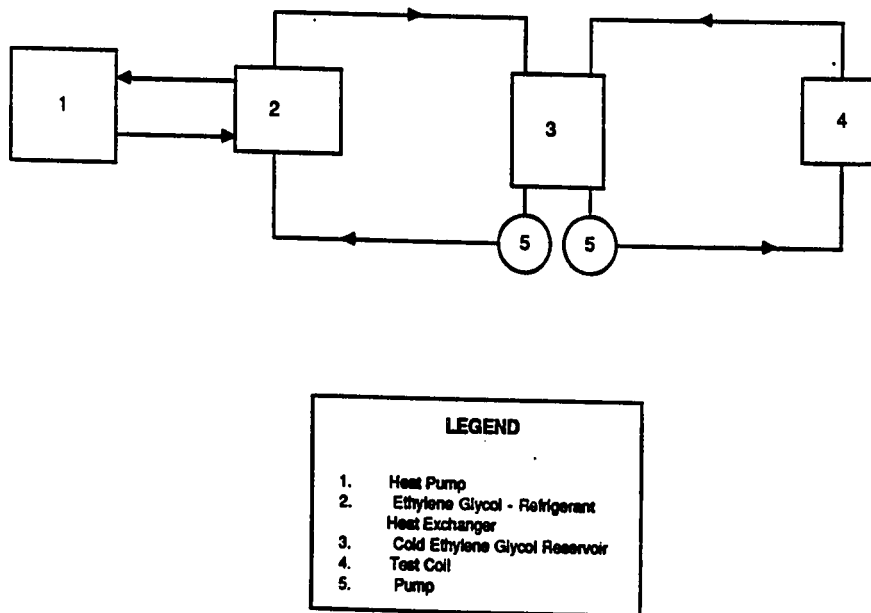
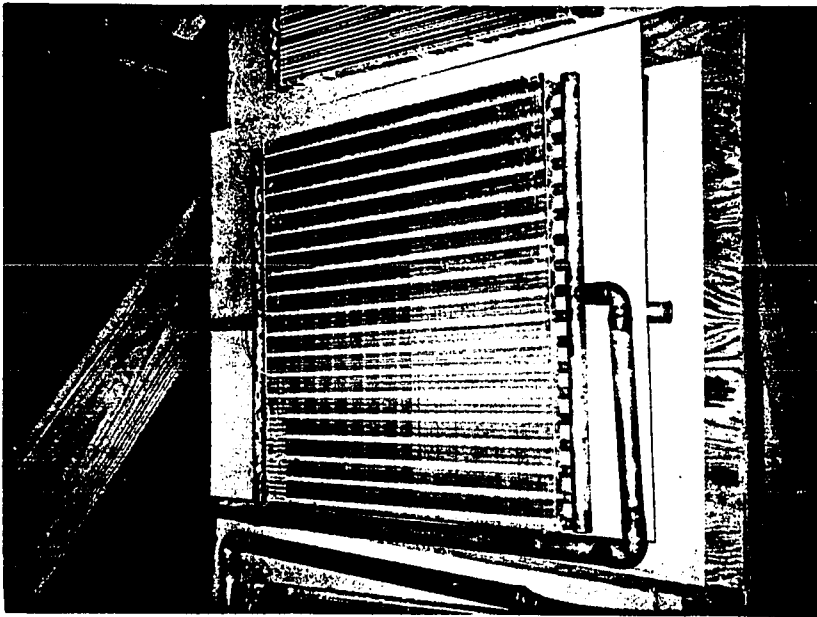
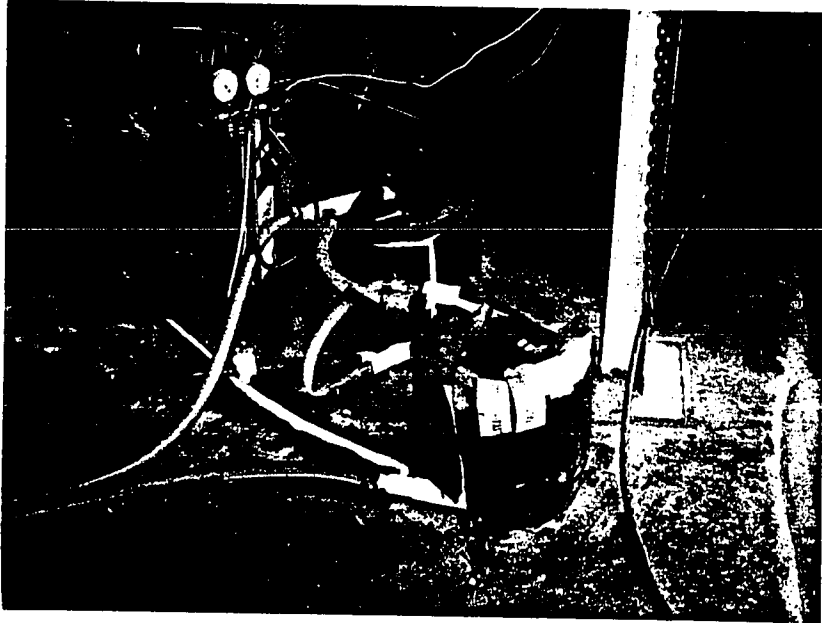


Figure 3.3 Schematic of Test Coil Configuration



Photograph 3.1 Test Coil



Photograph 3.2 Tube in Tube Heat Exchanger

residential heat pump operating in the heating mode. The presence of a cooling coil in addition to the test coil is warranted by the fact that the test coil alone will not be able to provide the required cooling and necessary temperature ranges for saturation and formation of the frost. Frost will typically not form unless the air temperature is in the range of 30 to 40 ° F.

The coil presently installed is a ' V ' shaped coil, 23.5 inches wide, with parallel rectangular Photograph fins. It is placed to allow for the use of a drain pan to collect condensate from the moist air. In addition, a sliding backboard has been constructed to control the path of the air flow across the fins of the heat exchanger coil.

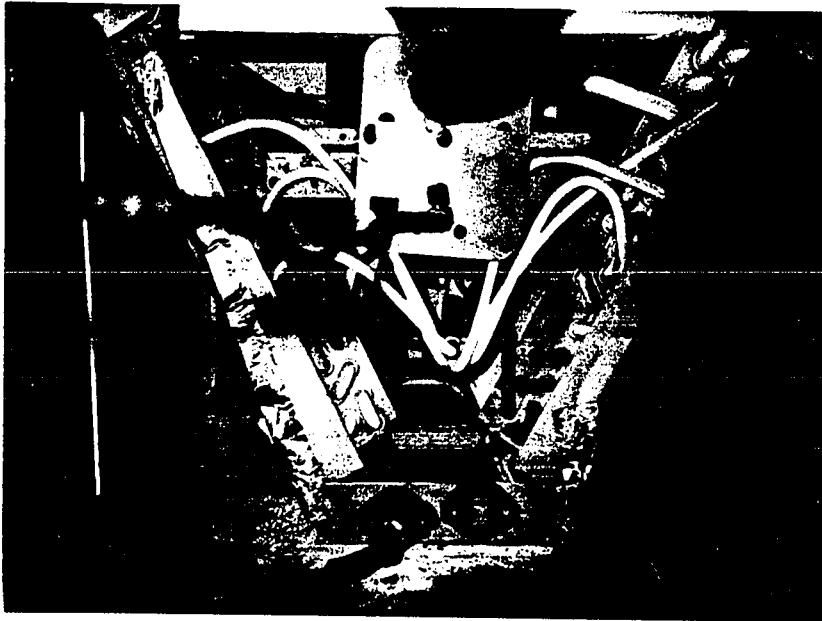
Photographs 3.3 and 3.4 show the layout of the condensing coil and the residential heat pump. R-22 was used since its properties well satisfied the operating range for the experiment.

Saturation System

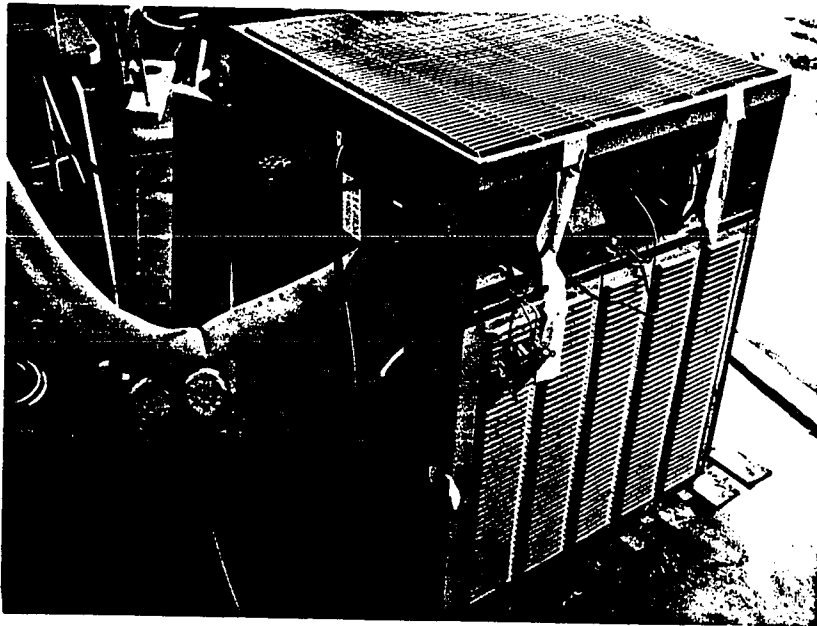
The saturation system is illustrated in Figure 3.4. It is designed to provide sufficient amounts of saturation to the air (to achieve the desired humidity levels).

There are two sections of the spray : a primary spray after the condensing coil and a secondary spray just prior to the test coil. Both the sections consist of a galvanized sheet metal tray, 2 inches in height, which contains a layer of water. Water is sprayed continuously into the tank via the use of a pump connected to a sump. The spray is a fine mist achieved via the use of atomizer nozzles.

As the water level in the tray increases as a result of the spray, the water



Photograph 3.3 Cooling Coil Configuration



Photograph 3.4 Residential Heat Pump connected to Cooling Coil

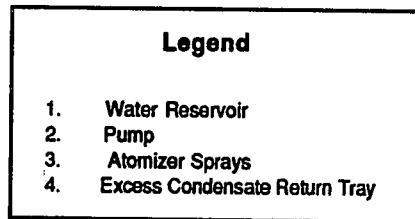
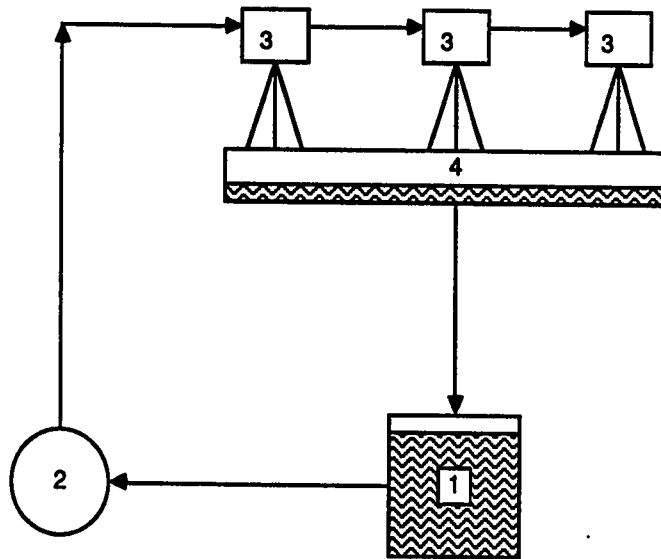


Figure 3.4 Schematic of Saturation Spray

level rises and drains out from a series of small drain ports leading back to the sump. The efflux of the water is approximately equal to the influx of the water ensuring the tray does not fill up and overflow. An immersion heater in the sump serves to raise the temperature of this water and thereby help the air to saturate faster.

The amount of water spray is controlled via the use of a hand valve. The flow needs to be adjusted so that the desired values of humidity are achieved in a relatively short time and maintained approximately constant. Relative humidities ranging from 60 to 85 % have been attained at different air temperatures.

Air Flow & Control

The source of air flow in the test circuit is a centrifugal blower. The blower is driven by a 240 V single phase motor. Air flow is controlled via the use of a damper. This is necessary to ensure a constant mass flow rate during a test. Since typical face velocities for heat pump evaporator coils range between 125 and 250 feet per minute, the suction (inlet) end of the blower is partially blocked off to attain the desired flow rates.

Heating Section

It is necessary to reheat the air to the desired range of air temperatures since the condensing coil cools the air down to values below required temperatures. (Figure 3.5) An on/off controller is used to turn the heaters on and off. Such an arrangement enables the system to control the air temperature to within the deadband of the controller. It has been successfully tested to operate within $\pm 1.0^\circ \text{F}$ of the desired temperature. The location of the temperature measurement

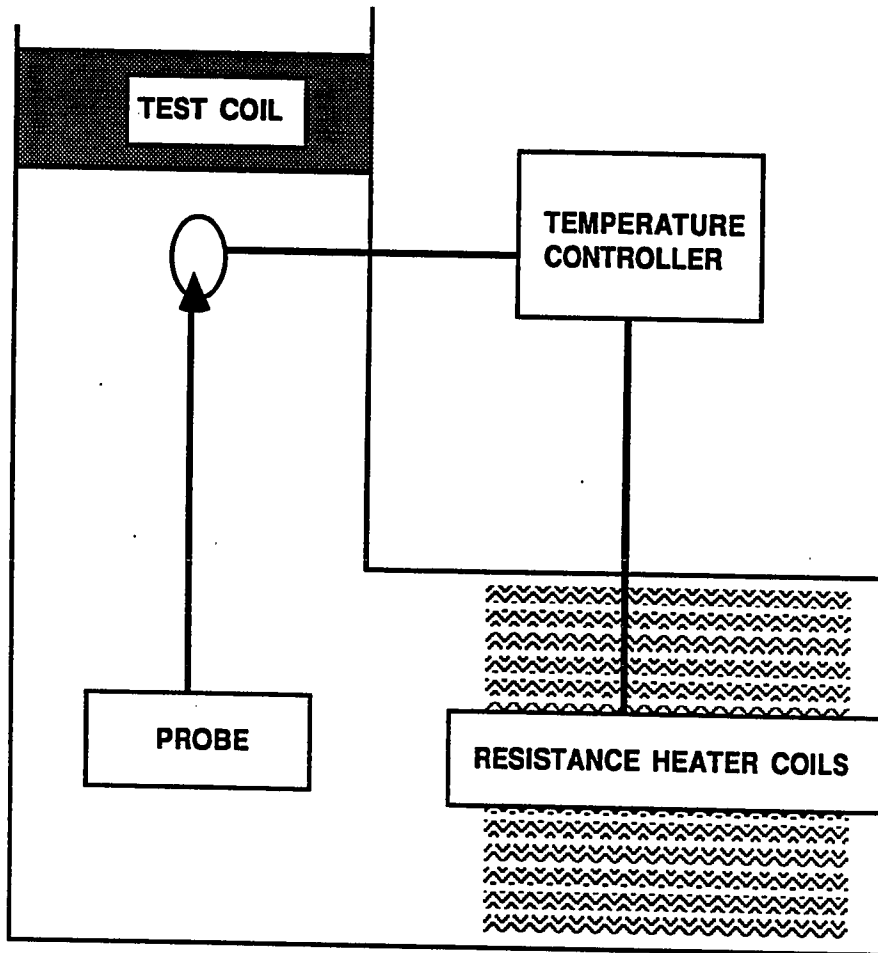


Figure 3.5 Resistance Heater Coils

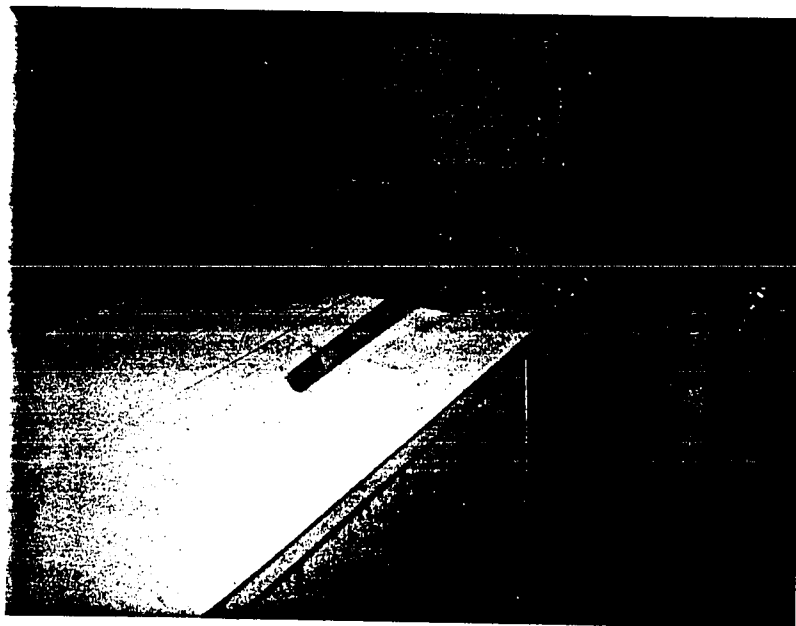
of the controller is just before the test coil.

Monitoring / Instrumentation

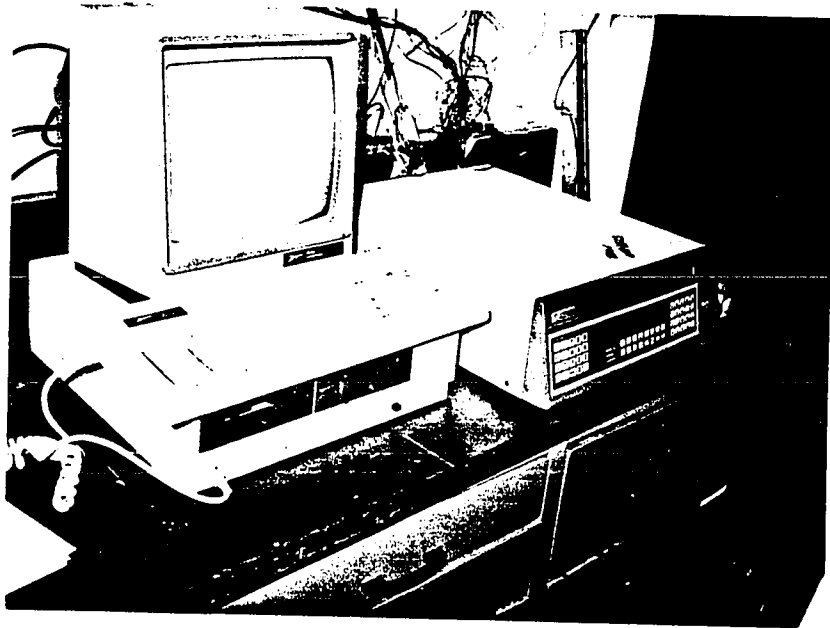
There are three measuring devices present in the test loop :

- a. Flow Nozzle connected to an inclined manometer. This will be used for monitoring the flow rate. The nozzle is a standard ASME 5 inch nozzle.
- b. Thermocouple Grids. 4 sets of Cu - Constantan thermocouple grids have been set in place as shown in Figure 3.1. Each grid consists of 9 thermocouples to provide an average temperature at that location. These thermocouples are connected individually to a datalogger whose output is directly in degrees F or C.
- c. Humidity Sensors. 2 humidity sensors have been calibrated and are in place before and after the test heat exchanger coil as shown in Figure 3.1. The calibration procedures involved the use of a high accuracy NBS-traceable Dew Point Meter in a humidity controlled environment. Photograph 3.5 shows a close up of one of the humidity sensors in use.

The datalogger is interfaced with a personal computer for initial data reduction. The data are reduced on the personal computer using a spreadsheet and later uploaded to the mainframe computer for further analysis. Photograph 3.6 shows the datalogger and computer used for data collection and storage.



Photograph 3.5 Humidity Sensors



Photograph 3.6 Datalogger and Computer

CHAPTER IV

ANALYTICAL MODEL

This chapter describes the development of an analytical model used to predict the performance of finned tube heat exchangers under frosting conditions. The model includes the growth mechanisms of the frost, the heat exchanger attributes, as well as the system characteristics.

A. ASSUMPTIONS

The governing equations for the model are derived with the following assumptions :

1. All local heat transfer surface temperatures are below frost point. i.e., frost will occur at all locations of the heat exchanger.
2. There is a homogeneous distribution of frost on the fins and tubes of the heat exchanger. This is strictly not true, but is a necessary assumption.
3. The problem is assumed to be quasi-steady in nature.
4. The frost layer will be characterized by average properties (density, porosity etc.) at any given time step.
5. The thermal conductivity of the frost varies with its density.
6. The air flow is steady and the velocity profile is fully developed.
7. The air and water vapor behave as ideal gases.
8. Heat and mass transfer is one dimensional (from the air to the heat exchanger surface).
9. Radiation exchange between the moist air and frost is negligible.

The assumption of quasi-steady state conditions enabled the governing equations to be developed for a particular time step. During this time step, the properties of the air stream across the heat exchanger and that of the frost layer were assumed to be constant. Therefore, the heat and mass transfer and the frost properties for each time step could be calculated. A forward march in time results in the recalculation of these quantities based on the previous time steps.

The use of the ideal gas equation of state to describe the behavior of air and water vapor was an important assumption in describing the diffusion of the water vapor into the frost layer. Such an assumption has been used previously by O'Neal [25].

If heat conduction and mass transfer parallel to the layer of frost is neglected, then the heat and mass transfer is one dimensional. This will occur if the frost layer is thin and there are no significant axial thermal or concentration gradients.

The mass transfer potential decreases as moist air flows across the coil because, as the water vapor condenses on the coil surface, the air loses moisture. Therefore, the frost deposition is maximum along the leading edges of the coil and progressively decreases towards the back of the coil. While the model can simulate this trend, for the purposes of average heat transfer performance, an average frost thickness is calculated and used.

B. GOVERNING EQUATIONS

The problem was divided into three basic parts :

- a. Frost Layer - growth and properties
- b. Heat Exchanger - heat transfer parameters
- c. System Parameters - air flow, pressure drops and blower characteristics.

It should be noted that the above sections are very much related and need to be considered simultaneously.

Frost Layer

This section deals with the frost growth model and the variation of the frost thermal conductivity and density. These are modelled in a quasi-steady manner with respect to time using a forward marching technique.

The rate of deposition of frost can be expressed as the loss of humidity in the air as the water vapor condenses on the cold heat exchanger surface.

$$\dot{m}_f = \dot{m}_a(\omega_{a_i} - \omega_{a_o}) \quad (4.1)$$

The exit humidity is a function of the heat and mass transfer processes which occur and are dealt with in the later section on the heat exchanger.

Since it has been established that as frost forms and continues to grow, it increases in density in addition to height. Therefore, it is assumed that part of the water vapor, which converts to frost, goes to increase the frost density and the rest to increase the frost height. Such an assumption is similar to that made by Jones and Parker [19].

$$\dot{m}_f = \dot{m}_\rho + \dot{m}_\delta \quad (4.2)$$

where,

\dot{m}_ρ = the density component

\dot{m}_δ = the height component.

The frost layer was considered to be very thin, and this allowed for the assumption that the mass transfer of water vapor into the frost layer, occurred from the moist air towards the cold heat exchanger surface and not axially through the frost. In addition, the frost is a porous media and not solid like ice. The mass of water vapor diffusing through the frost layer has been given to be [17] :

$$\dot{m}_\rho = A_T D_s \left[\frac{(1 - \frac{\rho_f}{\rho_i})}{\tau_f} \right] \left(\frac{d\rho_v}{dx} \right)_s \quad (4.3)$$

The diffusion coefficient, D_s , was calculated from an empirical expression given by Eckert and Drake [39]. D_s is a function of the temperature and vapor pressure which are functions of time. The tortuosity factor, τ_f , is a measure of the mean free path of the water vapor molecules in the frost layer as compared to that in free space (with no obstructions). It is a measure of the porosity of the frost layer. The expression used for the tortuosity was that of Sanders [29] :

$$\tau_f = 1 + \left(\frac{\rho_f}{\rho_i} \right)^{0.5} \quad (4.4)$$

Other expressions exist such as the Satterfield correlation [17], but there are no data to indicate which is the best.

The last term in the right hand side of Equation 4.3, $\left(\frac{d\rho_v}{dx} \right)_s$, can be modified using the ideal gas equation and applying the chain rule of differentiation :

$$\left(\frac{d\rho_v}{dx}\right)_s = \frac{1}{RT_s} \left(\frac{dT_v}{dx}\right)_s \left[\left(\frac{dP_s}{dT}\right)_s - \frac{P_s}{T_s} \right] \quad (4.5)$$

The gradient of the saturated vapor pressure with respect to the temperature at the surface of the frost layer, $\left(\frac{dP_s}{dT}\right)_s$, can be calculated by applying the Clausius-Clapeyron equation for the case of sublimation :

$$\left(\frac{dP_s}{dT}\right)_s = \frac{i_{sv}}{T_s v_g} \quad (4.6)$$

In the above equation, the change in specific volume from gaseous to solid state has been modified to that of the gaseous state alone, since the specific volume in the gaseous state is much greater than that in the solid state.

The above expressions are substituted into Equation 4.3, and the ideal gas equation is once again applied to Equation 4.6. The resulting expression is :

$$\dot{m}_\rho = A_T D_s \left[\frac{(1 - \frac{\rho_s}{\rho_v})}{RT_s^2 \tau_f} \right] \left(\frac{i_{sv}}{v_g} - P_s \right) \left(\frac{dT_v}{dx} \right)_s \quad (4.7)$$

The only unknown quantities in the above expression are the temperature gradient of the vapor at the surface of the frost and the temperature of the frost surface. The saturated vapor pressure, P_s , is a function of the temperature at the surface of the frost.

The energy transferred to the frost surface is the sum of the heat transferred from the air to the frost layer and the latent energy of sublimation of the water vapor as it diffuses into the frost layer and solidifies. An energy balance on the frost surface yields :

$$A_T k_f \left(\frac{dT_v}{dx} \right) + \dot{m}_p i_{s,v} = \dot{m}_a Q \quad (4.8)$$

Combining Equations 4.7 and 4.8 results in the following expression for the amount of water vapor increasing the frost density :

$$\dot{m}_p = \dot{m}_a \left[\frac{\beta Q}{k_f + i_{s,v} \beta} \right] \quad (4.9)$$

where,

$$\beta = \left[\frac{P_s D_s (1 - \frac{\rho_f}{\rho_i}) (\frac{i_{s,v}}{RT_s} - 1)}{\tau_f RT_s^2} \right] \quad (4.10)$$

The frost surface temperature is still required to obtain a closed form solution. This will be determined from psychrometric and heat transfer considerations on the heat exchanger and is discussed in a later section.

Now that a complete expression for the amount of water vapor diffusing into the frost layer to increase density, has been developed, the amount of water vapor which contributes to the increase in frost height can be determined from Equations 4.1, 4.2, and 4.9. For each time step, a new value of frost density and height needs to be determined. The change in frost density is given by :

$$\Delta \rho_f = \frac{\dot{m}_p \Delta t}{A_t \delta_f} \quad (4.11)$$

This is added to the value of frost density at the previous time step to obtain the density at the current time step. Now consider the growth rate of the frost layer. The growth rate of the frost is determined from the following equation :

$$\Delta \delta_f = \frac{\dot{m}_p \Delta t}{A_t \rho_f} \quad (4.12)$$

Similar to the density, this is added to the previous frost height to get the new frost height.

If a functional relationship, F , between the frost thermal conductivity, frost density and thickness is assumed, the new thermal conductivity can be determined for the current time step.

$$k_f = F(\delta_f, \rho_f) \quad (4.13)$$

For the present model, the following relationship was assumed [9] :

$$k_f = (1.202 \times 10^{-3}) \rho_f^{0.963} \quad (4.14)$$

From Equations 4.1, 4.2, 4.9, 4.11 and 4.14, the growth of the frost can be monitored and the variation of the properties (thermal conductivity and density) can be predicted.

Heat Exchanger

The various parameters related to the performance of the heat exchanger include :

1. The Fin Efficiency, η_F
2. The Overall Heat Transfer Coefficient, U_o
3. The Enthalpies of the Air Flow (entering and leaving), i_a
4. The Enthalpy of the Frost Surface, i_f .

Each is discussed below :

Fin Efficiency, η_F

Fin efficiency is defined as the ratio of the actual heat transferred from the fin to that which would have been transferred if the entire fin had been at base temperature.

For a dry unfrosted fin, with a fin length much greater than its width, the fin efficiency can be determined from :

$$\eta_F = \frac{\tanh(m_F L)}{(m_F L)} \quad (4.15)$$

where

$$m_F = \sqrt{\left[\frac{h_a}{k_F \delta_F} \right]} \quad (4.16)$$

L is the equivalent length of the fin.

For the case of a fin with an even layer of frost, the above expression can be modified by incorporating the thermal resistance of the frost layer in the air side heat transfer coefficient.

$$h_o = \left[\frac{1}{h_a} + \frac{\delta_f}{k_f} \right]^{-1} \quad (4.17)$$

The expression for the fin efficiency, Equation 4.14, remains the same except for a modified fin parameter, $m_{F,f}$.

$$m_{F,f} = \sqrt{\left[\frac{h_o}{k_F \delta_F} \right]} \quad (4.18)$$

It should be noted that the above expression reduces to that for the dry, unfrosted case when the frost thickness reduces to zero.

The Overall Energy Transfer Coefficient, E_o

The overall energy transfer coefficient is the primary measure of the thermal performance of the heat exchanger. It is similar to the concept of a heat transfer coefficient, except in that it is based on total energy transfer and not only sensible heat transfer. This is discussed in more detail in Chapter V. The overall energy transfer coefficient can be expressed in terms of the air side heat transfer coefficient, h_a , the surface area of interest, the total surface area, A_T , (the sum of the total finned surface area and the tube surface area) and the 'surface efficiency', η_s . For the purposes of this study, the surface area of interest is the total finned surface area.

The overall energy transfer coefficient (based on fin area) is :

$$E_o = \left[\frac{A_F}{\eta_s h_a A_T} + \frac{A_F}{A_r h_r} \right] \quad (4.19)$$

where the surface efficiency of the heat exchanger is :

$$\eta_s = 1 - (1 - \eta_F) \frac{A_F}{A_T} \quad (4.20)$$

The total surface area of heat transfer is the sum of the finned area and tubes.

$$A_T = A_P + A_F \quad (4.21)$$

The above three equations can be combined into a single expression :

$$E_o = \left[\frac{1}{\left[h_o \left(\eta_F + \frac{A_F}{A_r} \right) \right]} + \frac{A_F}{A_r h_r} \right]^{-1} \quad (4.22)$$

The air side heat transfer coefficient, h_a , is a function of the Reynolds and Prandtl Numbers and the geometry of the heat exchanger. An expression for the laminar air side heat transfer coefficient for flat rectangular plate fin type heat exchangers was adapted from a correlation suggested by Gray and Webb [40] :

$$h_a = \dot{G}_f c_p Pr^{0.667} X_j R_j \quad (4.23)$$

where,

$$X_j = 0.14 Re^{-0.328} \left(\frac{S_t}{W_t} \right)^{-0.502} \left(\frac{S}{D_s} \right)^{0.0312} \quad (4.24)$$

$$R_j = 0.991 \left[2.24 Re^{-0.092} \left(\frac{N_t}{4} \right)^{-0.031} \right]^{0.607(4-N_t)} \quad (4.25)$$

- \dot{G}_f = Mass velocity based on free flow area
- S_t, W_t = Tube spacings
- S = Fin spacing
- D_s = Tube diameter
- N_t = Number of tube Rows (less than 4)

The values of Reynolds Number and Prandtl Numbers are functions of the properties of the air : specific heat, viscosity, density, temperature and velocity. These values were calculated from simple curve fits adapted from data given by

Incropera and Dewitt [41].

The above correlation was developed for heat exchangers operating under dry conditions and not for frosting conditions. However, in the case of frost formation there is a perceivable change in geometry in that the free flow area constantly changes with an increasing frost layer. This leads to a decreased fin spacing and affects the correlation. Hence a modified correlation needed to be developed in order to obtain a better correlation.

A possible correction was in one of the exponents of X_j :

$$X_j = 0.14Re^{-0.326} \left(\frac{S_t}{W_t} \right)^{-0.502} \left(\frac{S}{D_s} \right)^c \quad (4.26)$$

The exponent, 'c', can be varied to account for the variable fin spacing and the particular environmental conditions. It must be clarified that such a correction needs to be justified by experimentation before it can be generalized. It is beyond the scope of the present study to justify such a modification, although it appears that such a change would present a better correlation with the experimental results.

For the purposes of the present model, the only change made in the above correlation is to account for the constantly changing fin spacing, S , due to the increasing frost layer.

Air and Frost Surface Enthalpies

Standardized psychrometric relations for moist air are used to determine the enthalpies of the air as it approaches the heat exchanger. To achieve a convergent

and numerically stable solution, the heat exchanger coil is divided into a number of elemental sections. The exit properties from a particular elemental section form the inlet properties for the next section. The inherent advantage of such a solution is that the variation in the height of the frost along the length of the heat exchanger can be simulated. The exact number of elements is determined from numerical convergence and stability. The following analysis can be applied progressively from one element to the next.

In a typical evaporator coil in a heat pump or air conditioner, the refrigerant temperature is approximately constant. Therefore the tube surface temperature is almost constant. If one assumes that the enthalpy at the tube surface can be approximated by the enthalpy of saturated air at the refrigerant temperature, the following energy balance can be derived for the air flowing across an elemental section of the heat exchanger* :

$$i_{a_r} = i_{a_i} - (i_{a_i} - i_r) \left[1 - e^{-\frac{E_o A_F}{m_a c_p t}} \right] \quad (4.27)$$

The derivation for the above expression is in Appendix A.

The enthalpy of the air at the frost surface for a particular elemental section can be determined by placing :

$$i_{f_s} = i_a - (i_a - i_r) \left[\frac{E_o A_F}{h_a A_t} \right] \quad (4.28)$$

* This analysis is for a counterflow heat exchanger. Similar expressions can be derived for other geometries.

Since the above set of equations is applicable at any location along the heat exchanger surface, the enthalpy of the air as it finally leaves the heat exchanger can be determined. It is also reasonable to assume that the air at the frost surface is saturated and the frost surface temperature can be found from standard psychrometric relations.

The heat transfer for each element can be determined from a LMED (Logarithmic Mean Enthalpy Difference) in the following manner :

$$Q = \frac{E_o A_F}{c_{p_a}} \left[\frac{(i_{a_i} - i_{a_e})}{\ln \left[\frac{i_{a_i} - i_r}{i_{a_e} - i_r} \right]} \right] \quad (4.29)$$

The total heat transfer can be determined by taking a sum of the above elemental heat transfer values.

Air Temperatures and Humidities

In order to determine the temperature of the air at any particular elemental section it is assumed that there is a proportional relationship between enthalpy and air temperature :

$$\left[\frac{T_{ae} - T_{ai}}{T_{ai} - T_s} \right] = \left[\frac{i_{ae} - i_{ai}}{i_{ai} - i_s} \right] \quad (4.30)$$

From the above expression, the temperature of the air leaving the elemental section can be determined. Once the temperature and enthalpy of the air at any given element are known, the humidity of the air can be found from :

$$\omega_a = \frac{i_a - c_{pd}T_a}{i_{fg} + c_{pw}T_a} \quad (4.31)$$

where,

c_{pd} = specific heat of dry air

c_{pw} = specific heat of moist and saturated air

Therefore, from the above elemental analysis, it is now possible to determine the progressive values of air temperature, humidity, enthalpy, frost height and frost surface temperature, as the moist air passes through the heat exchanger. This is achieved by the simultaneous solution of Equations 4.1 through 4.32. However, for simplicity, certain parameters such as heat transfer coefficients and pressure drops (as explained in the following section) utilize an average value of the frost height.

System Parameters

As the frost forms on the fins and tubes, it blocks off the free flow area. This results in an increased pressure drop, ΔP_{HX} across the heat exchanger coil. From classical heat exchanger theory [14], this pressure drop can be expressed in the following manner :

$$\Delta P_{HX} = \frac{(\rho_a V_a^2)}{2} \left[f \cdot \frac{A_t}{A_{free}} \right] \quad (4.32)$$

The air flow rate supplied by the blower depends on the pressure characteristics of the blower in the system :

$$\Delta P_B = a_0 + a_1 \dot{V} + a_2 \dot{V}^2 + a_3 \dot{V}^3 \quad (4.33)$$

The total pressure drop in the system can be expressed as a sum of the pressure drop across the heat exchanger, ΔP_{HX} and the remaining components of the system (elbow losses etc.), ΔP_o .

$$\Delta P_T = \Delta P_{HX} + \Delta P_o \quad (4.34)$$

Therefore, as the pressure drop across the heat exchanger increases, so does the total pressure drop in the system, ΔP_T . This total pressure drop is what is experienced by the blower and in turn, affects the air flow rate in the system. Typically, with an increase in pressure, the air flow rate drops.

The velocity of the air flowing through the heat exchanger is a function of the air flow rate, the free flow area and the air density.

$$V_a = \frac{\dot{V}}{\rho_a A_{free}} \quad (4.35)$$

The Reynolds Number can be determined based on the mass flow rate, the free flow area and the viscosity of the air. The Prandtl Number is evaluated at a bulk mean temperature which is the mean of the air temperature and the frost surface temperature.

The free flow area is a function of the frost thickness, the fin density (spacing), number and spacing of tubes and overall heat exchanger geometry. If the frost is allowed to grow, it will finally block off the entire heat exchanger. The

variation of the free flow area with time is determined by considering the additional blockage resulting from the growth of the frost layer in the previous time step, and subtracting that from the previous value of free flow area.

This completes the mathematical formulation of the model. The three sections on frost growth, heat exchanger characteristics and system pressure parameters need to be solved simultaneously. A computer program has been written and successfully executed.

C. NON-DIMENSIONAL DESIGN PARAMETERS

This section describes the development of three non-dimensional variables for use in evaluating the effects of frosting on finned tube heat exchangers :

1. NTU (Number of Transfer Units)
2. ϵ (Heat Exchanger Effectiveness), and
3. Non-dimensional analysis of the fins in terms of efficiency, temperature distribution and heat transfer.

NTU - Number of Transfer Units

The number of transfer units, NTU, is a dimensionless indicator of the performance of the heat exchanger. The higher the NTU's, the better the performance of the heat exchanger. The overall heat transfer coefficient, U_o , accounts for the frost growth and can be used directly in the standard expression for NTU. The following expression for an NTU is defined for a heat exchanger :

$$NTU = \frac{U_o A_F}{\rho \dot{V} C_{p_{min}}} \quad (4.36)$$

Since the evaporator coils can be considered to effectively have an infinite refrigerant mass flow rate, it is assumed that the mass capacity of the air is much less than that of the refrigerant. In such a case, the above expression can be rewritten as :

$$NTU = \frac{U_o A_F}{\rho \dot{V} C_{p_{air}}} \quad (4.37)$$

Since both, U_o and \dot{V}_a are strong functions of the frost growth, the effects of the frost are manifested in the expression for NTUs.

Heat Exchanger Effectiveness : ϵ

Another measure of expressing heat exchanger performance is its effectiveness, ϵ . If the mass capacity of the air is less than that of the refrigerant, the following expression can be derived for a counterflow heat exchanger in the presence of frosting on its surfaces is given as :

$$\epsilon = \left[\frac{1 - e^{-NTU(1 - \frac{\rho \dot{V} C_{p_{air}}}{\rho \dot{V} C_{p_r}})}}}{1 - \left(\frac{\rho \dot{V} C_{p_{air}}}{\rho \dot{V} C_{p_r}}\right) (e^{-NTU(1 - \frac{\rho \dot{V} C_{p_{air}}}{\rho \dot{V} C_{p_r}})})} \right] \quad (4.38)$$

If the mass flow rate of the refrigerant is much greater than that of the air, the above expression reduces to :

$$\epsilon = (1 - e^{-NTU}) \quad (4.39)$$

As the frost grows, U_o decreases, the NTUs decrease, and hence the effectiveness also decreases. A very common way to express heat exchanger performance is with NTU- ϵ charts. From the above analysis, such charts as a function of frost growth could be easily developed.

The above mentioned methodology of presenting the detrimental effects of frost growth in standardized non-dimensional parameters has not been presented to date in the literature. With proper usage of this model and the related analysis, it is possible to develop a full range of NTU- ϵ charts for a variety of geometries and conditions. This would prove to be a very useful design tool for designers and manufacturers.

Non-Dimensional Analysis of Fin Performance

The following expressions which represent the temperature distribution along the fin length, the heat transfer from the fin surface and the fin efficiency, all in a non-dimensional manner can be derived* :

The temperature distribution along the length of the fin :

$$\theta(x^*) = \frac{\text{Cosh}\left[m_f(1-x^*)\right]}{\text{Cosh}(m_f)} \quad (4.40)$$

where, m_f is the frosted fin parameter :

$$m_f^2 = H_F \times H_f \quad (4.41)$$

* These expressions are only for rectangular plate fins but can be applied to other fin geometries with appropriate modifications

and the dimensionless heat transfer coefficient for the frost, H_f :

$$H_f = \left[\frac{2k^*}{(2k^* + Bi_F \delta_f^*)} \right] \quad (4.42)$$

and the dimensionless fin heat transfer parameter H_F

$$H_F = \frac{Bi}{\delta_F^*} \quad (4.43)$$

For no frost, $\delta_f = 0$ and H_f reduces to unity.

The *dimensionless heat transfer rate* at the base of the fin can be expressed as a ratio of the heat transfer with frost as to that without frost :

$$q^* = \frac{m_f \text{Tanh}(m_f)}{m_o \text{Tanh}(m_o)} \quad (4.44)$$

where,

$$m_o = m_f \quad \text{when} \quad \delta_f = 0 \quad (4.45)$$

Applying the definition of fin efficiency, η_F :

$$\eta_F = \frac{\text{Tanh}(m_f)}{m_f} \quad (4.46)$$

We can define a *Fin Efficiency Ratio*, E , to be the ratio of the fin efficiency of the frosted fin to that of the unfrosted fin :

$$E = \frac{\eta_F}{\eta_o} \quad (4.47)$$

Detailed derivations of the above expressions are given in Appendix B.

In all the above expressions, the fin parameters can be reduced to that of the case with no frost by setting the dimensionless frost thickness, δ_f^* , to zero.

Using the above expressions, (Equations 4.40 through 4.47) the following non-dimensional charts can be developed :

1. Dimensionless temperature distribution as a function of dimensionless length for varying dimensionless frost thicknesses. (θ vs. x^* for varying δ_f^*).
2. Dimensionless heat transfer rates as a function of dimensionless frost thicknesses for varying dimensionless fin heat transfer coefficients. (q^* vs. δ_f^* for varying H_F).
3. Fin Efficiency Ratio as a function of dimensionless frost thickness for varying dimensionless fin heat transfer coefficients. (E vs. δ_f^* for varying H_F).

The overall mathematical model considers the variation of frost properties (conductivity and height) in time and these updated values can be used in the above analysis of fin performance. This would give a better estimate of the process, rather than considering an average value for frost thermal conductivity.

The above non-dimensional analysis should prove to be useful to designers since a methodology has been developed by which design charts can be developed for a variety of cases. However, any model is of limited value unless it can be shown to be valid with respect to experimental results. The comparison of this model with appropriate results from the experimental part of this investigation is done in Chapter VI.

D. MODEL APPLICATION AND EXPECTED RESULTS

The above equations can now be solved simultaneously for the solution. The large number of variables coupled with the complexity of the problem necessitate the use of a computer for a solution.

It is difficult to directly compare the results obtained from the model to what is available in the literature. This is mainly due to a lack of complete information about the exact experimental conditions of previous studies. To achieve a somewhat satisfactory comparison, a great many assumptions about the previous investigations would need to be made. Therefore, only qualitative comparisons are being made. However, since the present study is also experimental in nature, a complete comparison and validation process can be done .

Wherever appropriate, the similarities with available literature have been cited in support of the validity of the model. In cases where there are differences with the available literature, possible reasons for the inability of the model to predict the correct trends are also stated.

Figures 4.1 through 4.21 reflect the trends as established by the model under a variety of conditions : air humidity, air temperature, air flow and refrigerant temperatures. These trends are discussed briefly in the present section.

In addition, the model in its present form is applicable only for rectangular plate fins. Other fin geometries are more complex and a more accurate geometrical formulation (in terms of free flow area, total heat transfer surface area and other parameters) is beyond the scope of the present study.

Frost Growth Model

As discussed earlier, the frost growth model involves a variety of assumptions. One of the important assumptions was that part of the water vapor, which converts to frost goes to increase the frost density and the rest to increase the frost height. In addition, the model requires various inputs such as the heat exchanger geometry, environmental conditions, initial frost height and initial frost density. Figures 4.1 and 4.2 show the variation of frost density and frost height with time for different starting values of density. Both the frost density and frost height tend to converge reasonably fast.

Ideally the initial frost height should be as close to zero as possible since at time, $t = 0$, there is no frost. The lowest possible initial frost height that would lead to a numerically stable and convergent solution was found to be 2×10^{-4} inches. By a similar token, an initial frost density of 3.00 lb/ft^3 was found to have the maximum stability.

Effects of Humidity

A number of computer simulations were performed to determine the expected trends of humidity on the following parameters :

1. Frost accumulation,
2. Average frost height,
3. Pressure drop,
4. Overall energy transfer coefficient, and
5. Enthalpy drop

A higher humidity leads to more frost mass and consequently a higher frost

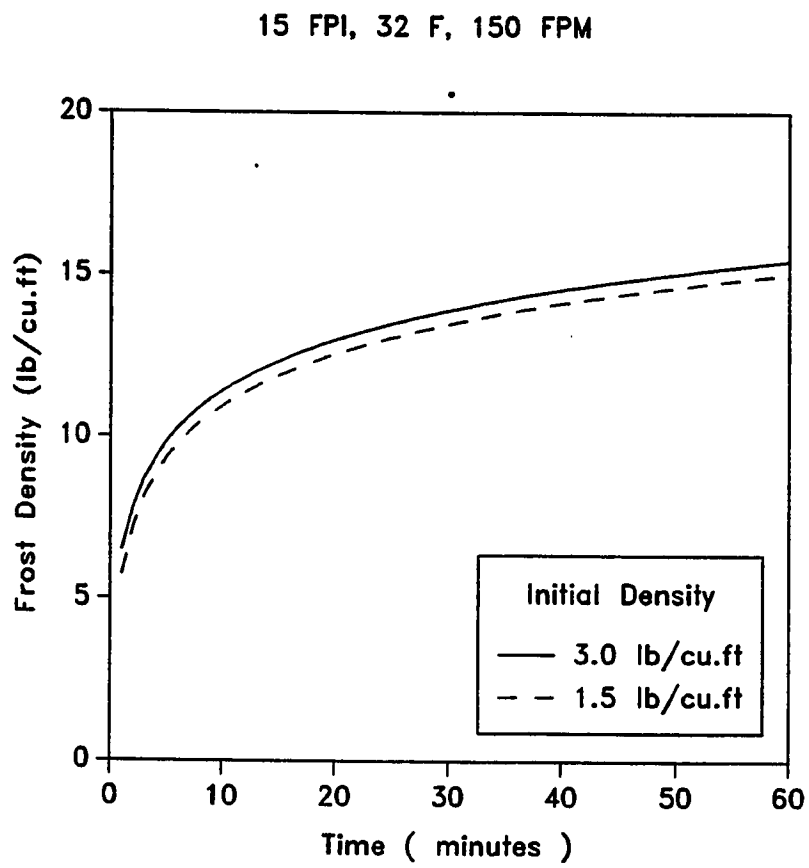
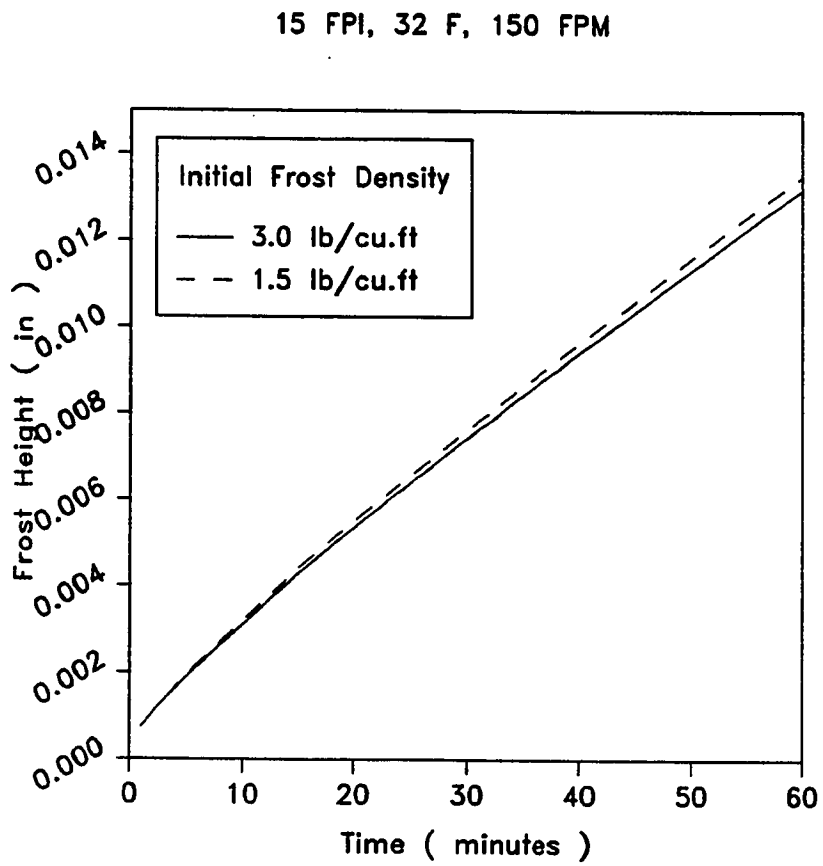


Figure 4.1 Convergence of Frost Densities



**Figure 4.2 Frost Growth Patterns for Different
Initial Frost Densities**

height. This is shown in Figures 4.3 and 4.4 respectively. However, the relative (proportional) increase of the mass accumulate is more than that of the frost height because part of the moisture goes to increase frost density and the rest goes to increase the frost height. Trends similar to this have been widely reported in the literature by Gatchilov and Ivanova [35] and Stoecker [31,32]

The pressure drop across the coil for the different humidities is shown in Figure 4.5. The rise in pressure drop is gradual at first, but as more frost accumulates, the slope becomes steeper. As expected, the pressure drop for the higher humidity is greater due to more frost and less free flow area. A similar trend is what has been reported in the literature by many including Gatchilov and Ivanova [35].

The coefficient, E_o , begins to decrease monotonically with time as frost accumulates. When the humidity of the approaching air is increased, the energy transfer coefficient, E_o , decreases more rapidly (Figure 4.6). This is because of the additional frost layer which insulates the heat exchanger coil. Almost all previous investigators have reported a slight increase in the heat transfer coefficient as the frost starts to form followed by a drop. The reasons suggested for this behavior are that, initially the frost surface results in an increased heat transfer surface area and a higher surface roughness which increases the heat transfer rate; however, later, the frost insulates the cold heat exchange surface from the air resulting in a drop in performance.

The model is unable to provide for such an initial increase in the energy transfer coefficient. E_o is a strong function of the air-side heat transfer coefficient, h_a , and there are insufficient data which give such information on h_a under frosting

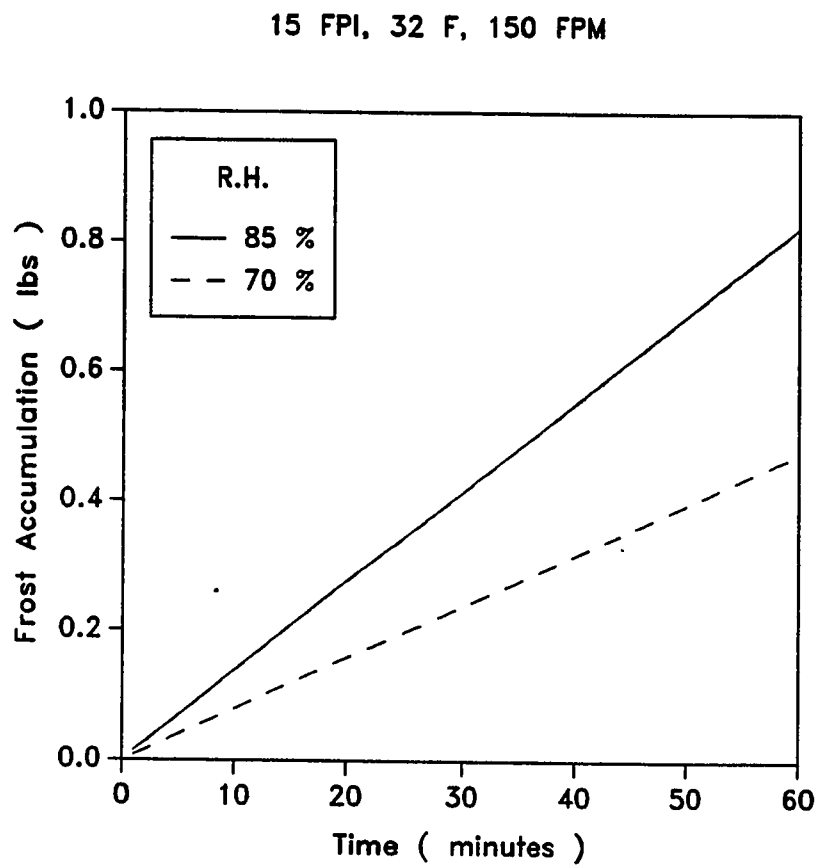


Figure 4.3 Effect of Humidity on Frost Accumulate

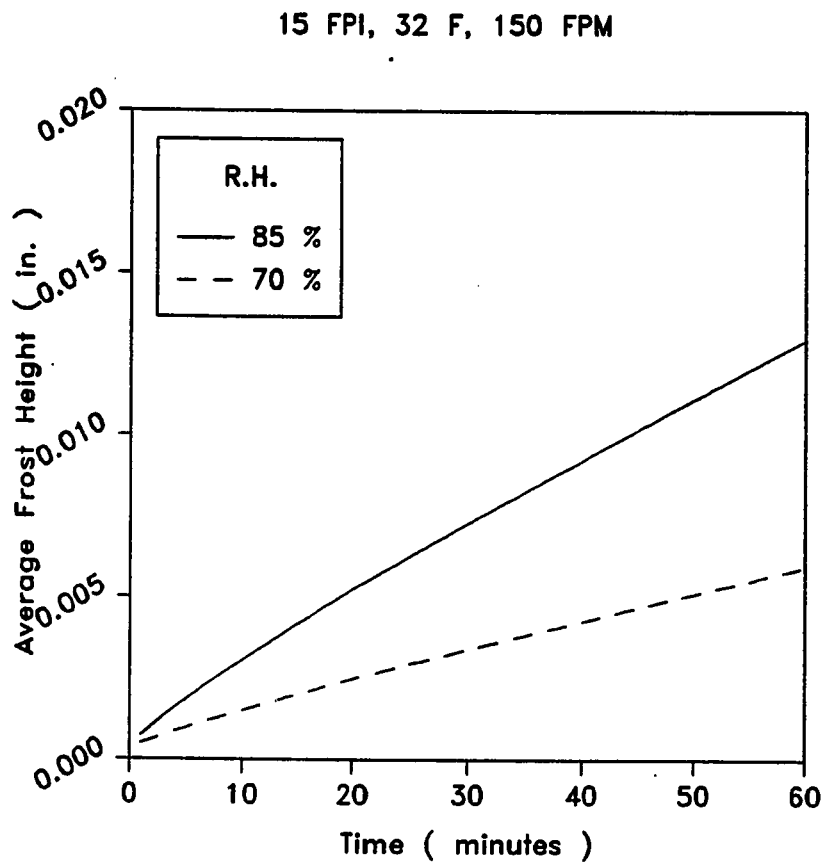


Figure 4.4 Effect of Humidity on Frost Height

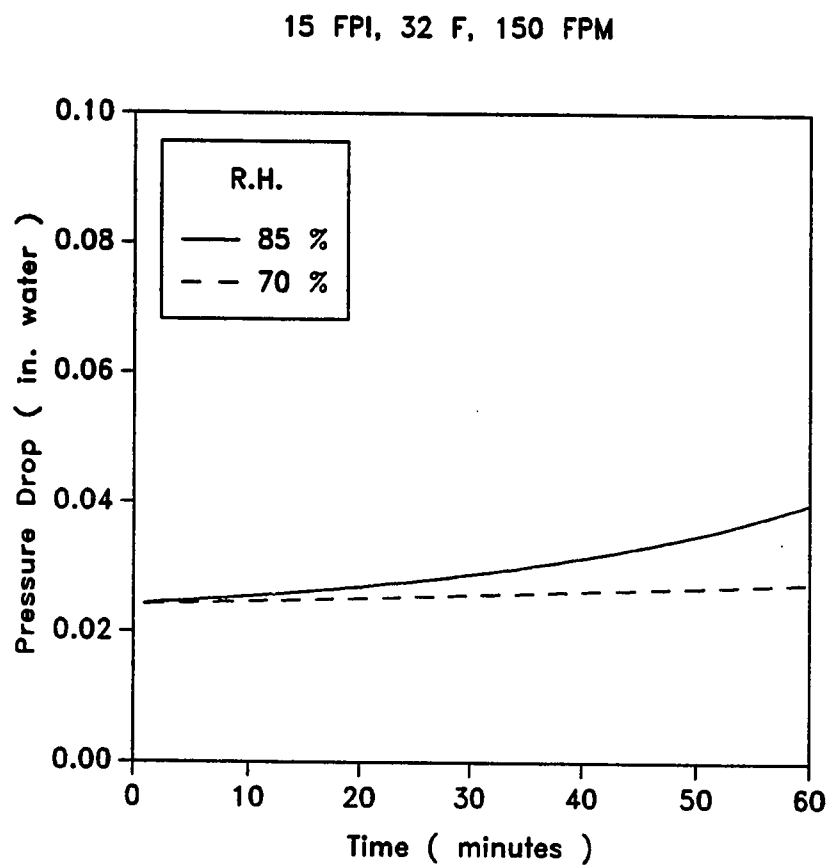


Figure 4.5 Effect of Humidity on Pressure Drop Across the Coils

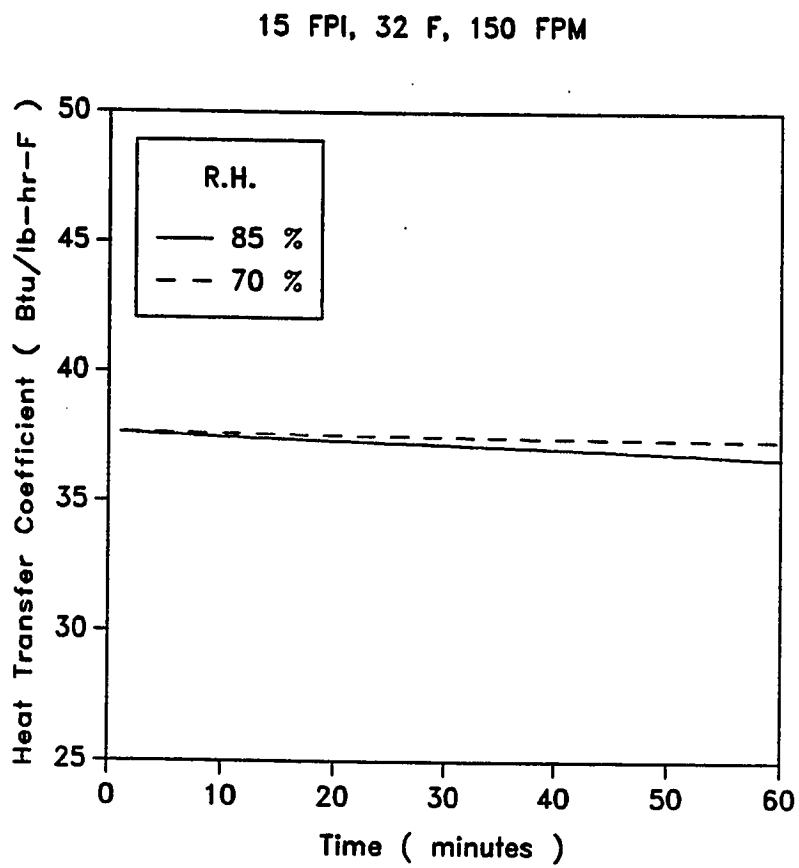


Figure 4.6 Effect of Humidity on Energy Transfer Coefficient

conditions. Data and correlations do exist for turbulent and transition regimes of flow [17,25], but not for laminar flow. Furthermore these data are only for more simple geometries such as flat plates or cylinders and not finned tube heat exchangers.

Therefore, the model is unable to reflect the initial increase in the energy transfer coefficient as observed from experiments. However, the general trends of a higher coefficient for a higher humidity are similar to that reported in the literature.

Figure 4.7 shows the effect of different humidities on the total energy transfer (enthalpy) per unit time across the heat exchanger. A higher humidity translates into a higher latent energy transfer. Therefore the enthalpy drop across the coil increases. As expected, with the onset of frost growth, the frost forms an insulating layer and the overall energy transfer decreases with time more rapidly at higher humidities.

Effect of Fin Density

When the fin density is increased, two effects occur :

1. An increase in heat transfer surface area, and
2. A decrease in the free flow area

The effects of increasing the fin spacing from 14 fins per inch to 20 fins per inch are shown in Figures 4.8 through 4.10. The three parameters of interest are :

1. Frost growth
2. Overall energy transfer coefficient, and

15 FPI, 32 F, 150 FPM

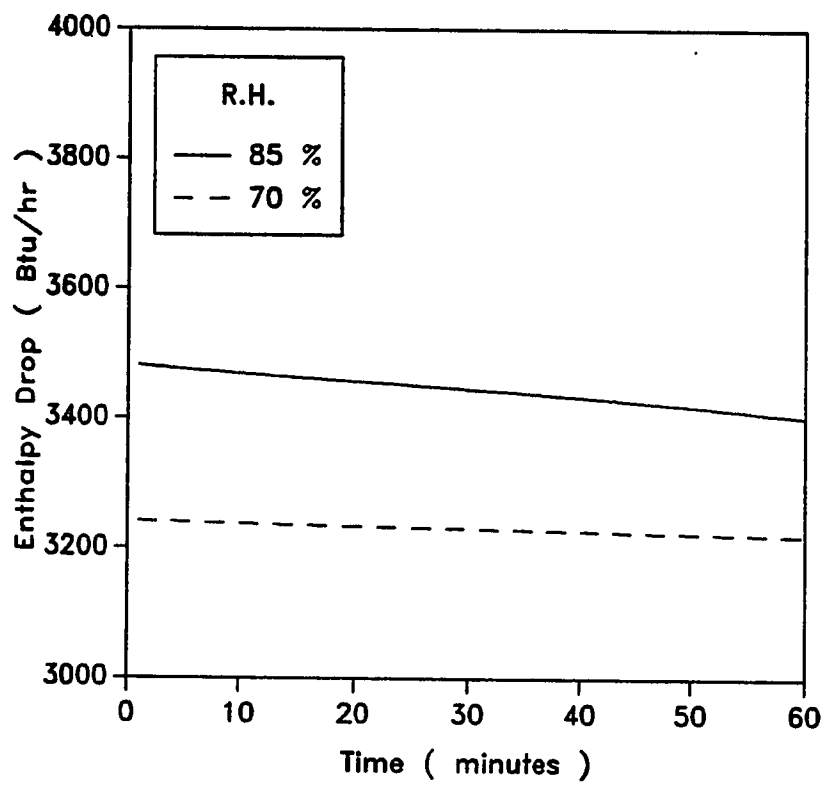


Figure 4.7 Effect of Humidity on Enthalpy Drop

3. Pressure drop across the coils

The frost growth patterns are seen in Figure 4.8. Under the same environmental conditions, there is more frost growth for the heat exchanger with a smaller fin spacing because of an increase in overall heat and mass transfer surface area. Similar trends have been reported by Stoecker [31,32].

The energy transfer coefficient increases with a decreased fin spacing. The reasons for such an increase in E_o are attributed to the increased heat transfer surface area and the increased latent energy transfer due to more frost accumulation. (Figure 4.9). As explained in the previous section, the trends are monotonically decreasing, unlike what has been reported in literature.

The pressure drop for the heat exchanger with a denser fin pattern (smaller fin spacing) is greater than the one with a larger fin spacing because of the decreased free flow area for the coil with a denser fin pattern. The larger pressure drop is further compounded by the frost accumulation, which causes the free flow area to decrease at a more rapid rate (Figure 4.10). Similar trends have been reported in literature by Stoecker [31,32].

Effect of Face Velocity

The effects of face velocity of the air approaching the heat exchangers are shown in Figures 4.11 through 4.13. A change in the face velocity has a direct effect on the Reynolds Number and hence the heat and mass transfer characteristics of the problem. The air-side heat transfer coefficient and the mass transfer characteristics increase due to a change in moisture content of the air. The three parameters of most interest which are discussed here are :

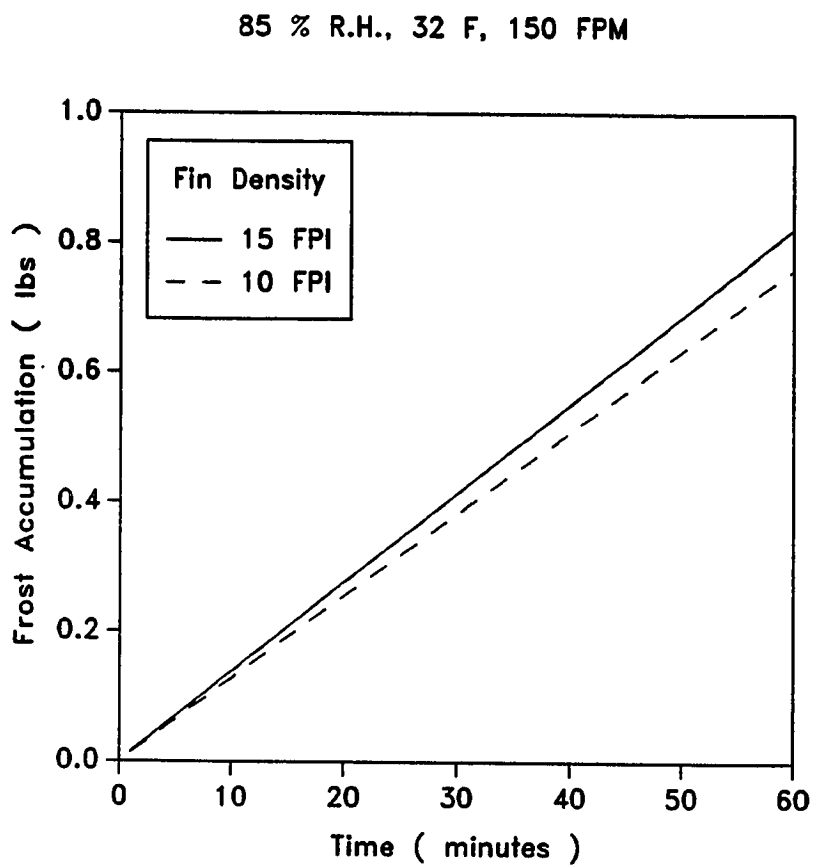


Figure 4.8 Effect of Fin Density on Frost Height

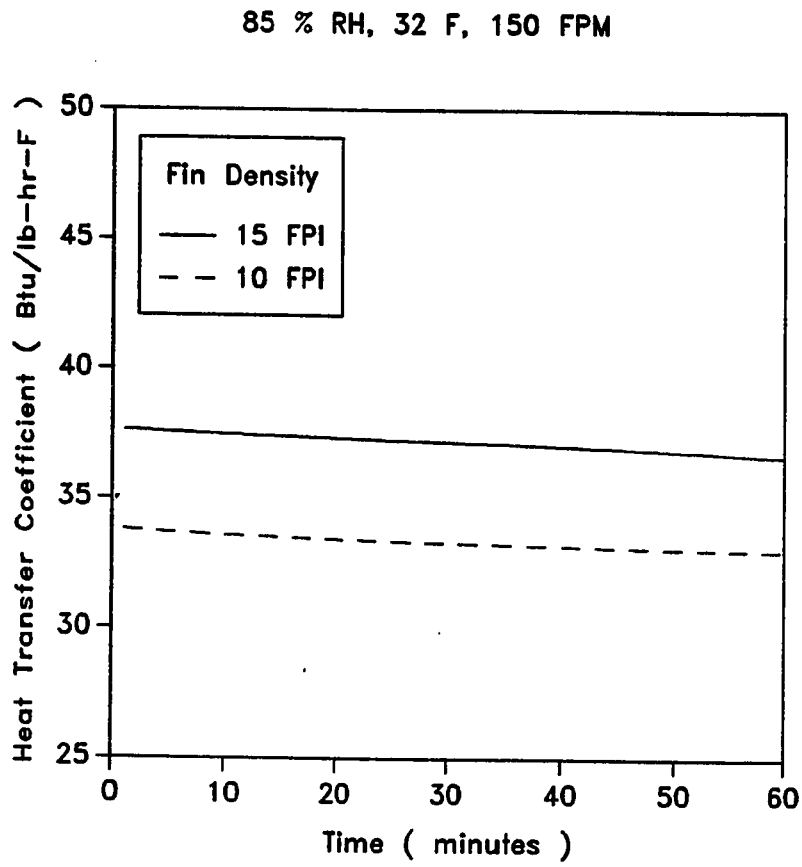


Figure 4.9 Effect of Fin Density on Energy Transfer Coefficient

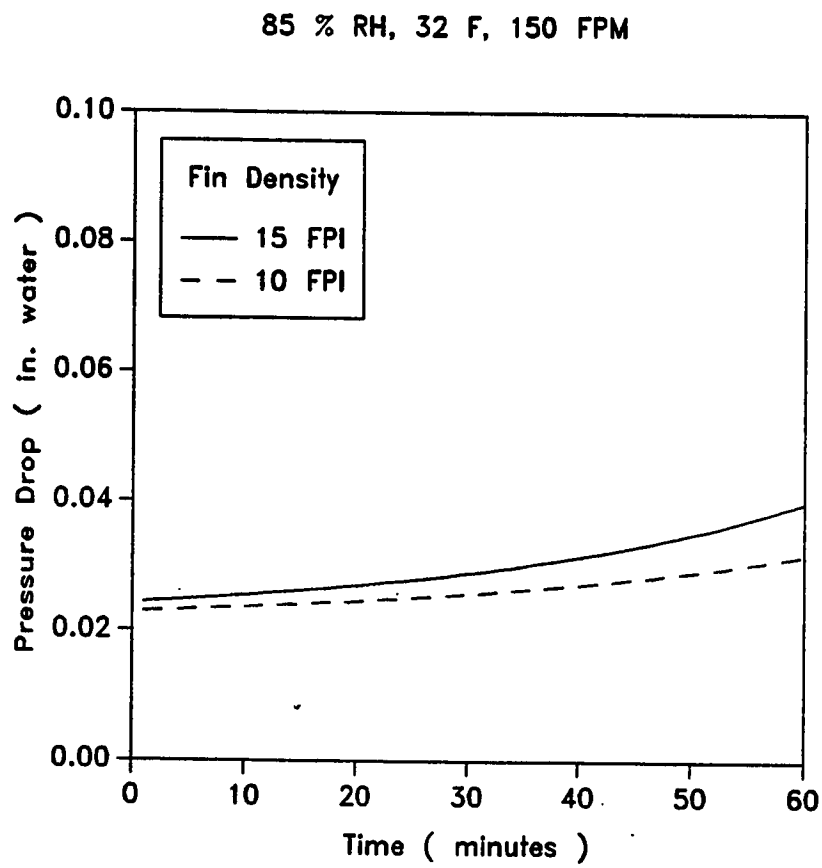


Figure 4.10 Effect of Fin Density on Pressure Drop Across the Coils

1. Frost growth (height),
2. Overall energy transfer coefficient, and
3. Pressure drop across the coils

The frost growth is more rapid at a higher face velocity (Figure 4.11). Frost growth is a strong function of the amount of moisture in the air, and the amount of moisture being carried by the air is much more at a higher velocity. In addition, the heat and mass transfer coefficients increases with velocity. The air-side heat transfer coefficient increases with velocity, and produces an increase in the overall energy transfer coefficient. (Figure 4.12)

Figure 4.13 shows the effect of velocity on the pressure drop. The pressure drop increases with velocity because it is directly a function of the mass velocity. In addition, with a higher rate of frost growth, the blockage effect has a compounding effect, causing a more rapid rate of pressure rise across the coil.

Effect of Refrigerant Temperature

Lowering the refrigerant temperature leads to an increased enthalpy potential between the refrigerant and the air which increases the heat and mass transfer (Figures 4.14 and 4.15). The two parameters which reflect this heat and mass transfer processes are :

1. Frost growth (height), and
2. Enthalpy drop (total energy transfer)

With an increased mass transfer potential, a lower refrigerant temperature leads to an increased frost accumulation and hence frost height (Figure 4.14).

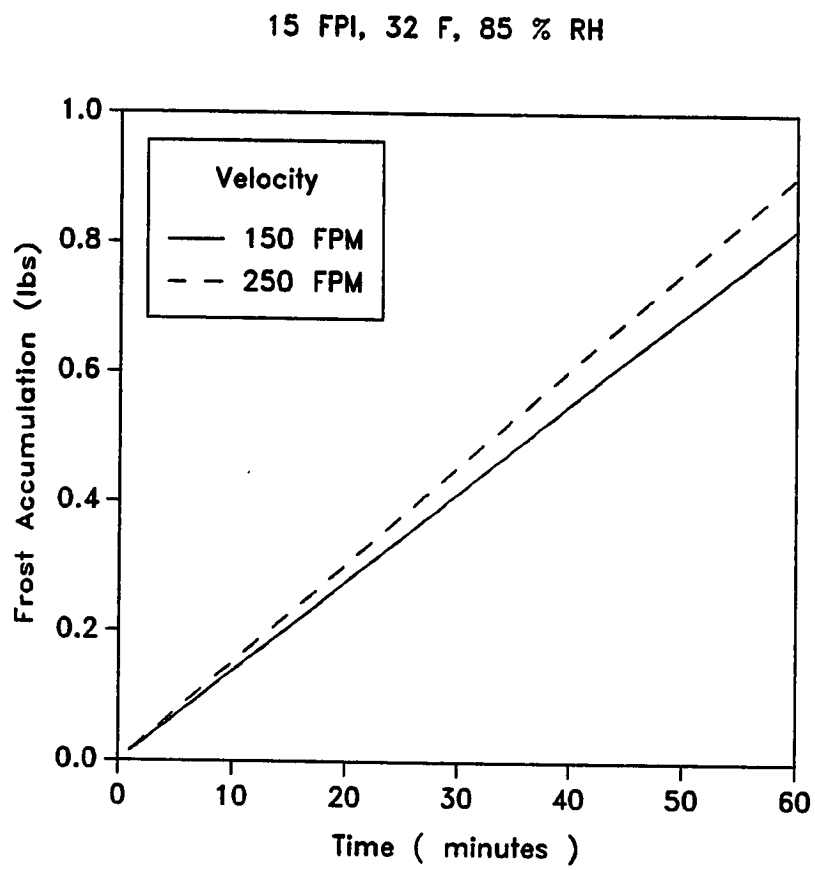


Figure 4.11 Effect of Face Velocity on Frost Height

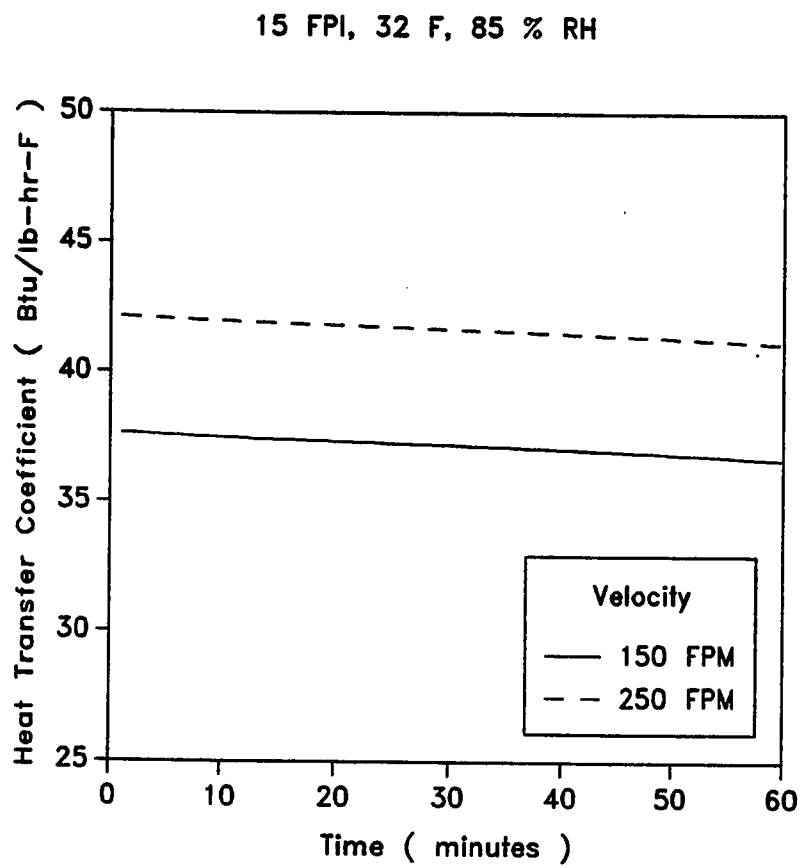


Figure 4.12 Effect of Face Velocity on Energy Transfer Coefficient

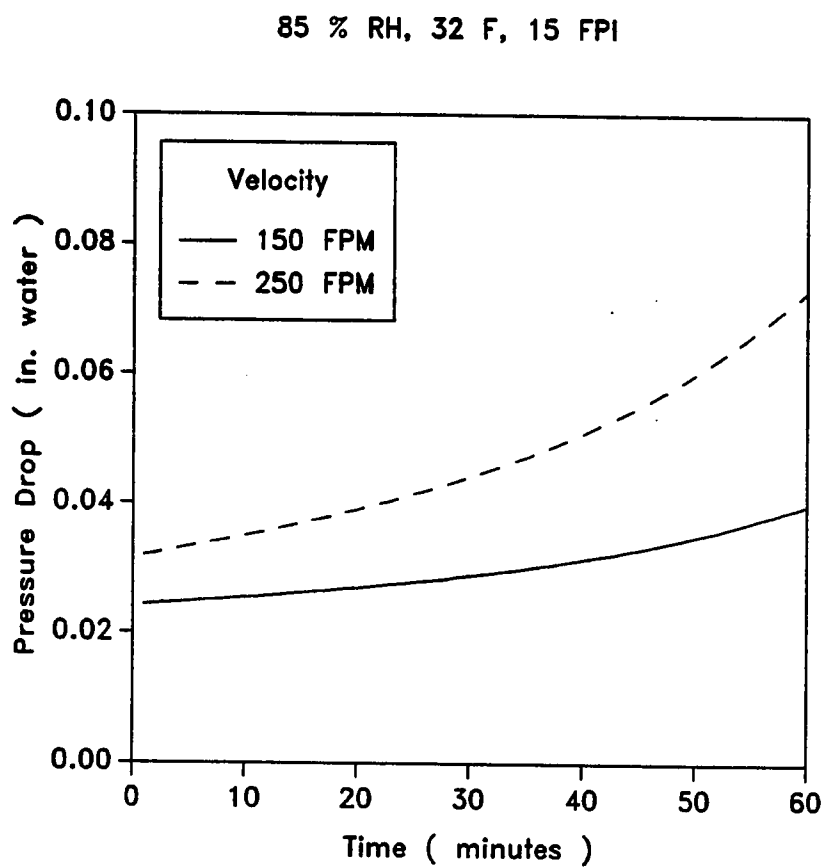


Figure 4.13 Effect of Face Velocity on Pressure Drop across the Coils

Figure 4.15 shows that the overall enthalpy drop (per unit time) also increases because of the increased thermal potential (sensible energy) as well the mass transfer potential (latent energy).

Non-Dimensional Parameters

The model also predicts a variety of non-dimensional parameters such as a Dimensionless Energy Transfer Coefficient, Effectiveness, Number of Transfer Units (NTU), and Dimensionless Fin Analysis. Figures 4.16 through 4.18 are a sample of the type of results which can be obtained. These are :

1. Effectiveness as a function of Fin Spacing, and
2. Number of Transfer Units (NTU) as a function of Face Velocity
3. Dimensionless Fin Analysis (Heat Transfer vs. Frost Height)

The effectiveness of the heat exchanger increases with fin density because the effectiveness is a strong function of the number of transfer units (NTU)(Figure 4.16) . A higher surface area results in a higher energy transfer coefficient as well as contributes to a higher NTU. The overall decreasing trend of the overall energy transfer coefficient, E_o results in a general decreasing trend for the effectiveness.

The number of transfer units (NTU) of the heat exchanger decreases with an increase in face velocity (Figure 4.17). The heat transfer due to the higher velocity is not in the same proportion as the increase in the mass flow rate across the heat exchanger.

$$NTU = \frac{U_o A_F}{\rho v C_{p_{air}}} \quad (4.37)$$

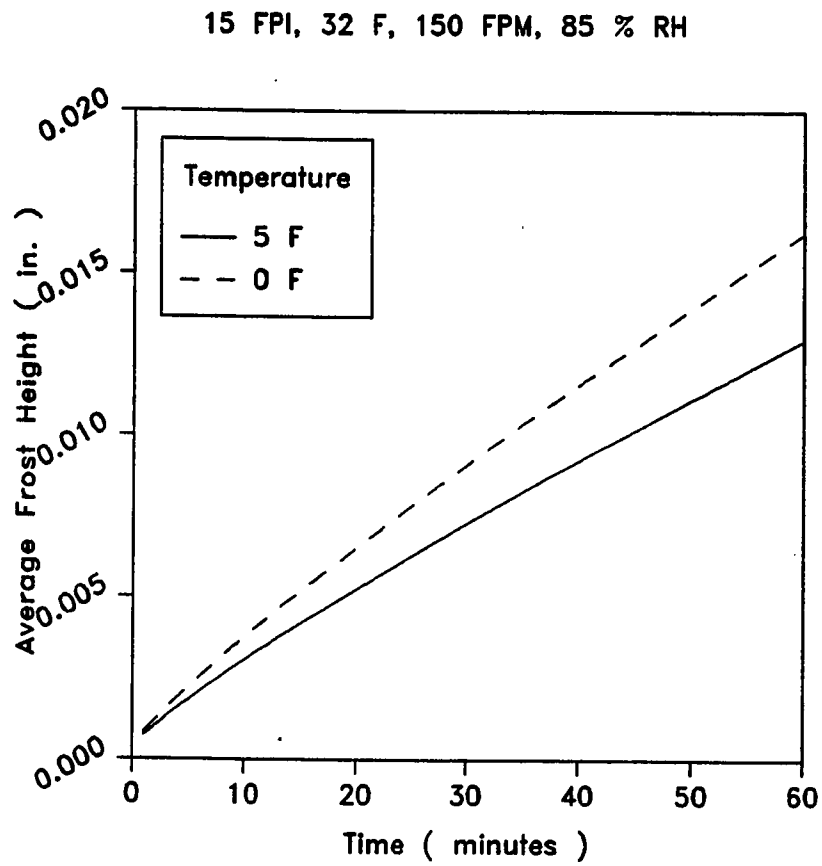


Figure 4.14 Effect of Refrigerant Temperature on Frost Height

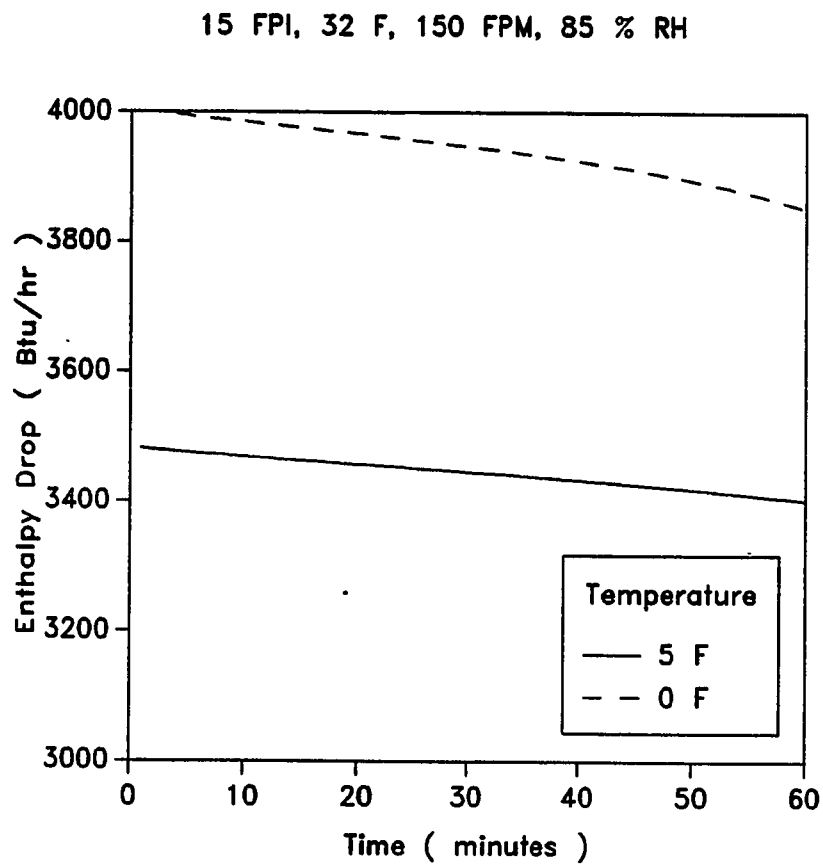


Figure 4.15 Effect of Refrigerant Temperature on Enthalpy Drop

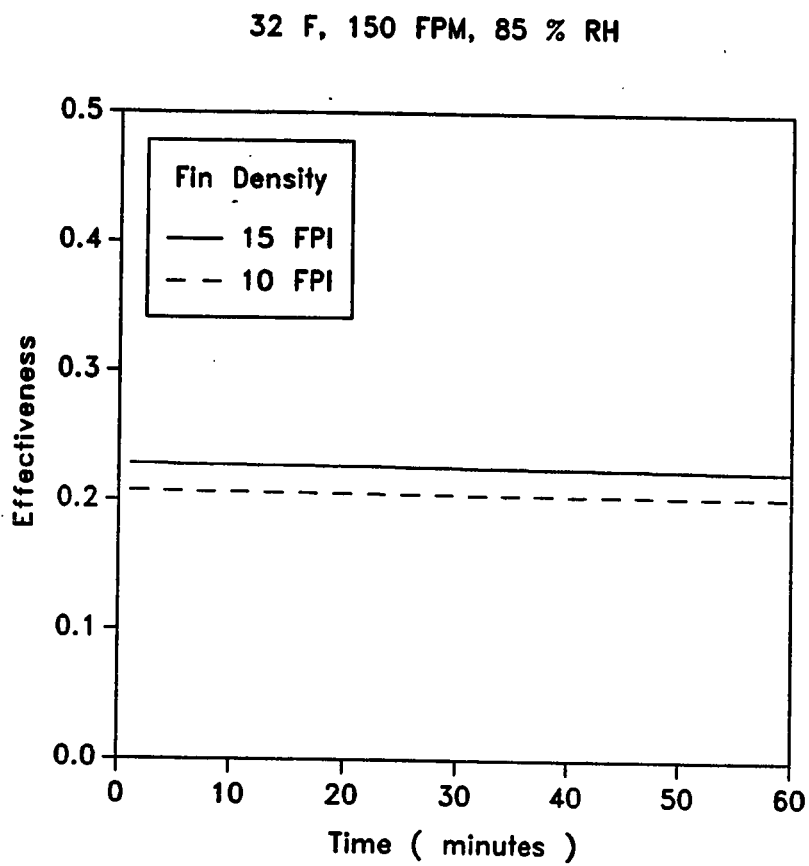


Figure 4.16 Effectiveness as a Function of Fin Density

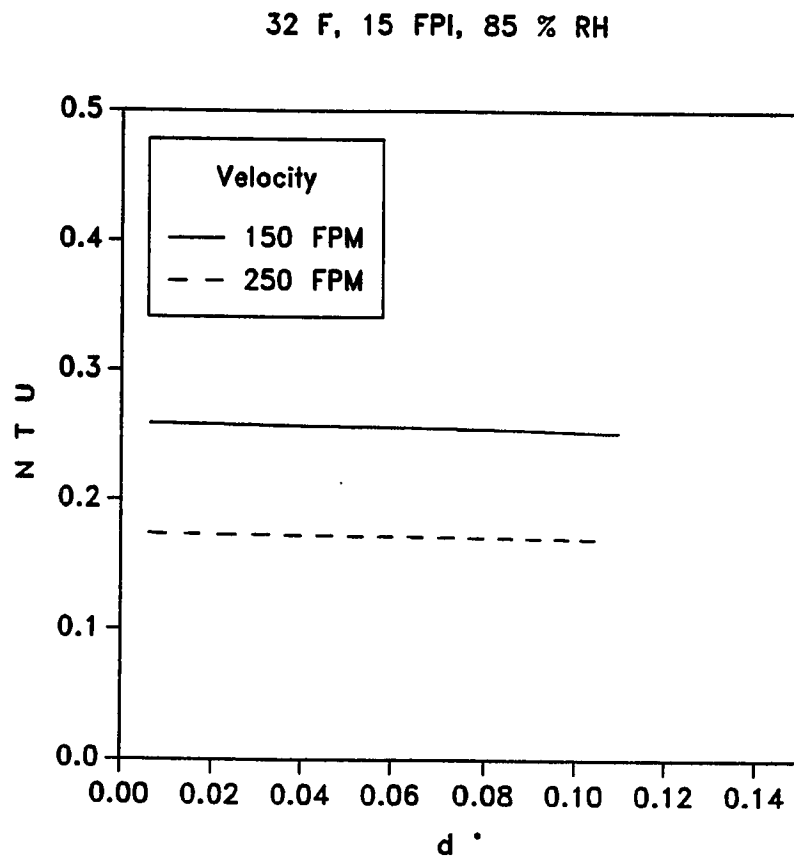


Figure 4.17 Number of Transfer Units as a Function of Face Velocity

The monotonically decreasing trend seen for the NTU's is a direct consequence of the behavior of the overall energy transfer coefficient, E_o .

The dimensionless heat transfer from the fin, q^* , is plotted as a function of the dimensionless frost thickness, δ^* (Figure 4.18). This is just a sample of the various dimensionless variables which can be obtained from the fin analysis.

Other Results

The effect of a leading edge in terms of frost growth, enthalpy of the air and frost surface temperatures can also be determined from the model. Figures 4.19 through 4.21 show this leading edge effect as a percentage of the heat exchanger length for two different times : 15 minutes and 45 minutes.

It is seen in Figure 4.19 that the frost height is maximum at the initial sections of the heat exchanger and gradually decreases (exponentially) towards the back of the coil . The driving potential for the frost growth is the moisture content of the air passing over a particular section of the heat exchanger. This moisture content gradually decreases as it passes over the heat exchanger, dumping some of the water vapor on the previous sections of the heat exchanger. Therefore, the driving force decreases, resulting in what has been termed as a leading edge effect.

The enthalpy of the air passing over the heat exchanger sections also decreases as it passes over the heat exchanger because the air is losing enthalpy to the refrigerant as it passes over the coil (Figure 4.20).

The model also can estimate the frost surface temperatures. This is shown

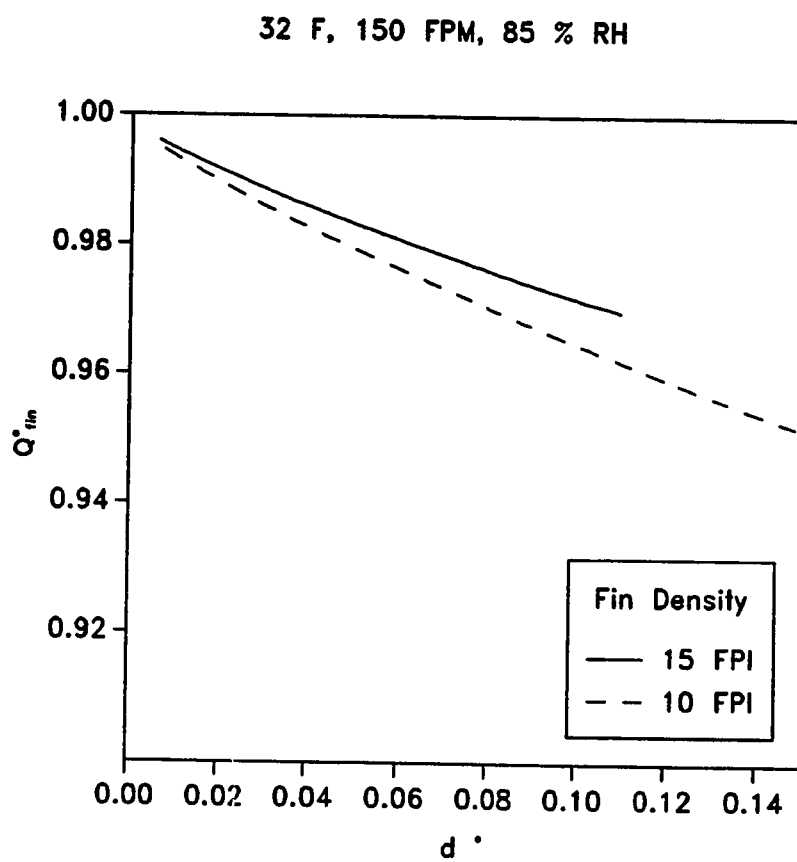


Figure 4.18 Dimensionless Heat Transfer for Individual Fin

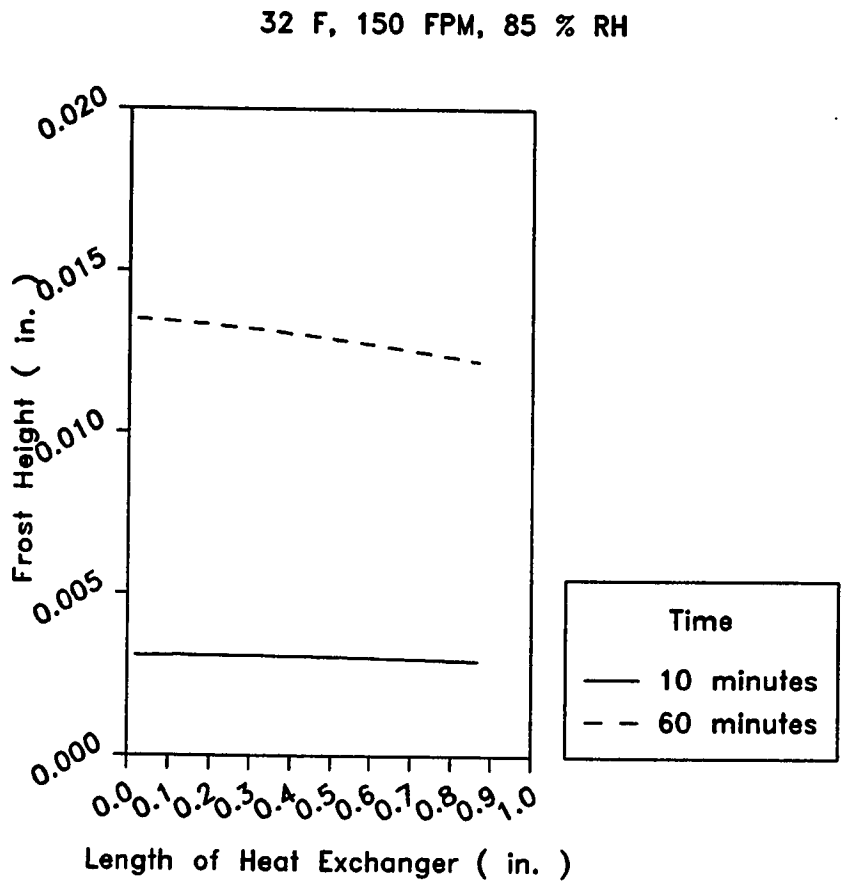


Figure 4.19 Frost Growth as a Function of Location

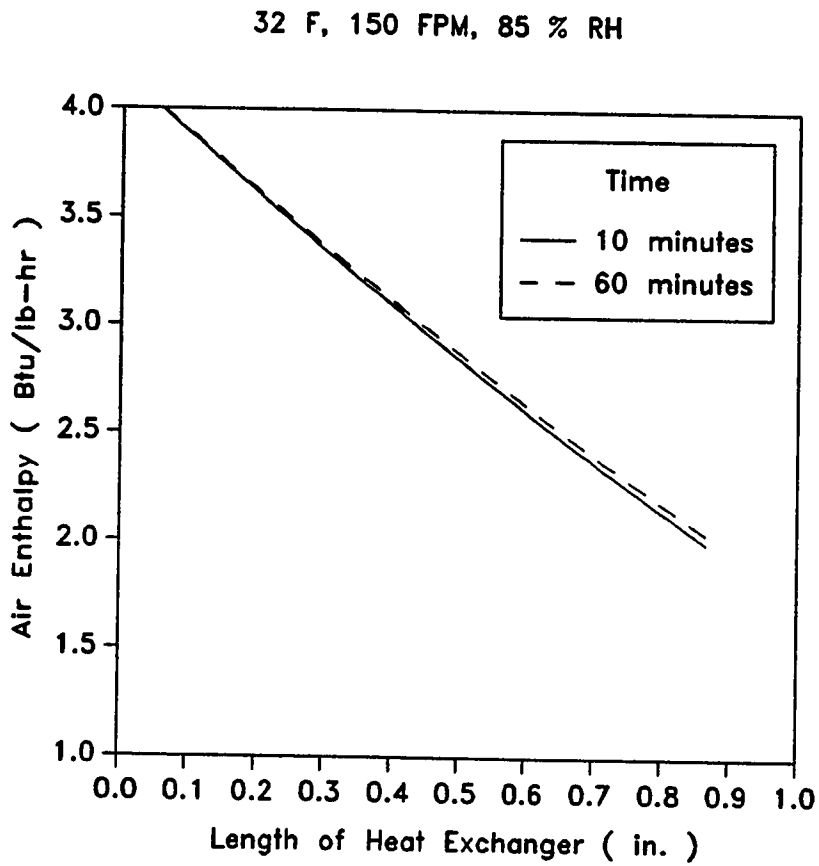


Figure 4.20 Air Enthalpy as a Function of Location

in Figure 4.21. The frost surface temperature is highest at the leading edge, ostensibly due to the amount of frost accumulating on a particular section. As more and more frost accumulates, the frost surface temperature approaches that of freezing (32 ° F).

E. CONCLUSIONS

This chapter has developed the basis for a comprehensive model to evaluate the performance of rectangular plate fin heat exchangers under frosting conditions. It has included a comprehensive frost growth model incorporating the variable nature of the frost properties, a heat exchanger performance model and also incorporated the effects of the system (pressure drops and blower characteristics). In addition to a dimensional analysis, the model also provides a non-dimensional set of variables which can be useful in the design of heat exchangers operating under frosting conditions.

Trends as predicted by the model are presented and discussed qualitatively to establish the validity of the model and its assumptions. It has been found that the results are good and appear reasonable. Most of the general trends are similar to those reported by previous investigators. This gives more credibility to the model and strengthens its validity. A more detail comparison with experimental results is done in Chapter VI.

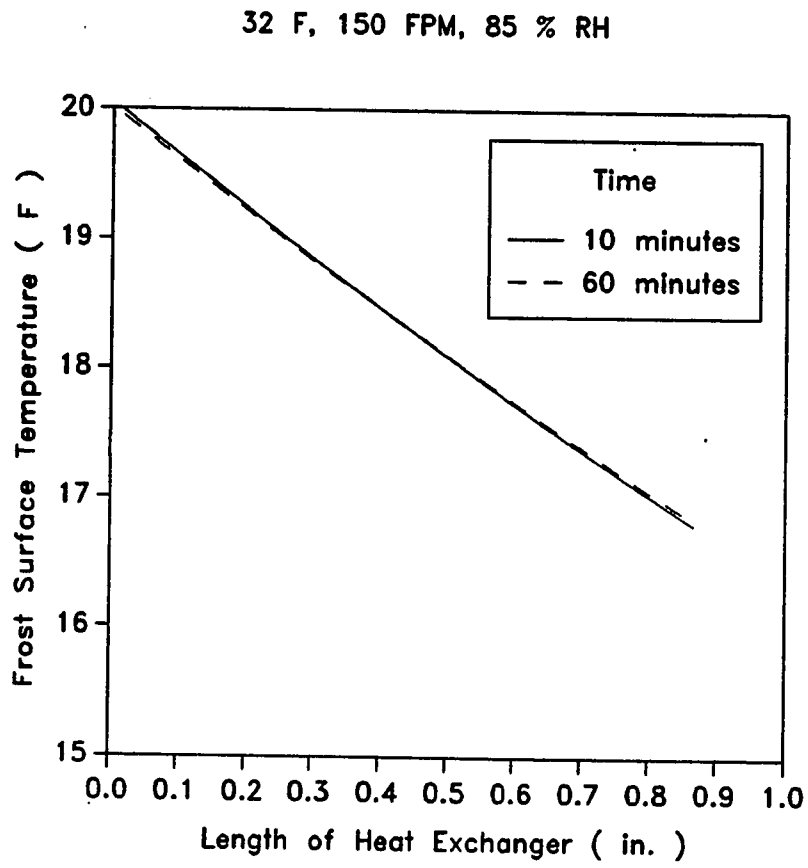


Figure 4.21 Frost Surface Temperature as a Function of Location

CHAPTER V

EXPERIMENTAL RESULTS AND DISCUSSION

This chapter discusses the results obtained from the experimental tests. These results are also discussed and compared with those from other investigators wherever possible. However, these comparisons are only for the flat, rectangular plate fin type, since all the previous studies have only dealt with this particular fin geometry.

A. DESIGN METHODOLOGY / TEST MATRIX

A design methodology which would evolve into a test matrix was sought and developed. The following variables were of interest :

1. The effects of different fin types (geometry).
2. The effects of fin density.
3. The effects of different humidities.
4. The effects of different approaching air temperatures.
5. The effects of different air flow rates.
6. The effect of a lower refrigerant temperature.

The above criteria were employed to evolve a test matrix (Table 5.1).

As seen from the test matrix, there are four plate fin types, namely Louvered, Sine Wave, Corrugated and Flat and also a Spine Fin type . The fin densities varied from 10 fins per inch to 20 fins per inch. Geometrical details of these coils are given in Appendix C . Three different relative humidities were considered along with two different air flow rates and air temperatures.

TABLE 5.1 Test Matrix

TEST CONDITIONS

HEAT EXCHANGER TYPE	H	M	L	R	A	V	
	Louvered 20 FPI	•					
	Louvered 18 FPI	•	•	•		•	•
	Louvered 14 FPI	•					
	Sine Wave 18 FPI	•	•	•			
	Sine Wave 10 FPI	•					
	Corrugated 18 FPI	•		•		•	•
	Flat Plate 18 FPI	•	•	•	•		
	Spine 20 FPI	•				•	
	Spine 24 FPI	•		•			

H	High Relative Humidity
M	Medium Relative Humidity
L	Low Relative Humidity
R	Lower Refrigerant Temperature
A	Higher Air Temperature
V	Higher Face Velocity (Air)

B. EXPERIMENTAL CONDITIONS AND LIMITATIONS

The measurements were conducted under the conditions specified below. If conditions were far different from the desired values, the test was conducted once again. A few tests were also repeated to ensure repeatability and correctness of data.

Air Temperature

All the tests were conducted at an average dry bulb temperature of 32 ° F except the tests which were designed to be conducted at a higher temperature of 37 ° F. These temperatures were chosen after some discussion with sources in industry, because these represented the temperatures of maximum utility and interest to the industry at large. The approaching air temperature was relatively constant in almost all the tests and there was little difficulty in controlling it. Figure 5.1 shows the typical variation in air temperatures during the course of a test.

Air Flow

All the tests were conducted at an average air flow rate of approximately 300 cubic feet per minute (face velocity of 130 feet per minute). This number was based on the approximate values used in industry for evaporator coils. The tests to study the effect of increased air flow rate were conducted at an approximate face velocity of 200 feet per minute.

Dampers were used to maintain the airflow approximately constant during the tests. As frost formed on the test coil and conditioning coil, the total pressure drop in the system increased. As a result the air flow rate decreased. The tests

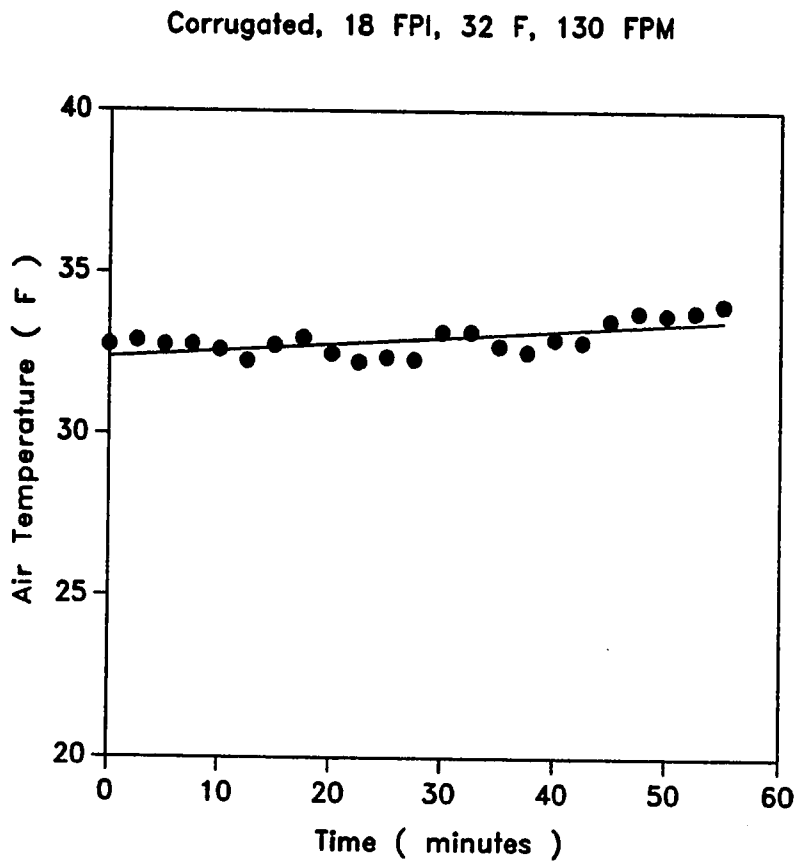


Figure 5.1 Variation of Air Temperatures in a Typical Test

were suspended once it was no longer possible to maintain the airflow rate to within 10 % of the initial value at the start of the test. Figure 5.2 reflects the typical variation in air flow rates during the course of a test.

Refrigerant Temperature

The refrigerant used was a 50 % ethylene glycol/ water solution with an average flow rate of 6.5 gallons per minute. In all the cases, average inlet temperature to the test heat exchanger was approximately 7 ° F. One set of tests was conducted at an average refrigerant inlet temperature of approximately 2 ° F to establish the effects of a lower refrigerant temperature on frost growth and heat exchanger performance.

The temperature of the ethylene glycol in the reservoir had to be lowered to approximately 0 ° F before the flow circuit through the test coil was activated. The problem was the initial “ chill down ” of the heat exchanger. A lot of mass required a lot of energy to bring it down in temperature. Therefore the refrigerant temperature in the sump would typically rise and settle down to approximately 7 ° F within 10 minutes into the test.

Humidity

The effects of humidity were studied by considering three relative humidities (R.H.). These were High (80 %), Medium (75 %) and Low (66 %). All the tests were conducted at a dry bulb temperature of 32 ° F and face velocity of 130 feet per minute. Some difficulties were encountered in maintaining approximately the same relative humidities between the tests. If in any test, the differences in

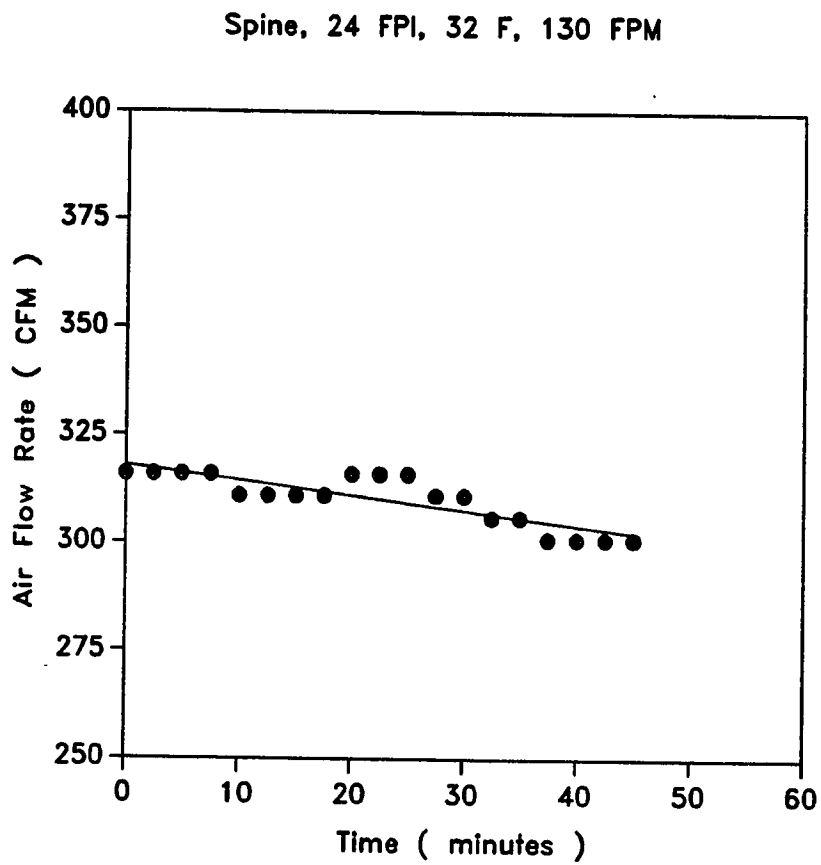


Figure 5.2 Variation of Air Flow Rates in a Typical Test

R.H. were more than $\pm 3\%$ off, the test was then repeated to ensure consistency in results. A typical variation of the relative humidity in a test is presented in Figure 5.3.

C. RESULTS

The results are presented in a dimensional as well as a non-dimensional format.

1. Frost growth (accumulation) vs. time .
2. Pressure Drop as a function of time .
3. Energy Transfer Coefficient*, E_o vs. time.
4. Dimensionless Sensible Heat Transfer Coefficient, U^* vs. time.
5. Heat Exchanger Effectiveness, ϵ vs time.

The above parameters are explained in detail along with a brief discussion. The data are presented in the form of graphs which have explanatory notes as to the exact environmental conditions and heat exchanger fin type. The data were collected at two to three minute intervals and averaged over time to reduce the error in taking an instantaneous value.

The data presented are indicative of the representative trends resulting from the experiments. Along with the results, a brief discussion of the trends is presented and appropriate comments are made. The data for the spine fin geometry are plotted separately because their geometry is so different that they cannot be easily compared with the other fin types.

* This is discussed in detail later in this chapter.

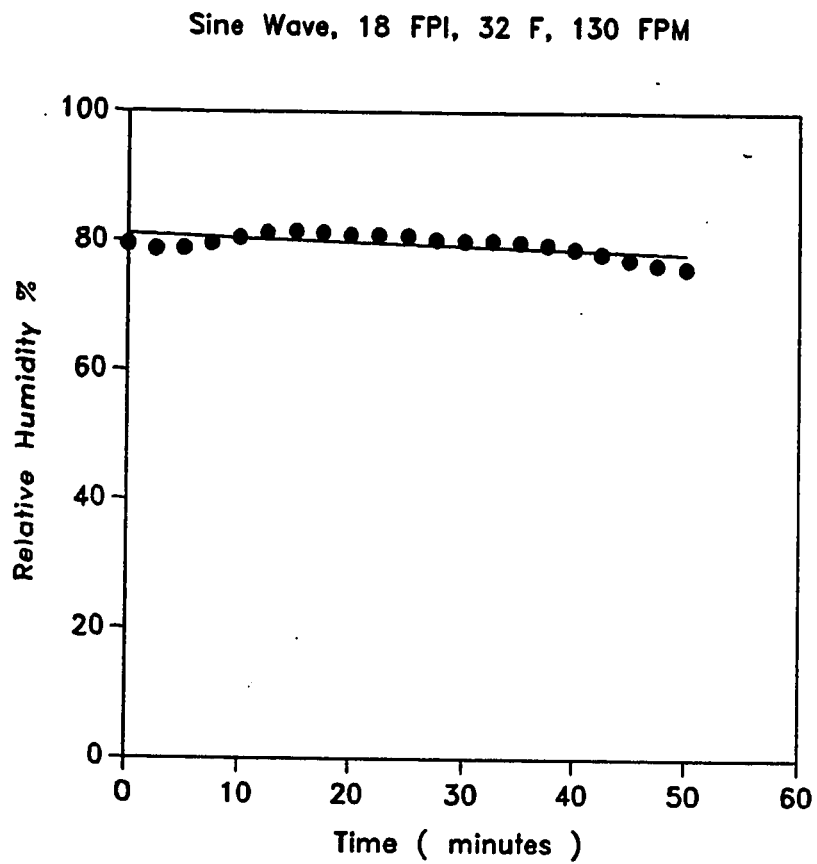


Figure 5.3 Variation of Air Relative Humidity in a Typical Test

Frost Growth

The growth of the frost on the heat exchangers as a function of time has been calculated and presented in graphs. The frost growth is based on the difference in the moisture content of the air approaching the coil and leaving the coil. This moisture difference is numerically integrated over time to determine the actual amount of frost deposited on the coil as a function of time. As a check, the total amount of condensate melting off the coil (when a test was completed) was collected and measured. This value was compared to the final value of the frost accumulation.

The condensate collected was found to be within 20 % of the amount calculated by using the numerical integration method. This difference can be attributed to the following reasons :

1. Due to surface tension effects and high fin densities, a small amount of the condensate remains trapped between the fins of the coil.
2. Some condensate is lost due to evaporation.

The complex geometry of the heat exchanger surfaces does not allow for a more accurate methodology than this. A photographic technique was tried but was unsuccessful. Such a method did not allow for a proper, quantitative estimation of the frost growth. A leading edge effect was observed, wherein the approaching surface of the heat exchanger (leading edge) has much more frost than the exit surface (trailing edge). This was noticed in all the tests conducted.

Figure 5.4 is a plot of the frost accumulation as a function of relative humidity.

Louvered, 18 FPI, 32 F, 130 FPM

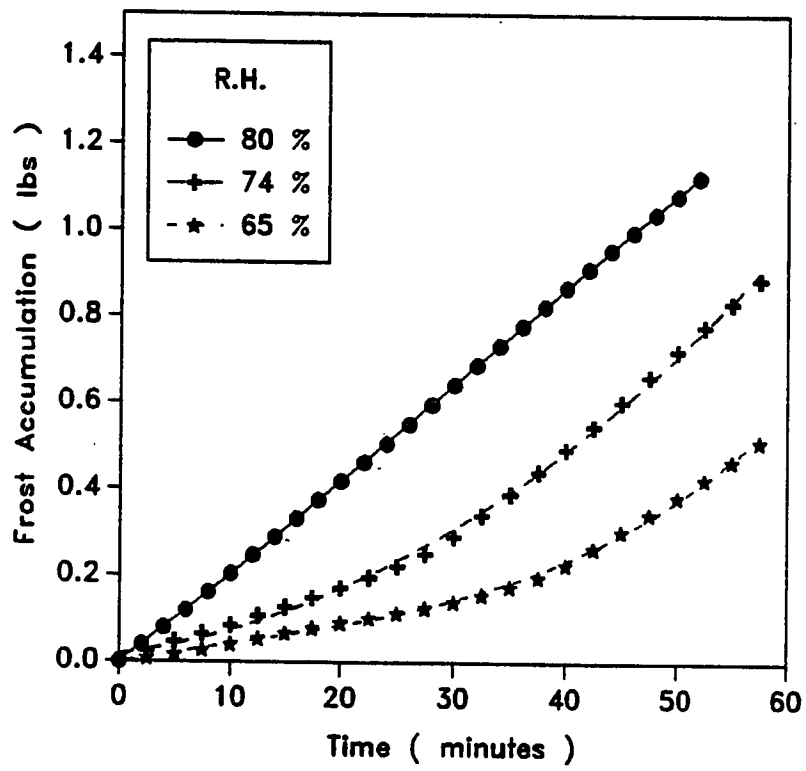


Figure 5.4 Effect of Humidity on Frost Accumulation

With an increase in relative humidity there is a tangible increase in the amount of frost. This is a consequence of the higher amount of moisture in the air which increases the mass transfer potential between the air and the heat exchanger surface. There is a steeper increase in frost growth in going from 65 % to 75 % R.H. than in going from 75 % to 80 % R.H. as a consequence of the difference in moisture content at these relative humidities. The two curves at the higher humidities have an almost parallel growth pattern. This trend of increasing frost accumulation with humidity was consistently seen in all the tests.

It has been demonstrated repeatedly by many investigators including Stoecker [31,32] and Gatchilov and Ivanova [35] that a higher level of moisture in the air increases the frost growth. For the same ambient dry bulb temperature, a higher relative humidity indicates a higher moisture content in the air leading to more frost growth. The results from the present study concur with previous studies.

Figure 5.5 reflects the effect of fin spacing on frost accumulation. By increasing the fin spacing, the amount of frost accumulating decreases, but not very significantly. Until about 20 minutes into the test, there is a difference in growth rates (slope with respect to time); however, after that the curves are almost parallel. A coil with a more dense fin pattern has a larger heat and mass transfer surface area. Therefore, with a larger mass transfer area, there is more frost growth.

Figure 5.6 shows that a higher face velocity leads to more frost. A higher face velocity leads to a higher heat and mass transfer coefficient, thereby increasing the amount of moisture being converted to frost in the same time period. The above trends are consistent with what has been reported by Shultze and Howell

Sine Wave, 32 F, 130 FPM, 80 % R.H.

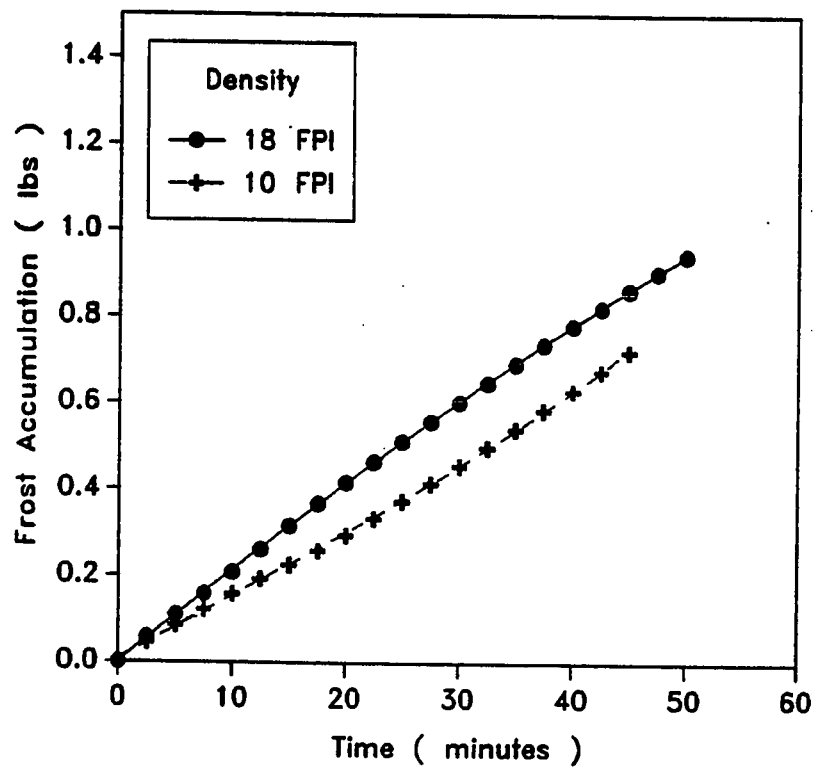


Figure 5.5 Effect of Fin Spacing on Frost Accumulation

Louvered, 18 FPI, 32 F, 80 % RH

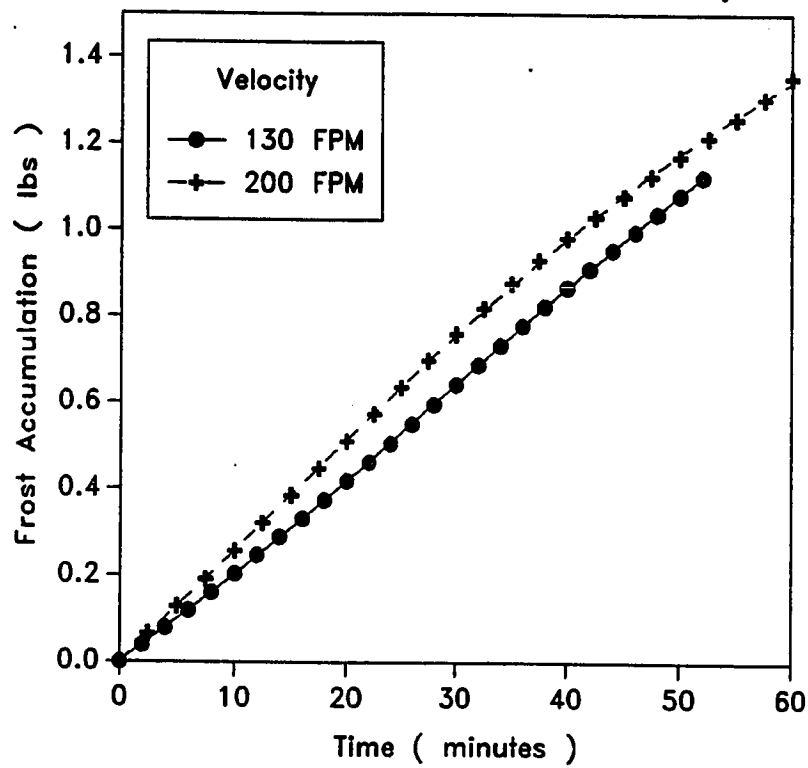


Figure 5.6 Effect of Face Velocity on Frost Accumulation

[42].

There is an appreciable increase in the frost growth when the dry bulb temperature of the approaching air is increased from 32 ° F to 37 ° F for the same relative humidity. This is shown in Figure 5.7. A higher air temperature for the same relative humidity has a higher absolute humidity and this leads to more frost growth. However, in another test the air temperature was raised to approximately 45 ° F, keeping the relative humidity at approximately 75 %. It was observed that the frost growth was minimal and only condensation on the heat exchanger surface occurred. It would therefore appear that there exists a limiting air temperature above which the effect of a higher temperature is more dominant than the effect of higher absolute humidity. This value will naturally be a function of the refrigerant temperature. For the current set of tests, it was found that the limiting temperature beyond which no frost will form is approximately 46 to 47 ° F.

When the refrigerant temperature was decreased by 5 ° F to 2° F, keeping the air temperature at 32 ° F, there was a dramatic increase in frost growth. This is shown in Figure 5.8. A lower refrigerant temperature will lead to colder fin and tube surface temperatures; therefore, with a greater mass and heat transfer potential there is more rapid frost growth. Other investigators such as O'Neal [17,25] have reported that there is more frost growth for a lower heat transfer surface temperature.

Figure 5.9 is a comparison of the frost accumulations for the four plate fin types being studied. The growth patterns are very close together and it is difficult to distinguish between them. The amount of frost accumulation for the louvered fins is higher than the other fin types. This can be attributed to the increased

Corrugated, 18 FPI, 130 FPM, 80 % RH

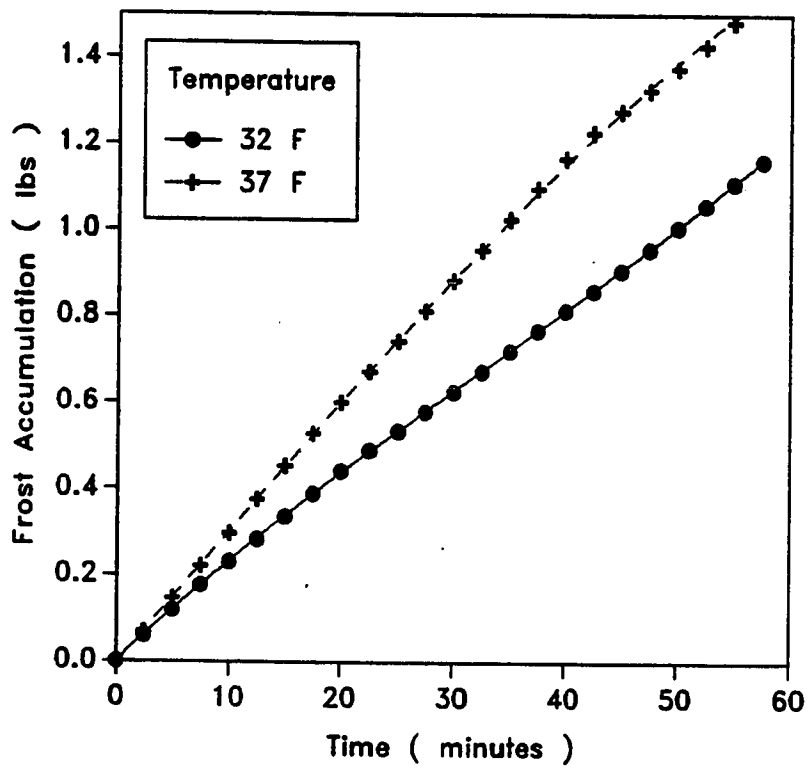


Figure 5.7 Effect of Air Temperature on Frost Accumulation

Flat, 32 F, 130 FPM, 80 % R.H.

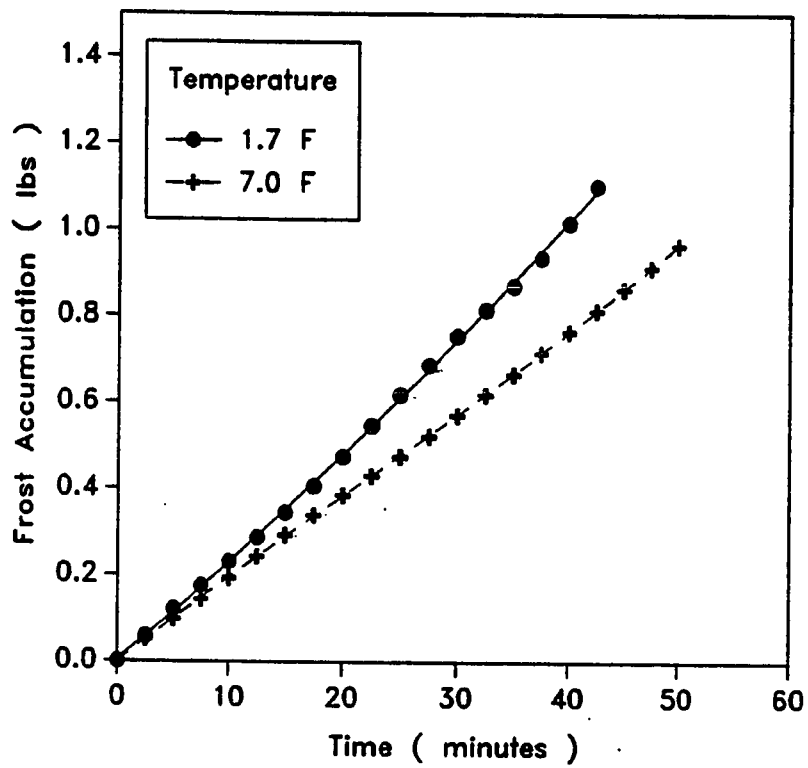


Figure 5.8 Effect of Refrigerant Temperature on Frost Accumulation

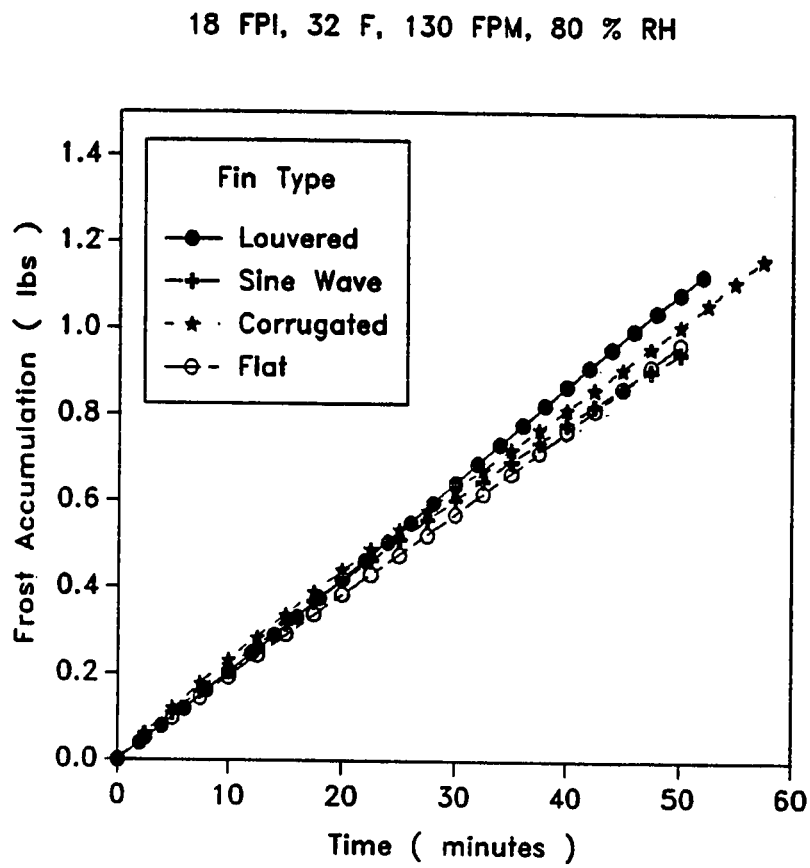


Figure 5.9 Frost Accumulation for Different Fin Geometries

surface area of contact for the mass transfer to occur and frost to settle down. The remaining three fin types : wavy, corrugated and flat are very close together, ostensibly because of similar geometries.

Figure 5.10 shows the effect of a higher humidity as well as a higher fin density on the frost accumulation on the spine fins. The 24 FPI coil has a higher amount of frost accumulation than the 20 FPI coil at the same humidity levels. There is also less frost growth at a lower humidity. These trends are similar to those found in the plate fin types and were expected. It is interesting to note that the amount of frost accumulated by the coils was also reasonably high (to the tune of 1 lb) within an hour. This can be attributed to the very dense interwoven mesh of the spine fins which causes turbulence and a very large surface area.

The above information can prove to be important in determining which fin types and what conditions are most conducive to frost growth. The following preliminary conclusions can be drawn :

1. An increase in humidity results in an increase in frost accumulation.
2. An decreased fin spacing results in an increase in frosting.
3. An increase in face velocity results in an increase in frost growth.
4. An increase in air temperature (as long it is below a limiting threshold value) results in an increased frost accumulation.
5. A lower refrigerant temperature increases the amount of frosting.
6. The louvered fin type has the maximum amount of frost accumulation in comparison to the other fin types.

Spine Fin, 32 F, 130 FPM

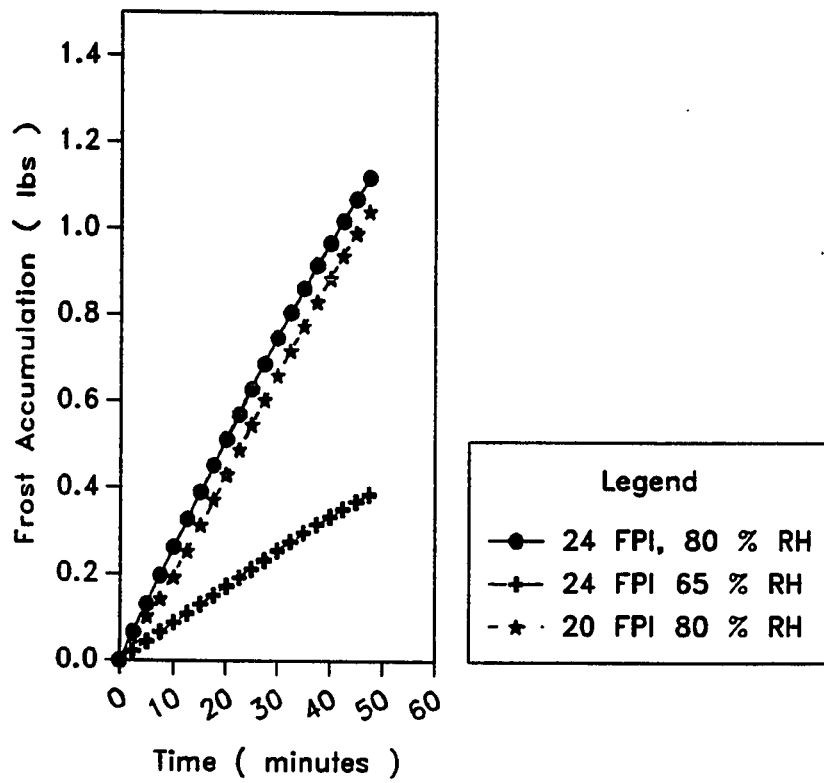


Figure 5.10 Frost Accumulation for Spine Fin Geometries

Pressure Drop Across Coil

The increase in pressure drop across the frosted coil as a result of the frost on the heat exchangers as a function of time was measured via the use of manometers. Figure 5.11 shows the effect of humidity on the pressure drop across the coil. Since there is more frost growth at higher humidities, there is less free flow area which leads to a higher pressure drop. Similar trends have been reported by Gatchilov and Ivanova [35].

The effect of fin spacing on pressure drops is presented in Figure 5.12. The coils with a higher fin density have a greater pressure drop due to the lower free flow area of these coils. The free flow area is further reduced by the higher frost accumulation. There are differences between the 20 FPI and 18 FPI heat exchanger, but the difference is far more perceivable in the 14 FPI coil. Stoecker [31] has reported similar trends with fin densities of 4 and 9 FPI.

As a consequence of an energy balance, the effect of an increased face velocity results in a greater pressure drop across the coils (Figure 5.13). In addition, since a higher velocity leads to more frost growth, there is a drop in free flow area which also contributes to a higher pressure drop. Stoecker [31] has reported the same trends.

Since a lower refrigerant temperature leads to more frost growth and to a reduced free flow area, there is a higher pressure drop for such conditions (Figure 5.14). Therefore the increase in pressure drop in this particular test is purely a frost growth “ blockage ” effect.

Figure 5.15 compares the pressure drops of the different fin types. The coil

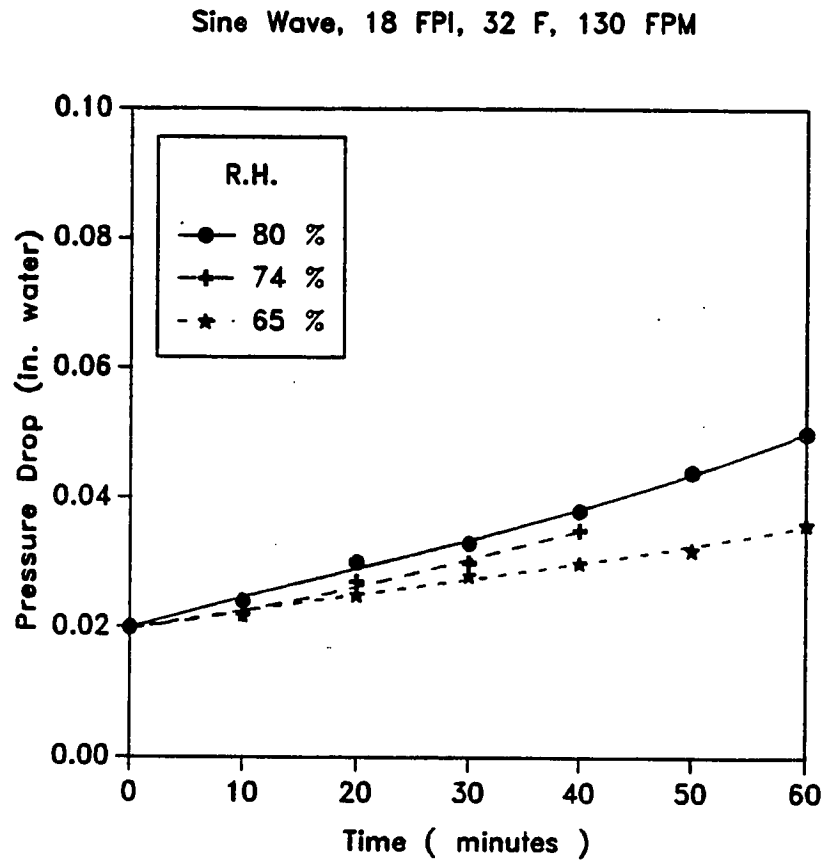


Figure 5.11 Effect of Humidity on Pressure Drop Across Coil

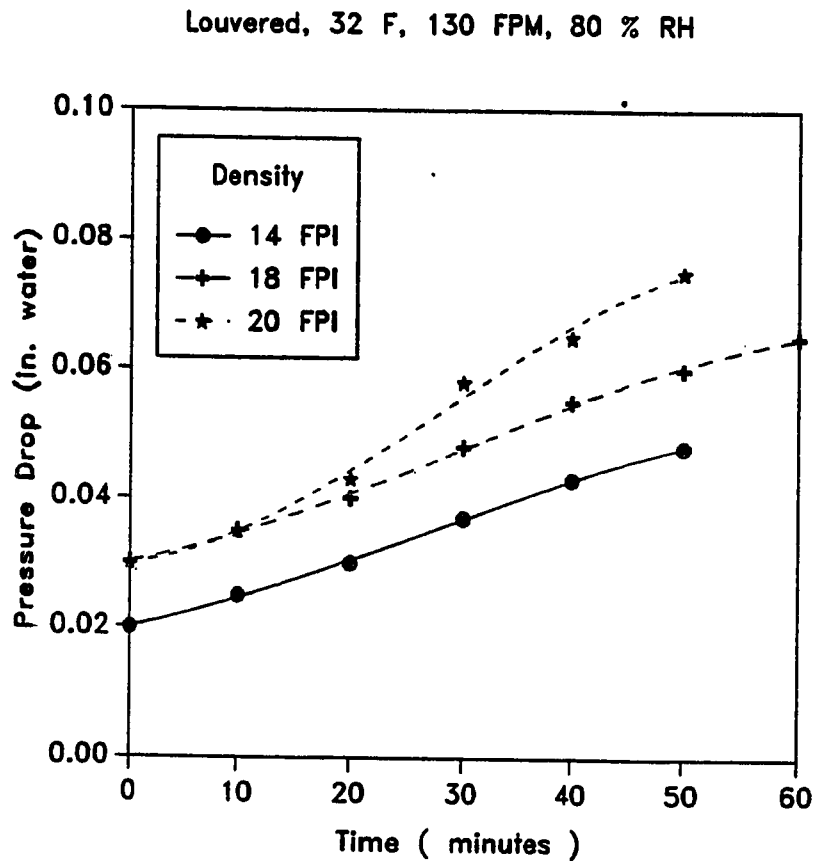


Figure 5.12 Effect of Fin Spacing on Pressure Drop Across Coil

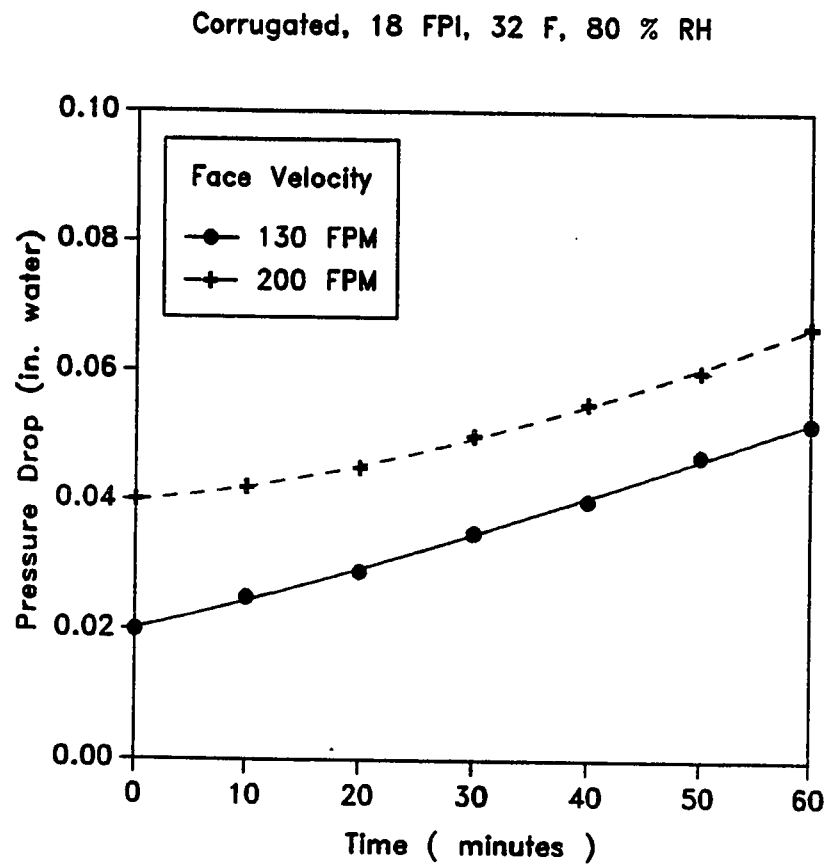


Figure 5.13 Effect of Face Velocity on Pressure Drop Across Coil

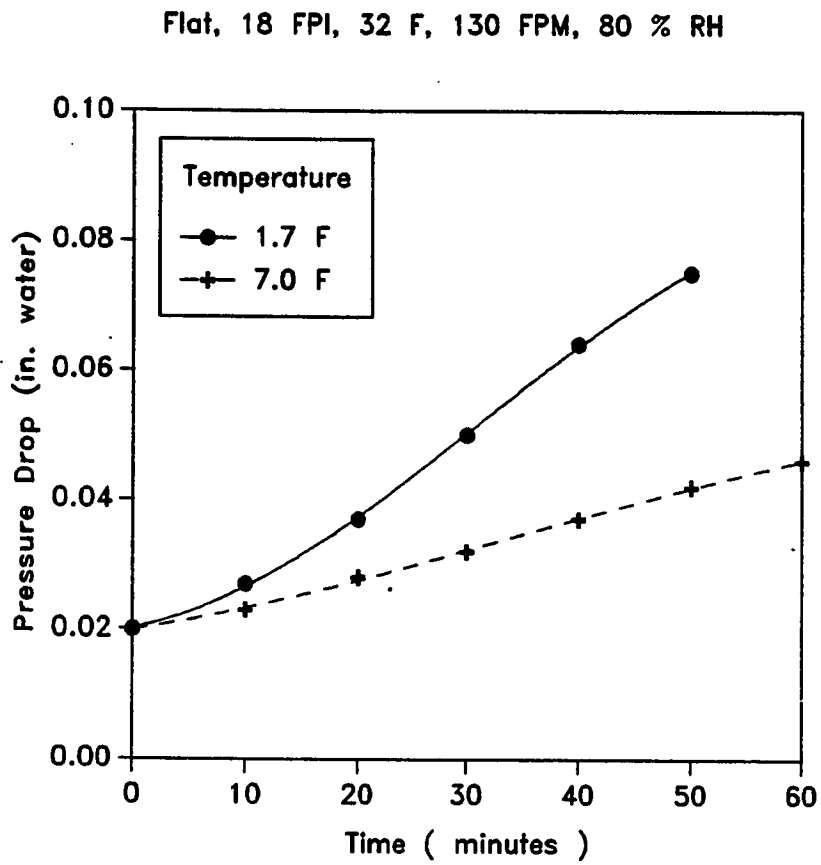


Figure 5.14 Effect of Refrigerant Temperature on Pressure Drop Across Coil

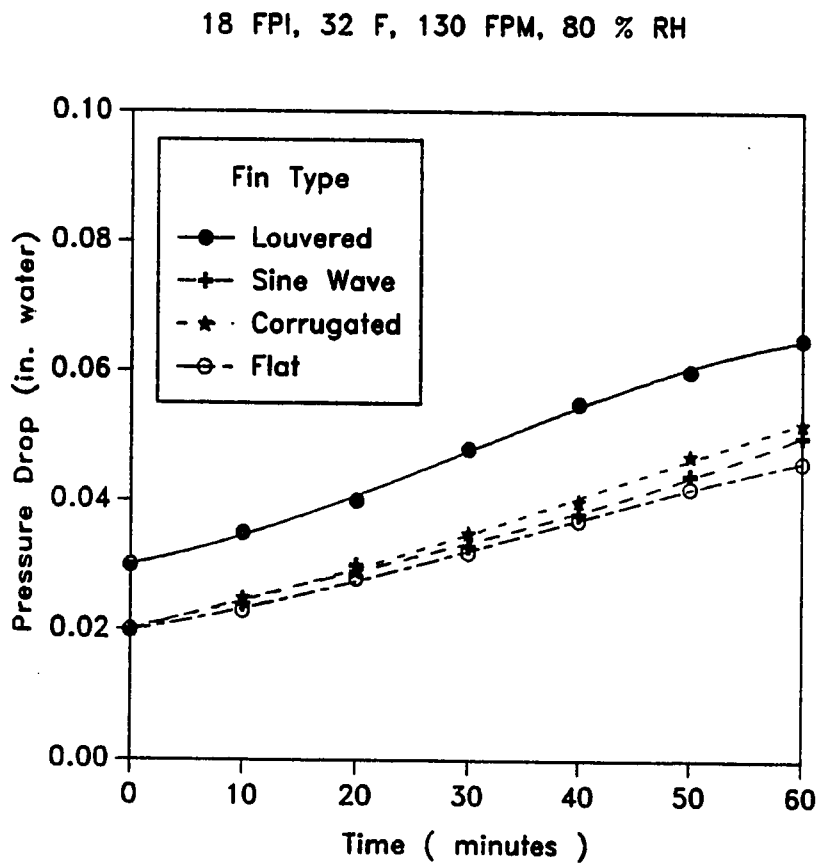


Figure 5.15 Pressure Drop Across Coil for Different Fin Geometries

with the louvered fin type has the greatest pressure drop because it has less free flow area than the other fin types. For the flat, wave, and corrugated fin types, the trends can probably be attributed to frost accumulation since their initial pressure drops and frost growth are comparable.

The spine fin geometries exhibit similar pressure drop characteristics to the plate fins. A higher humidity results in more frost growth and therefore a higher pressure drop. In addition, a higher fin density leads to less free flow area resulting in a higher pressure drop .

The above information is important since the pressure drop across the coil is a direct indicator of what is commonly termed as the “ blockage effect ”. The blockage affects the performance of the heat exchanger because it reduces the free flow area and therefore decreases heat transfer. From the above results it would appear that the major variables affecting the pressure drop are fin geometry and frost accumulation. In general, the following conclusions can be drawn :

1. A smaller fin spacing results in a higher pressure drop across the coils ostensibly due to a smaller free flow area. Louvered fins have the highest pressure drop because of the boundary layer separation and geometry.
2. In the case of the plate fin types, the pressure drop differences can be attributed to the frost growth patterns since their geometries are very similar.

Energy Transfer Coefficient, E_o

Traditionally, one of the more common ways to evaluate the performance of a heat exchanger is to calculate an overall heat transfer coefficient based on the

logarithmic mean temperature difference (LMTD). Such a methodology is well established and recognized as a useful approach in the case of sensible heat transfer.

Since frosting includes both sensible and latent energy transfer processes, the use of an LMTD approach is not strictly correct. A more appropriate method therefore, would be to consider the enthalpy differences instead of temperature differences in computing a logarithmic mean. Such a calculation would account for the sensible energy transfer as well as the latent energy transfer.

An overall energy transfer coefficient has been defined and presented for the various conditions. The calculations are based on a logarithmic mean enthalpy difference and an enthalpy potential formulation. Such a formulation is very advantageous in evaluating combined heat and mass transfer problems with humid air because it combines the separate heat and mass transfer processes into one simple equation. A similar type of formulation has been used previously in literature by Sanders [29] and Mitalas and Almahedy [43].

An energy transfer coefficient, E_o can be defined as (see Appendix D) :

$$E_o = \frac{C_p \dot{Q}_t}{\Delta i_m A_t} \quad (5.1)$$

E_o has to be defined relative to a particular heat transfer surface area, A . In this study, this area was set to the dry, unfrosted area of the tubes since this was a convenient reference area. E_o represents the combined heat and mass transfer analogy of the heat exchanger and is therefore a measure of the performance of the heat exchanger under frosting conditions.

As discussed in Chapter II, previous studies have reported the energy transfer coefficient increasing with initial frost growth and then decreasing as the frost grows. The reasons for the rise have been attributed to a larger surface area for heat and mass transfer resulting from an increased surface roughness of the frost layer. The fall in the energy transfer coefficient has been attributed to the frost insulating the cold heat exchanger surface from the relatively warm moist air and the increased blockage in airflow as the frost increases in thickness.

The effect of different relative humidities on E_o is shown in Figure 5.16. As the humidity increases, there is an increase in the energy transfer coefficient, E_o . For a constant refrigerant temperature, higher humidities produce an increase in mass transfer (since more frost forms on the coil) which increases the latent energy transfer. However, as time progresses, the energy transfer coefficient drops off more rapidly at higher humidities because the frost insulates the cold heat exchanger surface from the warm air. At higher humidities there is more frost and the insulating effect occurs earlier than at a lower humidity. It has been shown by Gatchilov and Ivanova [35] that the energy transfer coefficient at a higher humidity actually drops below that of a lower humidity after some time has elapsed. If the tests conducted in the present study were allowed to run long enough, the trends observed by Gatchilov and Ivanova [35] will probably surface.

Figure 5.17 reflects the effect of face velocity on E_o . A higher face velocity leads to a higher Reynolds Number and hence an increased rate of energy transfer. This is similar to the trends observed with a dry, unfrosted coil. Such trends have also been reported by Stoecker [31,32]. However, the energy transfer coefficient also starts to drop sooner (for the higher velocity) than at a lower

Sine Wave, 18 FPI, 32 F, 130 FPM

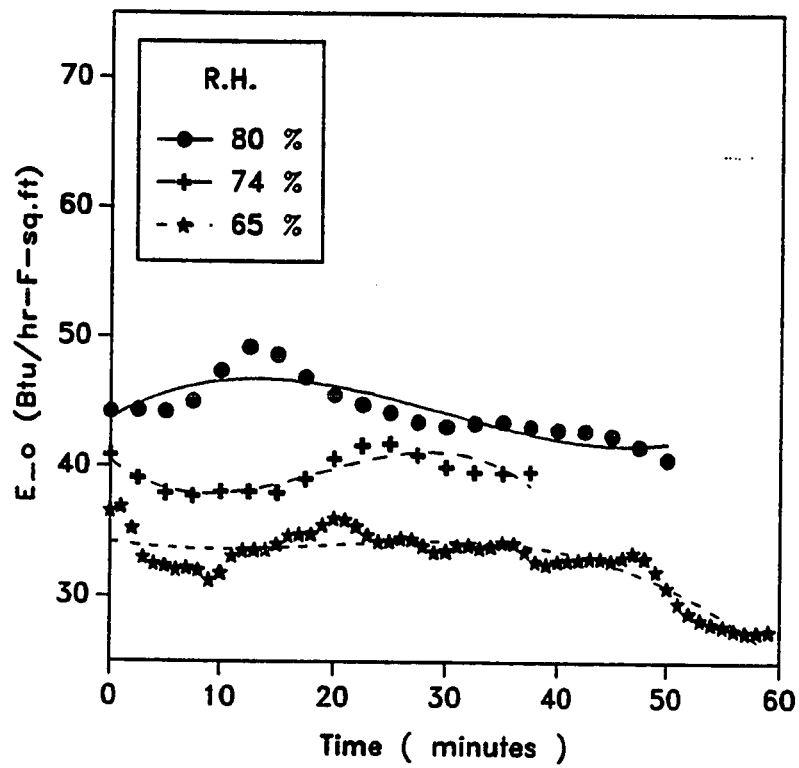


Figure 5.16 Effect of Humidity on Energy Transfer Coefficient

Corrugated, 18 FPI, 32 F, 80 % R.H.

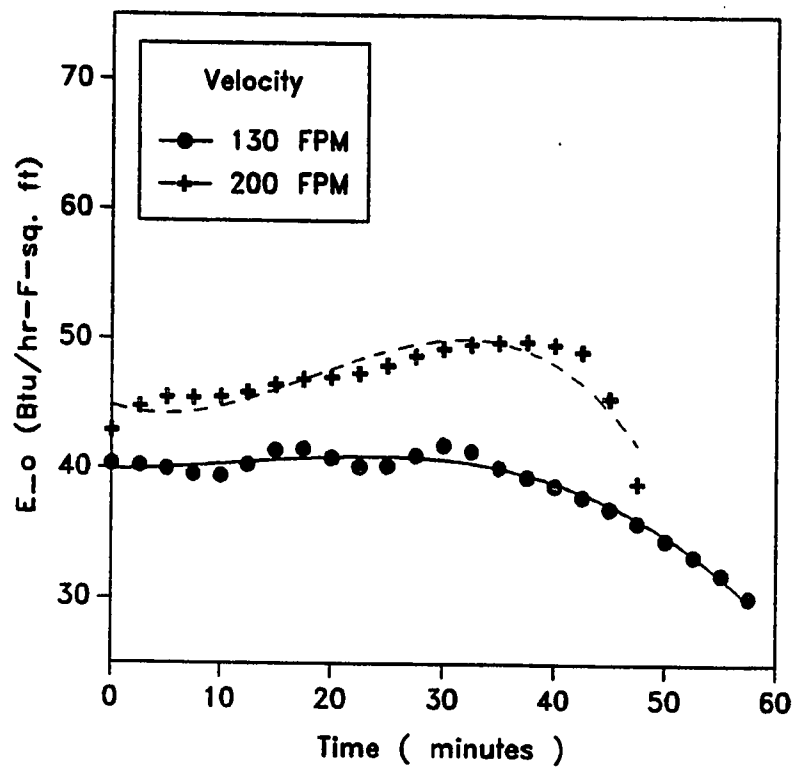


Figure 5.17 Effect of Face Velocity on Energy Transfer Coefficient

velocity. Because of a larger frost accumulation, the frost layer insulates the heat exchanger quicker.

For the same relative humidity, the energy transfer coefficient increases with air temperature (Figure 5.18). Air at 37 ° F, 80 % R.H. has a lot more moisture than air at 32 ° F, 80 % R.H. Such a trend can be attributed to the increase in latent energy transfer (increased moisture levels) as well as an increased sensible temperature difference between the air and refrigerant.

A lower refrigerant temperature results in a higher energy transfer coefficient (Figure 5.19) due to an increase in both latent and sensible energy transfer. The entire heat exchanger surface – fins and tubes becomes colder due to a colder refrigerant and this increases the heat and mass transfer between the air and the heat exchanger coil.

A higher fin density results in a higher energy transfer coefficient (Figure 5.20). This is a direct consequence of the increased energy transfer area and the increased frost. An increase in heat transfer should be accompanied by a corresponding (less desirable in the long run) increase in mass transfer which leads to an increase in the total (sensible and latent) energy transfer. The increased energy transfer is desirable to improve the overall thermal performance of the heat exchanger. However, as more frost accumulates, there is a more rapid performance degradation due to blockage and the insulating effects of the frost.

A comparison of the energy transfer coefficients for the different fin types is shown in Figure 5.21. The louvered fin type has the maximum energy transfer

Corrugated, 130 FPM, 32 F, 80 % RH

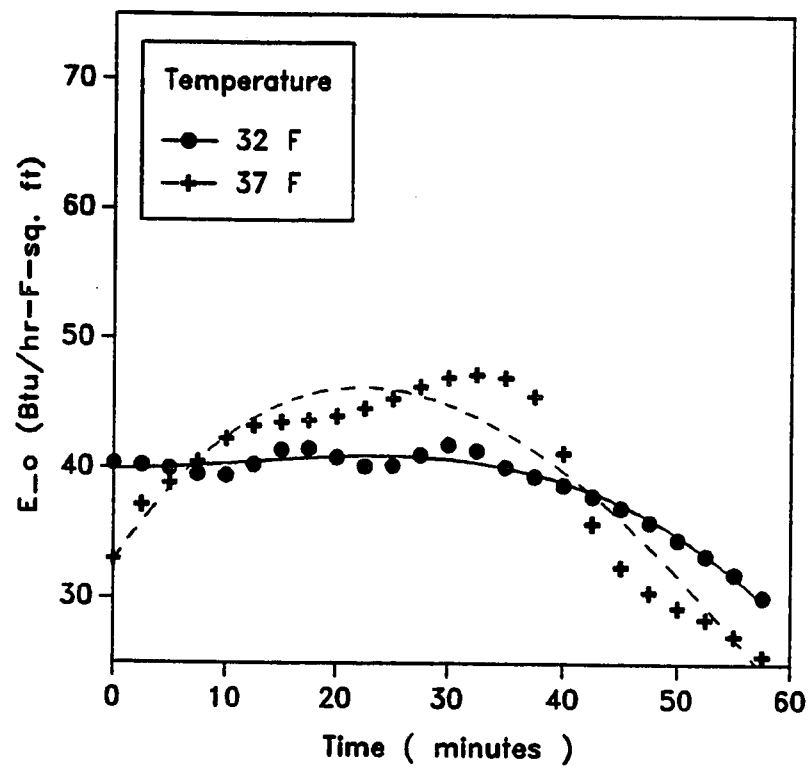


Figure 5.18 Effect of Air Temperature on Energy Transfer Coefficient

Flat, 18 FPI, 130 FPM, 32 F, 80 % R.H.

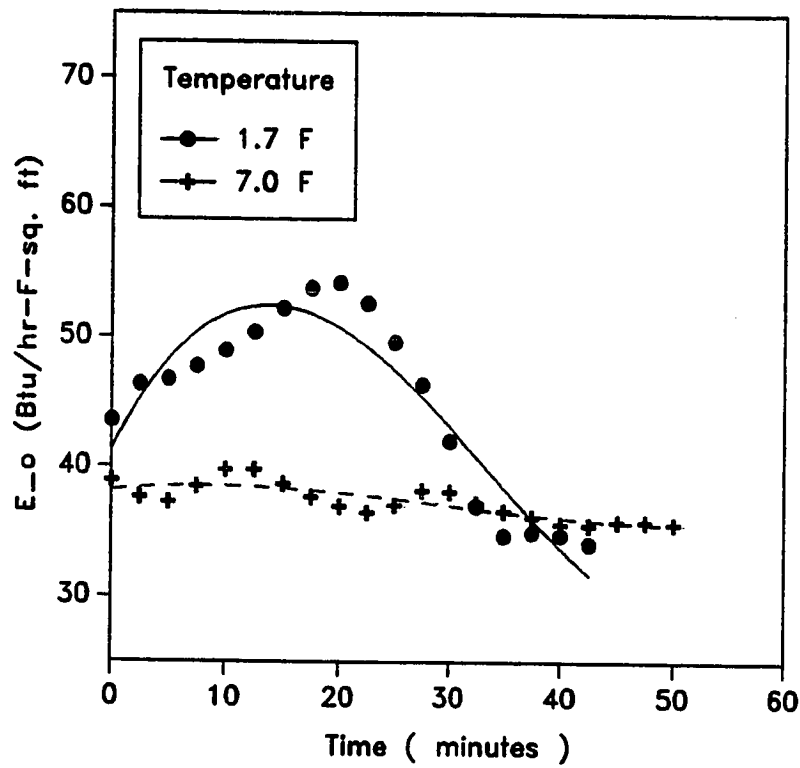


Figure 5.19 Effect of Refrigerant Temperature on Energy Transfer Coefficient

Louvered, 130 FPM, 32 F, 80 % R.H.

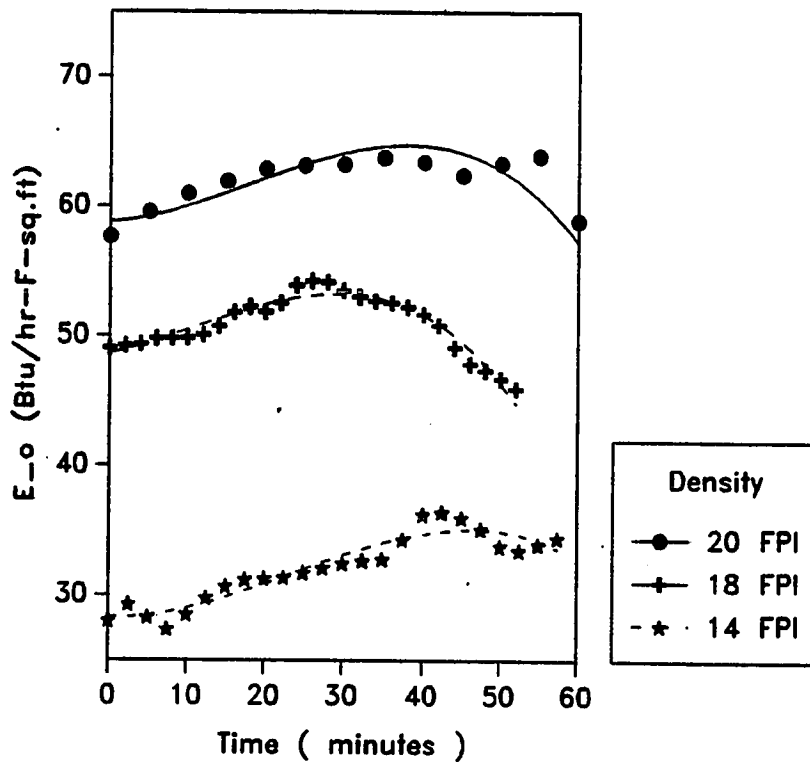


Figure 5.20 Effect of Fin Spacing on Energy Transfer Coefficient

18 FPI, 130 FPM, 32 F, 80 % R.H.

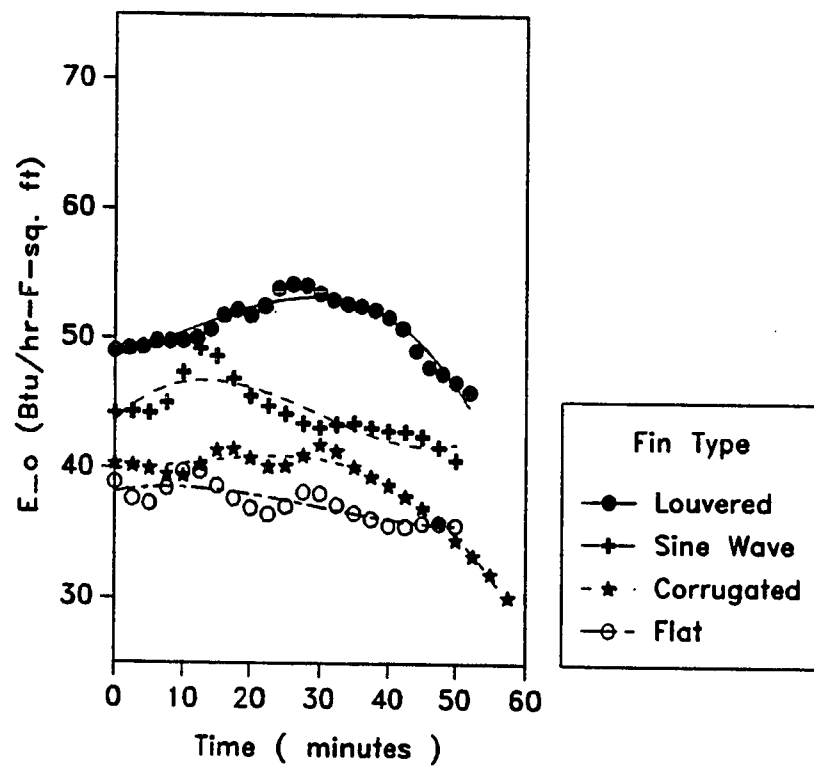


Figure 5.21 Energy Transfer Coefficient for Different Fin Geometries

coefficient. Considering that this fin type has the maximum frost accumulation and the maximum heat transfer surface area, this is to be expected. The latent and sensible contributions of the energy transfer process are maximum for the louvered fin type. The wavy fin has an overall energy transfer coefficient less than the louvered but more than the others. The corrugated and flat fins have the lowest energy transfer coefficient. Since the amount of frost accumulation is approximately the same in all three (wavy, corrugated and flat) fin types (Figure 5.9), the dominant factor is the sensible component of the energy transfer process.

Figure 5.22 shows the effect of fin density and humidity in spine fins on the energy transfer coefficient. In the case of the 24 FPI coil especially at a higher humidity, E_o can be clearly seen rising and then falling after some time. This effect is also present though not quite apparent in the other tests. The trends are similar to those reported above for the same reasons. A higher humidity leads to a larger amount of latent energy transfer and therefore the energy transfer coefficient, E_o is higher. Similarly, for a higher fin density the surface area for heat and mass transfer is increased considerably leading to a higher E_o .

In all the cases, there is generally a trend of the energy transfer coefficient going through a slight rise and then a fall. This is consistent with what has been reported in the literature. However, the exact reasons for this trend are not very clear. In an attempt to clarify this further, the energy transfer coefficient was split into a sensible component and a latent component. This was achieved by the LMED approach with the driving potential being either the sensible or latent energy.

Spine Fins 130 FPM, 32 F

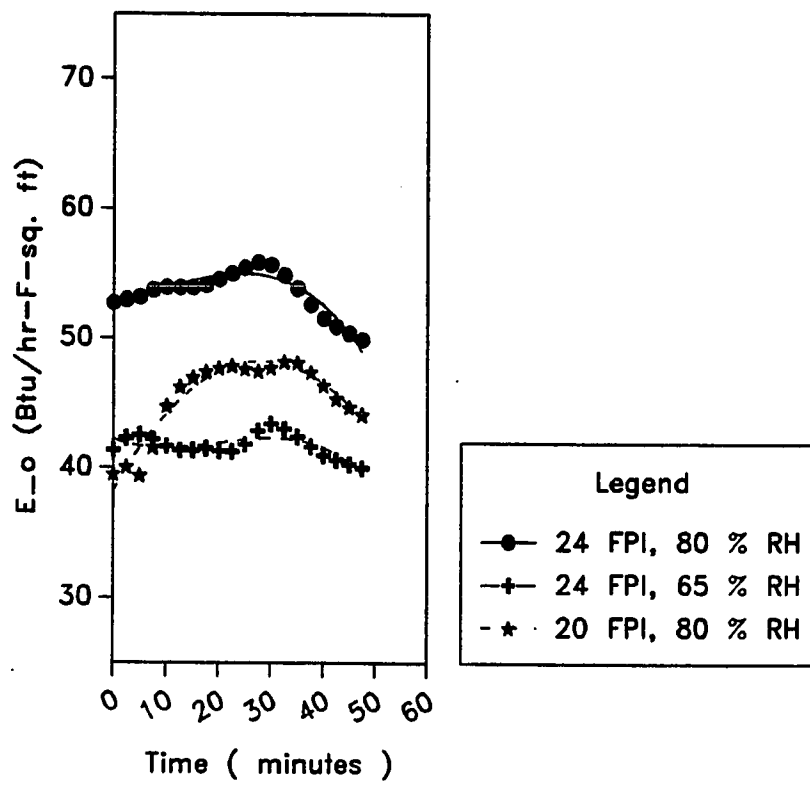


Figure 5.22 Energy Transfer Coefficient for Spine Fin Geometries

The following equations define the sensible and latent energy transfer coefficients :

$$E_s \Delta i_m A_t = C_p Q_{sensible} \quad (5.2)$$

$$E_l \Delta i_m A_t = C_p Q_{latent} \quad (5.3)$$

A typical breakup in this fashion is shown in Figure 5.23. For convenience, the above breakup into sensible and latent portions is presented in the form of an energy transfer coefficient with the LMED. The breakup could also be presented in the form of a fraction or any other similar form.

Initially, the sensible component goes through a slight rise, followed by a practically constant trend and with the passage of time it starts a downward trend. It would appear that the insulating effect of the frost layer begins to take effect, causing that downward trend. Similarly the latent contribution also goes through a slight rise and then remains approximately constant. Combining the two, the rise is seen more easily followed by a fall. The latent contribution forms approximately 30 % of the total energy transfer which is not a negligible amount. It would therefore appear that the latent portion of the energy transfer plays an important role in the performance of the heat exchanger coil. This is in contradiction to what Stoecker [31] had found in his study of frosting in finned refrigeration coils. He found that the latent contribution was less than 5 % and therefore presented his results as a sensible heat transfer coefficient instead of a combined sensible and latent energy transfer coefficient.

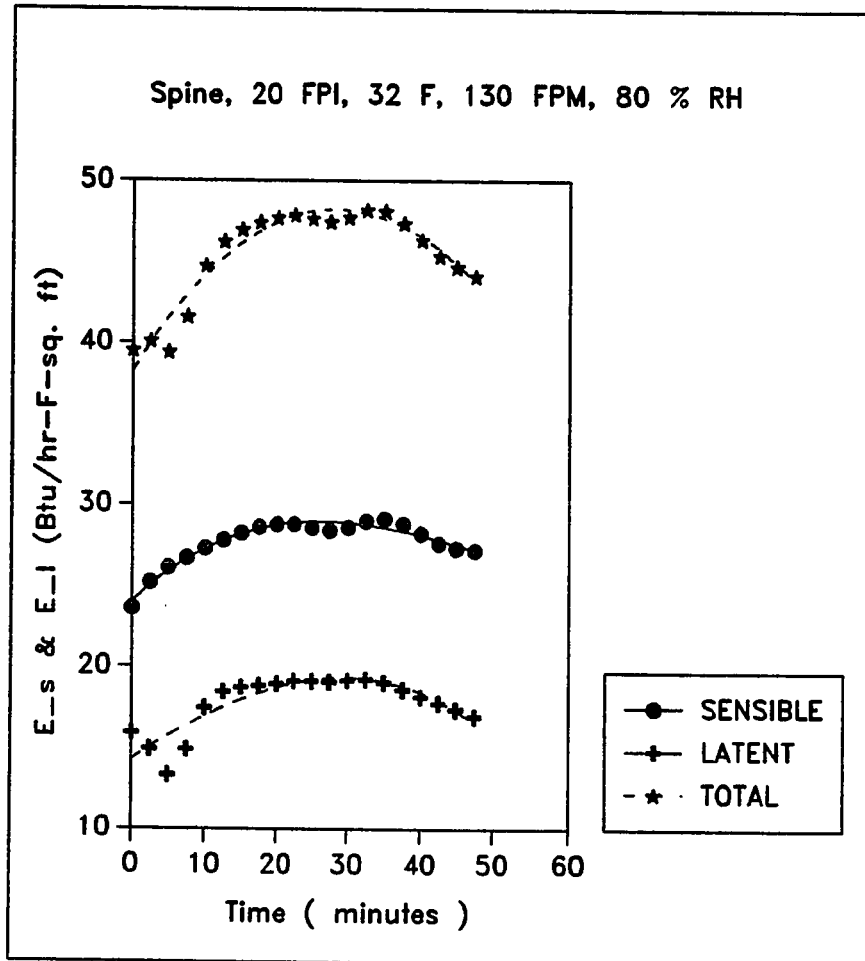


Figure 5.23 Sensible and Latent Energy Transfer Coefficients

Another way to present the data is to look at the energy transfer coefficient in a non-dimensional manner. This can be done by defining a non-dimensional energy transfer coefficient with respect to a dry coil (non frosting case) in the following manner :

$$E^* = \frac{E_o}{E_{dry}} \quad (5.4)$$

where the dry energy transfer coefficient is similarly defined as the frosted case (Eq. (5.1)) with the test being performed under dry conditions (no frosting). The above non-dimensional parameter is a form of normalization with respect to standard dry (non - frosting) conditions. Such information is very important in that it gives a clearer picture of the performance degradation of the heat exchangers with respect to the the dry case.

The trends seen in the dimensionless energy transfer coefficient, E^* are the same as the dimensional case (Figures 5.24 through 5.28). In general, the dimensionless overall energy transfer coefficient increases by 20 to 30 % over the dry case but this drops down to 10 % after about an hour of frosting.

Figure 5.27 is a comparison of the various fin types on a common ground. The louvered fin type has the poorest performance in relation to the other fin types. The flat fin type performs the best on a normalized basis and the wavy fin and corrugated fin types lie in between. It appears that the dry heat transfer coefficient is part of the reason behind such a trend, since the flat fin type has the least dry heat transfer coefficient and the louvered fin type the maximum. In addition it appears that the increase in localized turbulence due to the increased surface

Sine Wave, 18 FPI, 32 F, 130 FPM

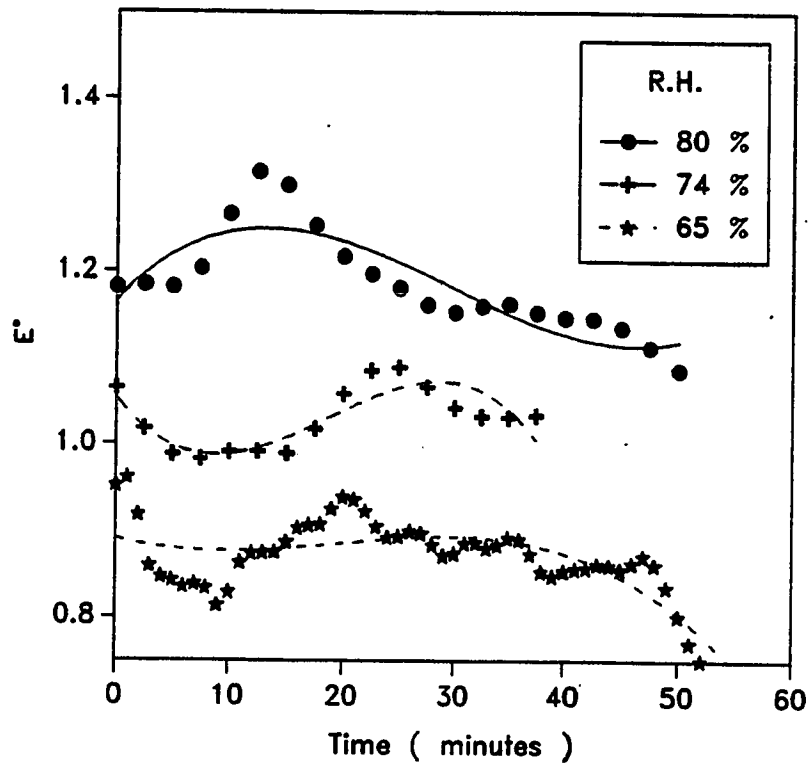


Figure 5.24 Effect of Humidity on Dimensionless Energy Transfer Coefficient

Flat, 18 FPI, 130 FPM, 32 F, 80 % R.H.

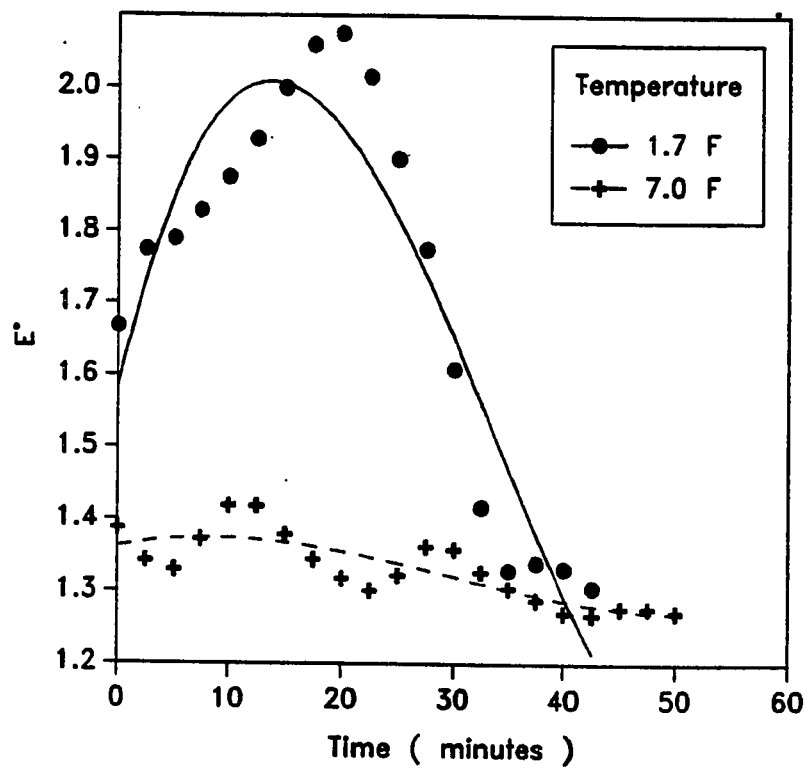


Figure 5.25 Effect of Refrigerant Temperature on
Dimensionless Energy Transfer Coefficient

Corrugated, 18 FPI, 130 FPM, 80 % R.H.

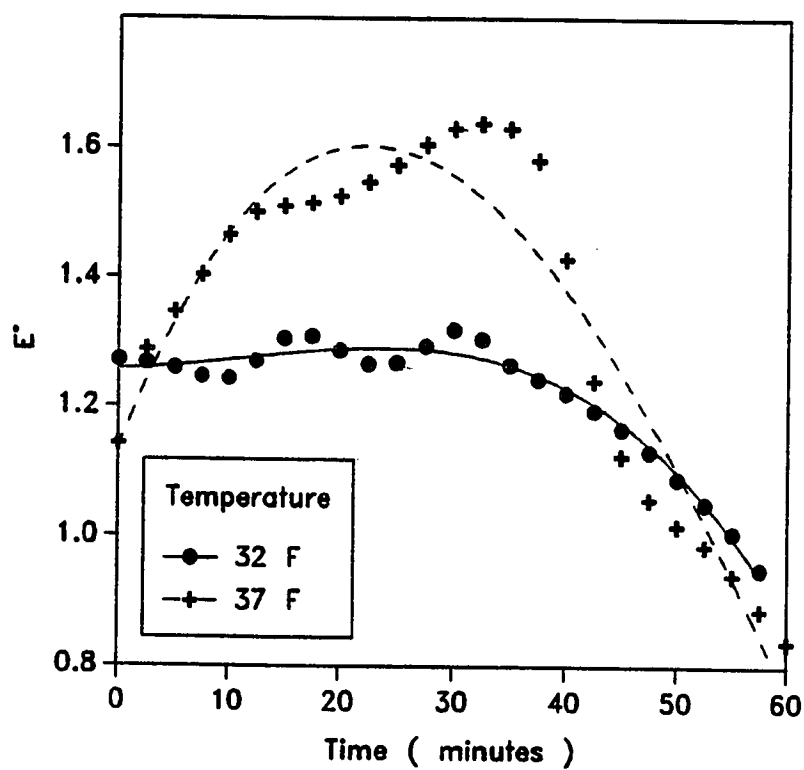


Figure 5.26 Effect of Air Temperature on Dimensionless Energy Transfer Coefficient

18 FPI, 130 FPM, 32 F, 80 % R.H.

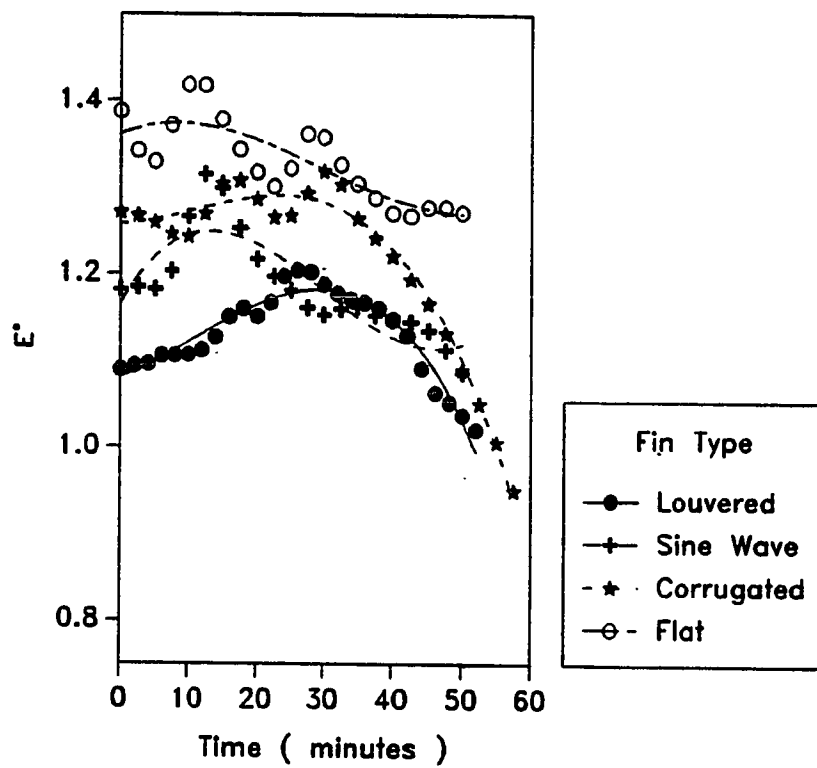


Figure 5.27 Dimensionless Energy Transfer Coefficient
for Different Fin Geometries

Spine Fin, 130 FPM, 32 F, 80 % R.H.

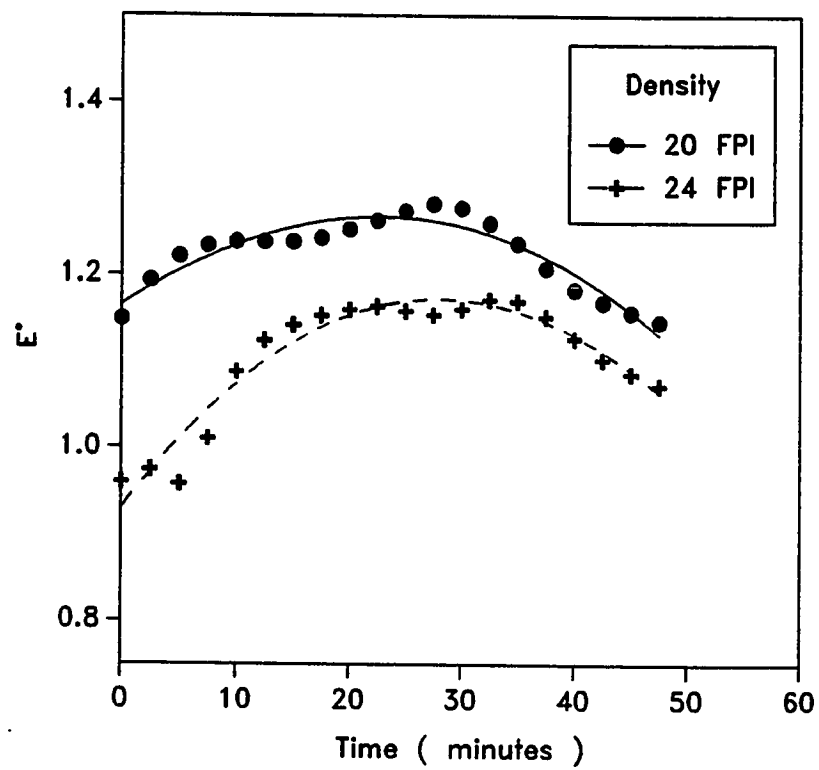


Figure 5.28 Dimensionless Energy Transfer Coefficient for Spine Fin Geometries

roughness of the frost has a greater impact on the flat fin than the louvered fin. Ostensibly, this behavior could be attributed to the fact that the presence of slits and perforations on the louvered fins already increase the localized turbulence and the additional turbulence afforded by the frost does not have much of a perceivable impact on the energy transfer. Whereas in the case of the flat, wavy and corrugated fins, the additional turbulence due to the frost enhances the energy transfer.

The following preliminary conclusions can be drawn from the above discussion :

1. Frosting results in an initial increase in the overall energy transfer coefficient, E_o , followed by a decrease. Therefore, any process in which increased frosting occurs (such as increased humidity or decreased refrigerant temperature) will lead to an initially higher energy transfer coefficient. This can be attributed to the initial increase in latent energy transfer which is later compensated by a drop in the sensible energy transfer.
2. The louvered fin type has the highest energy transfer coefficient in an absolute sense when compared with the other fin types. The flat fin type has the least value of E_o .
3. On a normalized basis, when compared on a common ground of dimensionless energy transfer coefficients, E^* , the trend is exactly reversed. It would appear therefore, that the louvered fin type has the poorest performance with respect to other fin types. The flat fin type has the best performance on this scale.

The above information is useful from a practical viewpoint. In terms of

absolute heat and mass transfer performance, the louvered fin type appears to be the best. However, on a relative scale, the flat fin type is the best.

Dimensionless Sensible Heat Transfer Coefficient, U^*

Another variable which is of interest in evaluating the performance of the heat exchangers is the sensible heat transfer coefficient. Using the standard approach of a Logarithmic Mean Temperature Difference (LMTD), and the dry heat transfer coefficient, one can define a dimensionless coefficient :

$$U^* = \frac{U_s}{U_{dry}} \quad (5.5)$$

where,

$$U_s \Delta T_m A_t = Q_{sensible} \quad (5.6)$$

The effects of humidity on the dimensionless sensible heat transfer coefficient, U^* are given in Figure 5.29. It is seen that an increase in humidity results in an increase in the sensible heat transfer. This can be possibly explained by the increased surface area and surface roughness due to more frost. However, the difference is within 10 % and could be a function of the experimental conditions.

Figure 5.30 shows the effect of a higher approaching air temperature on the dimensionless sensible heat transfer coefficient, U^* . There is an increase in the thermal driving potential between the air and the refrigerant which could explain the slightly higher heat transfer coefficient at higher temperatures. The more rapid decline of U^* at 37 ° F, when compared to the case at 32 ° F, can be attributed to the increased insulating effect of the frost.

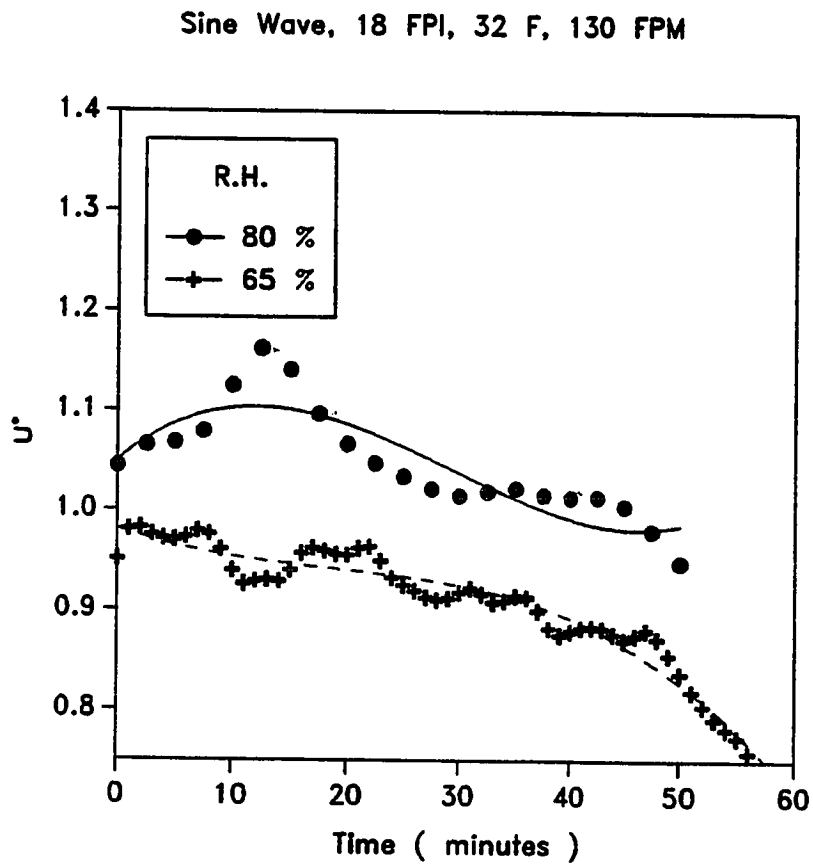


Figure 5.29 Effect of Humidity on Dimensionless Sensible Heat Transfer Coefficient

Corrugated, 18 FPI, 130 FPM, 80 % R.H.

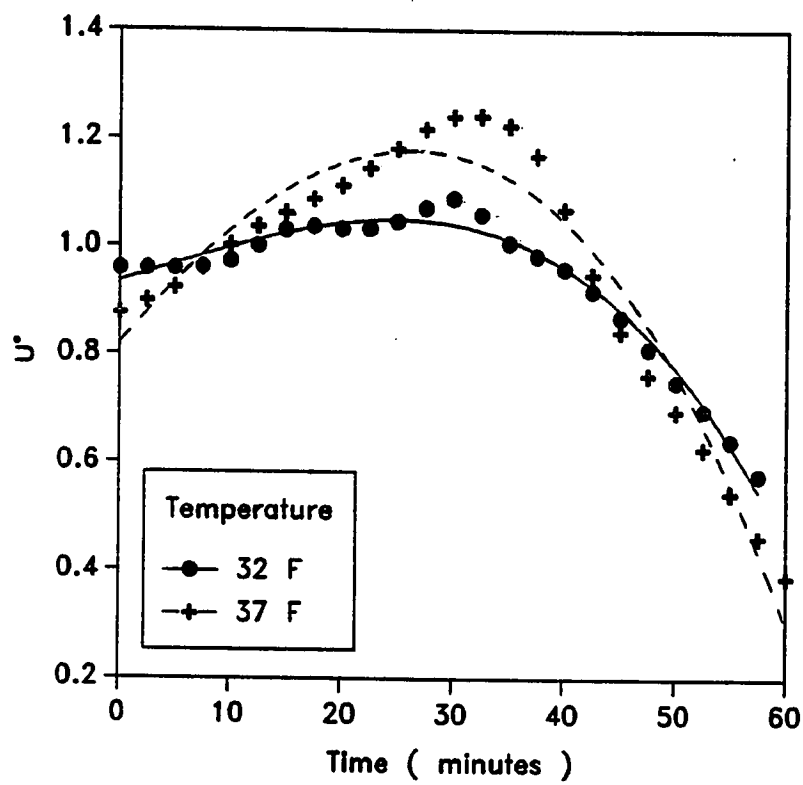


Figure 5.30 Effect of Air Temperature on Dimensionless Sensible Heat Transfer Coefficient

When the refrigerant temperature is decreased, the amount of sensible heat transfer increases dramatically until the insulating effect of the increased frost produces a rapid decline in U^* . This trend is shown in Figure 5.31.

A comparison of the dimensionless sensible heat transfer coefficient, U^* , for the different plate fin types is shown in Figure 5.32. The flat fins appear to consistently have the highest U^* , with the louvered and corrugated fin types having the lowest U^* . However, these values are very close together and a definitive conclusion is difficult to draw.

Figure 5.33 shows the dimensionless heat transfer coefficients for the spine fin geometries. There is some rise followed by a drop in all the cases. This is similar to what has been generally reported in the literature for all fin types.

It would therefore appear that the onset of frosting has a definite impact on the sensible heat transfer process. The following preliminary conclusions can be drawn :

1. The effect of an increased thermal potential between the air and refrigerant results in an increased heat transfer coefficient. This also results in an increased amount of frosting and therefore, U^* tends to have a much steeper fall.
2. There is an increase in the dimensionless heat transfer coefficient, U^* , which can be ostensibly explained by the increase in surface area and roughness of the frost layer. This is followed by a drop in U^* because of the insulating effect of the frost. Typically, U^* rises by about 10 to 20 % of its initial value before beginning to drop.
3. Not much can be concluded from a comparison of the different fin types. It

Flat, 18 FPI, 130 FPM, 32 F, 80 % R.H.

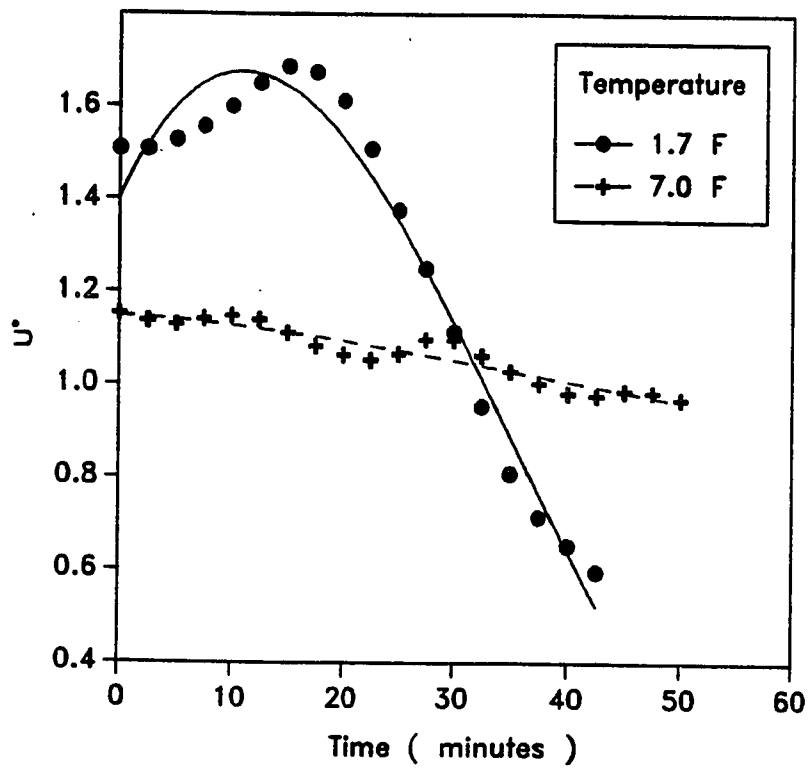


Figure 5.31 Effect of Refrigerant Temperature on Dimensionless Sensible Heat Transfer Coefficient

18 FPI, 130 FPM, 32 F, 80 % R.H.

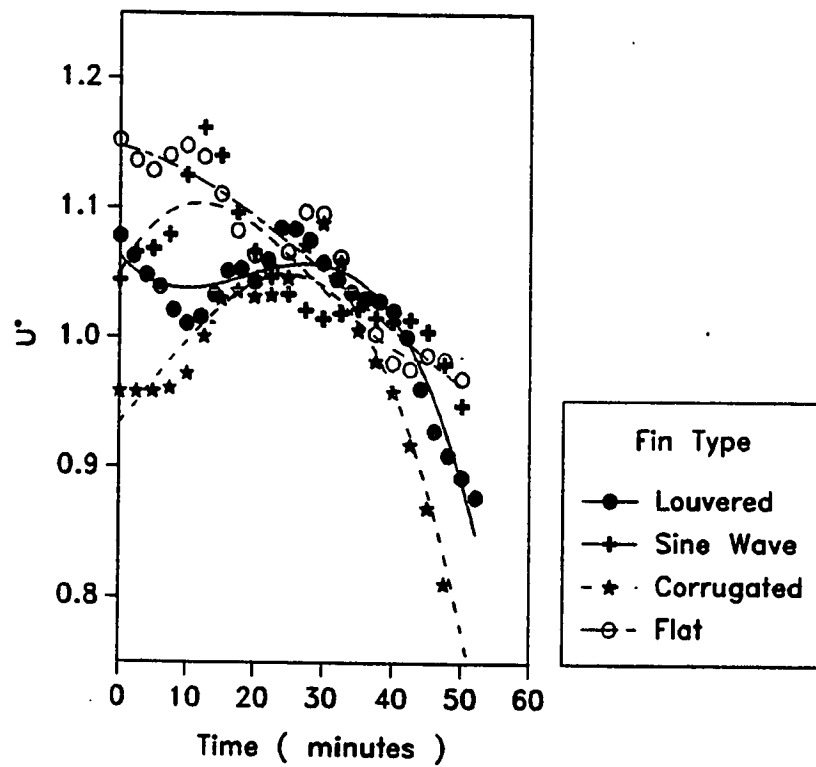


Figure 5.32 Dimensionless Sensible Heat Transfer Coefficient
for Different Fin Geometries

Spine Fin, 130 FPM, 32 F, 80 % R.H.

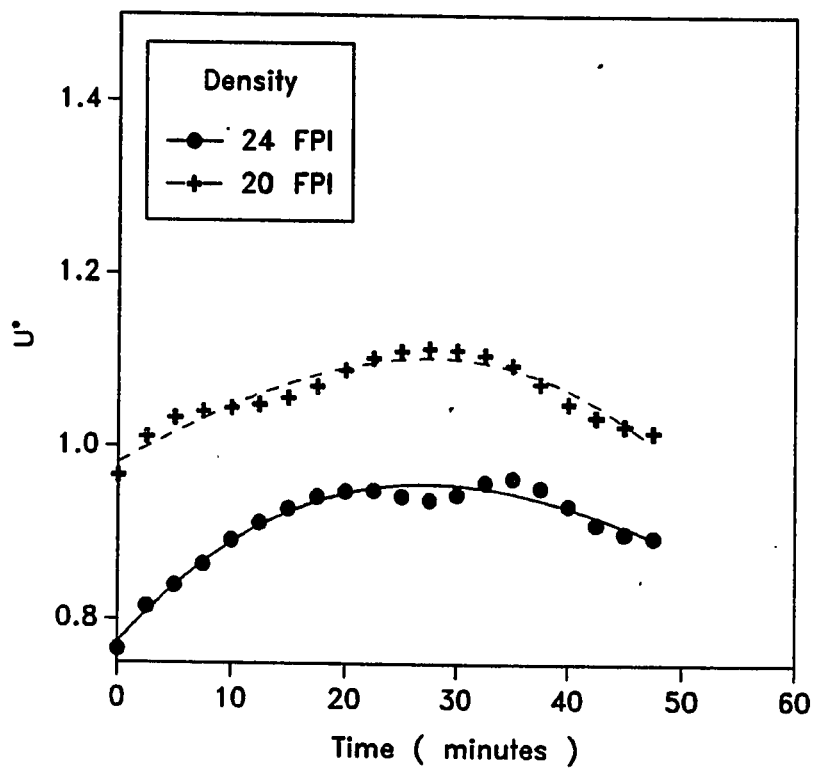


Figure 5.33 Dimensionless Sensible Heat Transfer Coefficient
for Spine Fin Geometries

would appear that the flat fin type has a better relative performance than the louvered fin type.

Heat Exchanger Effectiveness, ϵ

Heat exchanger effectiveness, ϵ , is another common method of evaluating the performance of coils. The effectiveness is defined as the ratio of the actual heat transfer to that of the maximum possible heat transfer. It is defined by the following equation :

$$\epsilon = \frac{C_h(T_{hi} - T_{he})}{C_{min}(T_{hi} - T_{ci})} \quad (5.7)$$

where,

C_h = Thermal mass capacity of hot fluid (Btu/° F)

C_{min} = Minimum thermal mass capacity (Btu/° F)

If the mass capacity of the hot fluid is the smaller of the two thermal mass capacities, the above expression reduces to :

$$\epsilon = \frac{(T_{hi} - T_{he})}{(T_{hi} - T_{ci})} \quad (5.8)$$

Instead of the above approach, considering the combined latent and sensible heat transfer occurring during frosting, the above expression can be modified using enthalpies :

$$\epsilon = \frac{(i_{hi} - i_{he})}{(i_{hi} - i_{ci})} \quad (5.9)$$

This expression was used to evaluate the effectiveness of the various heat exchangers tested. Figures 5.34 through 5.40 reflect the results obtained from the above approach.

The effectiveness of the heat exchanger increases with humidity (Figure 5.34). When more frost forms on a coil, the enthalpy difference of the air across the coil (upstream and downstream of the coil) is much more, since more latent energy transfer occurs.

Figures 5.35 and 5.36 reflect the effect of increased air temperature and a lower refrigerant temperature on the effectiveness of the heat exchangers. As has been said before, the effects of the above parameters is twofold. There is the effect of an increased thermal driving potential and frost. Together, they contribute to an increase in the enthalpy difference across the coil. There is also a steeper drop in the effectiveness relative to the base case. This is because of a drop in the sensible energy transfer.

Increasing the face velocity decreased the effectiveness (Figure 5.37). Initially this result appears contradictory but can be explained quite simply. For larger air flow rates, the amount of energy transferred across a coil is more than that with a lower air flow rate but the heat transfer rate per unit mass is less. Although the effectiveness of the heat exchanger drops as a result of the increased air flow, the overall heat transfer actually increases.

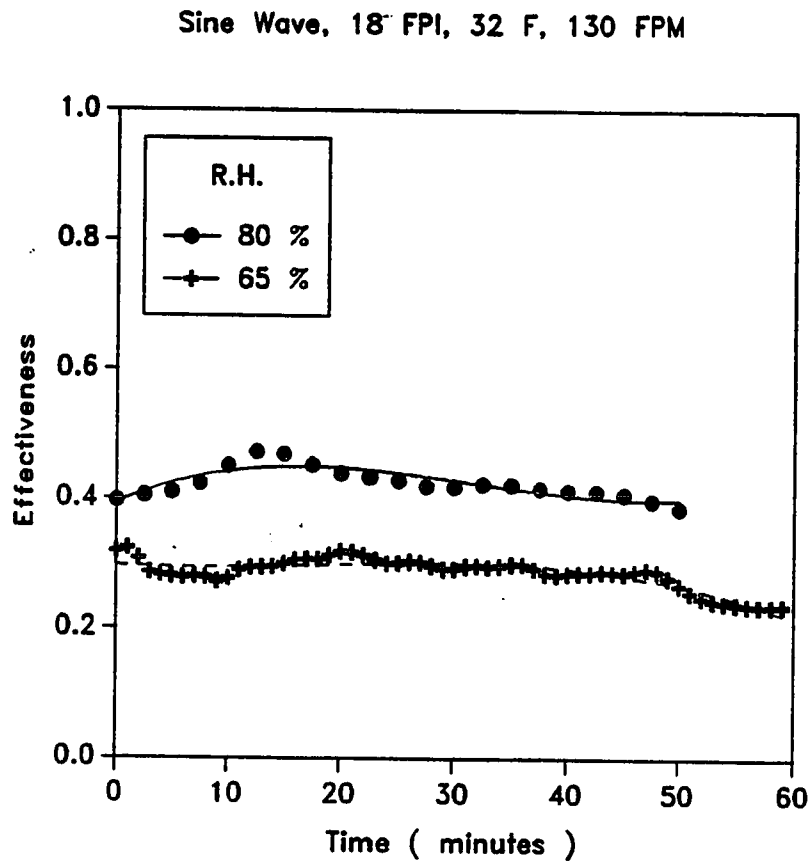


Figure 5.34 Effect of Humidity on Effectiveness

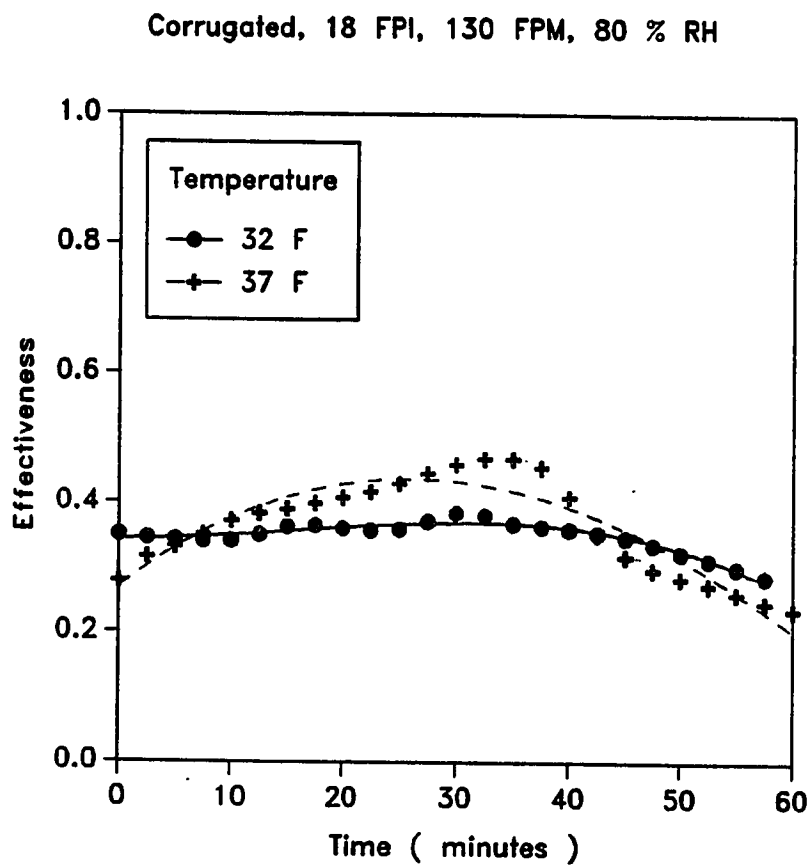


Figure 5.35 Effect of Air Temperature on Effectiveness

Flat, 18 FPI, 130 FPM, 32 F, 80 % R.H.

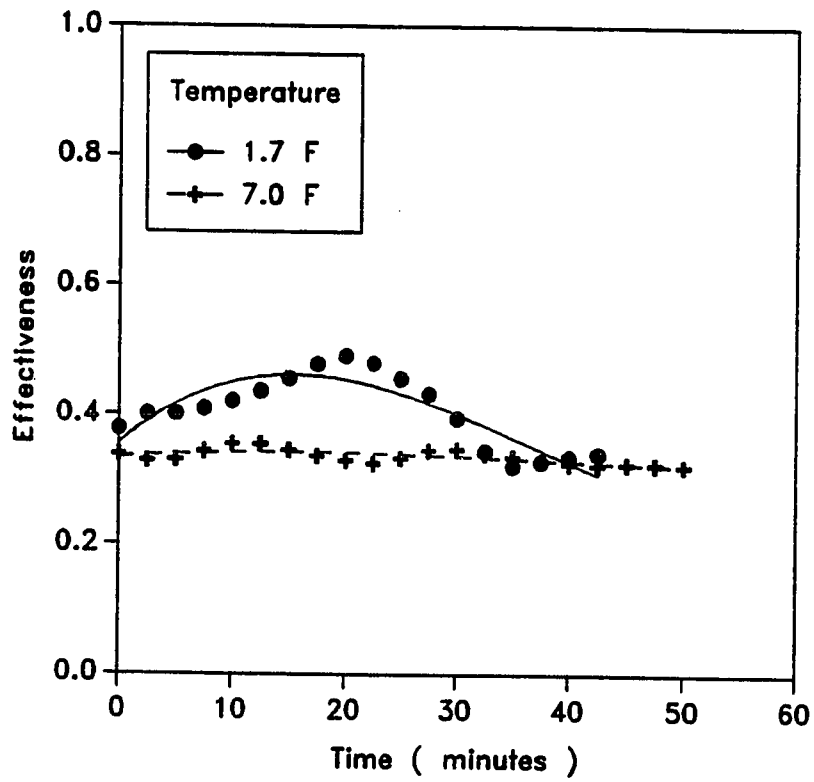


Figure 5.36 Effect of Refrigerant Temperature on Effectiveness

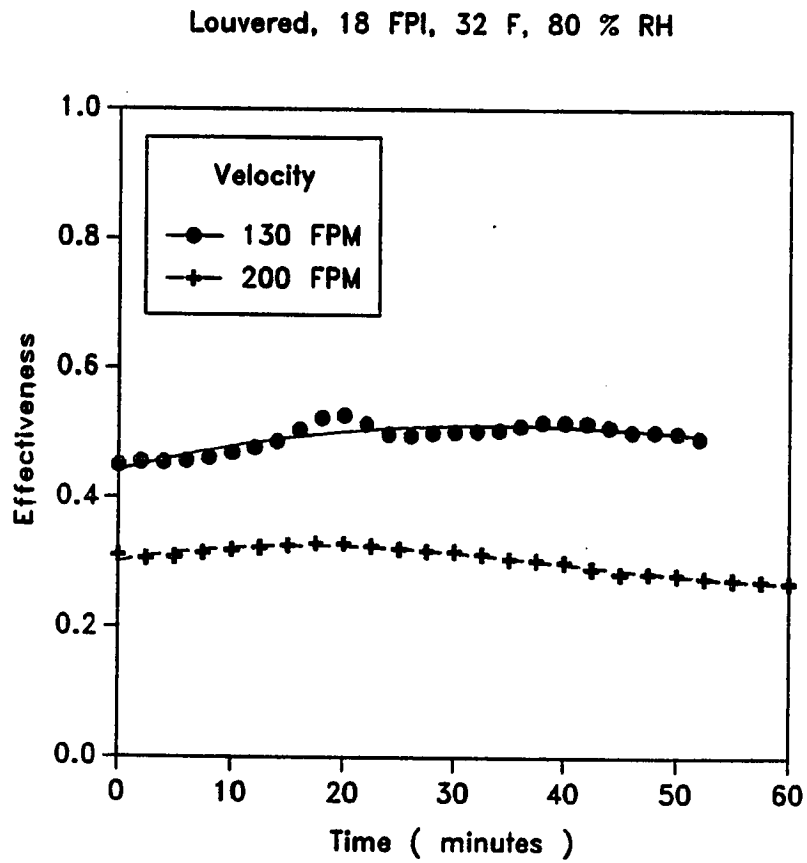


Figure 5.37 Effect of Air Face Velocity on Effectiveness

Increasing the fin density resulted in an increased effectiveness (Figure 5.38). There is almost a 50 % difference between the effectiveness of the 18 FPI and 10 FPI heat exchangers.

The effectiveness of the louvered fin is the maximum when compared to the other fin types (Figure 5.39). The flat fin has the lowest effectiveness. In general, the effectiveness goes through a slight rise followed by a decrease, similar to the trends observed in the energy transfer coefficient, E_o . The reasons for this behavior can be attributed to the latent energy contribution which causes the rise and the drop in sensible contribution which causes the decline.

Figure 5.40 shows the effectiveness for spine fins and the trends are similar to those of the other coils. The values of the effectiveness are low, ostensibly because the test coils have only one row of tubes and the fins are very small. This can be seen from the overall dimensions of the heat exchangers presented in Appendix C. To date, there is no literature available which reflects effectiveness of heat exchangers under frosting conditions.

The following conclusions can be drawn based on the above observations :

1. The effectiveness of the heat exchangers have similar trends to that of the overall energy transfer coefficient, E_o .
2. The effectiveness is a strong function of the amount of frost accumulation, fin spacing, humidity and the thermal driving potential.

D. CONCLUSIONS

In this chapter, the experimental results have been presented and discussed.

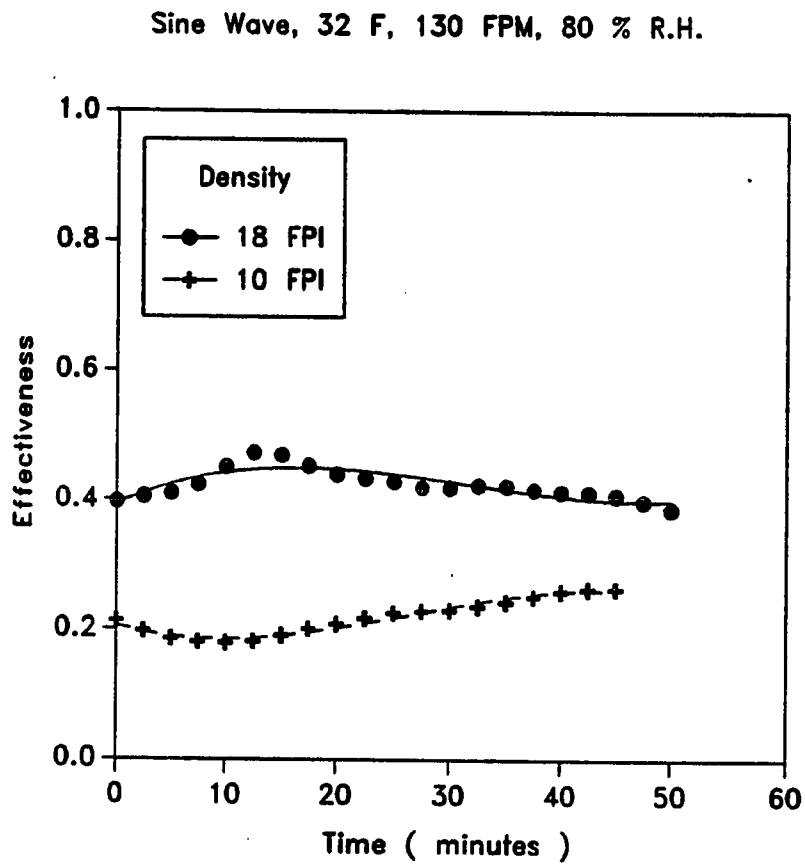


Figure 5.38 Effect of Fin Spacing on Effectiveness

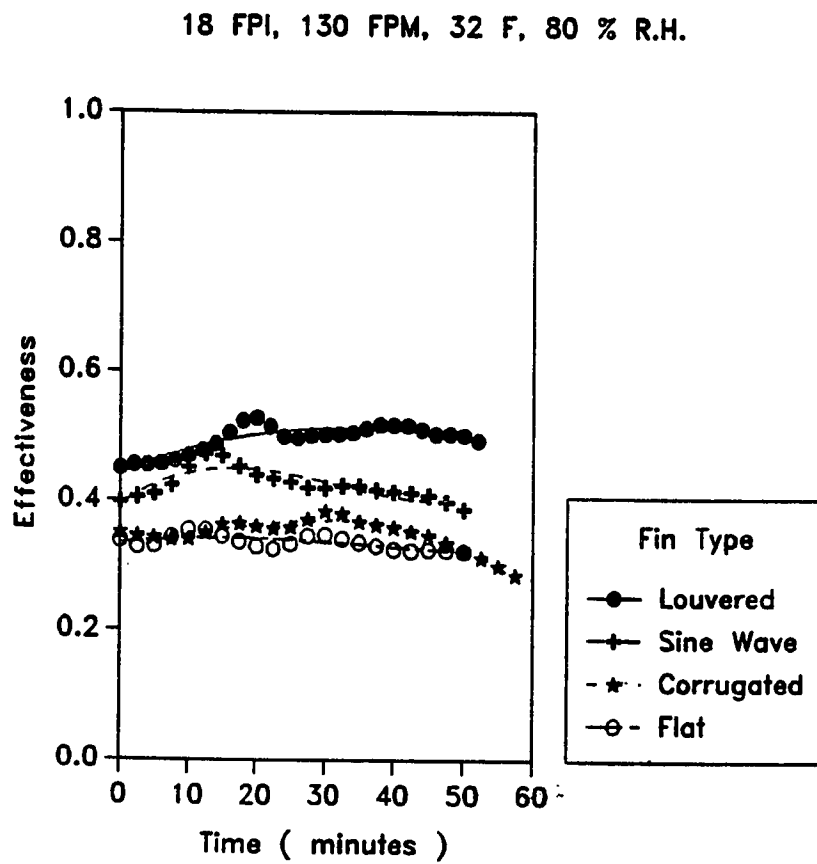


Figure 5.39 Effectiveness for Different Fin Geometries

Spine Fin, 130 FPM, 32 F, 80 % R.H.

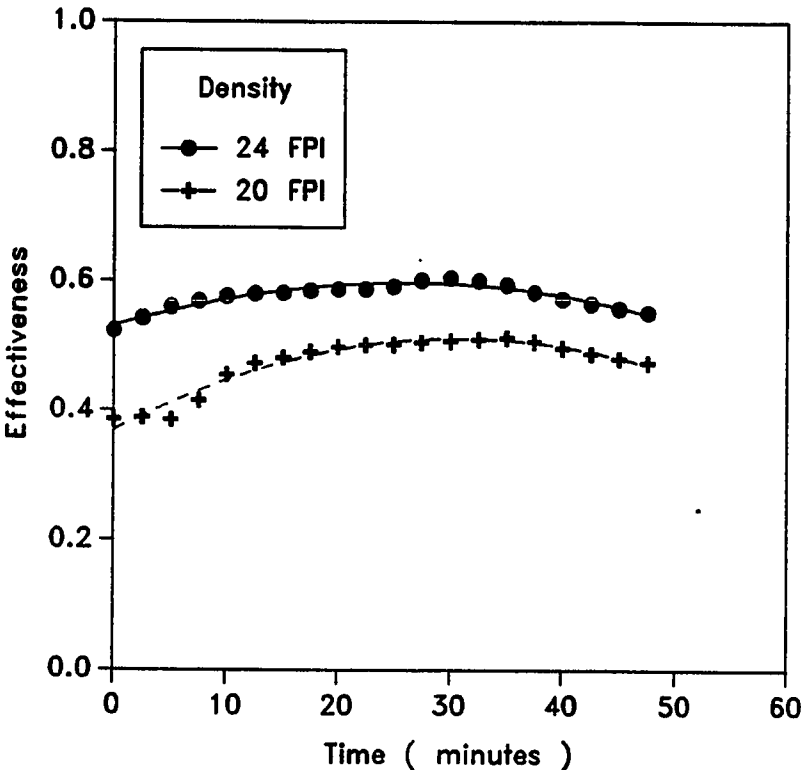


Figure 5.40 Effectiveness for Spine Fin Geometries

The effects of the various environmental conditions and fin geometries on frost growth, pressure drops, energy transfer coefficients – dimensional and non-dimensional and effectiveness of the heat exchangers have been presented.

Wherever possible, the results have been qualitatively compared with what has been reported in literature. In general, the experimental results from the present study compare well with what has been reported by other investigators. However, since previous studies have been based on flat fin geometries, the comparisons are qualitative.

New information for different fin geometries as well as some new terms (with respect to frosting conditions) such as energy transfer coefficient, E_o , heat exchanger (dimensional and non-dimensional) and effectiveness, ϵ , have also been presented.

CHAPTER VI

COMPARISON OF EXPERIMENTAL RESULTS WITH MODEL

In this chapter, the experimental results are compared to those predicted by the analytical model. General trends are discussed and discrepancies explained. In addition, the shortcomings and possible improvements to the model are suggested.

The following variables are of interest in terms of comparing the model with the experimental results :

1. Frost Growth
2. Pressure Drop
3. Energy Transfer Coefficient
4. Enthalpy Drop
5. Heat Exchanger Effectiveness

These will be discussed relative to humidity, air and refrigerant temperatures, air velocity and fin spacing. Comparisons are made for an 18 FPI coil at 32 ° F, 130 FPM air velocity, 80 % RH with a refrigerant temperature of 5 ° F.

It should be noted that in the comparisons which follow, the scales on the graphs have been exploded in order to give a close up view of the trends. This leads to an illusionary effect that the discrepancies between the model and experimental results are very large. In reality, the results compare within 15 to 20 % of each other.

A. FROST GROWTH

It has been seen in the experimental results that a higher humidity, a higher air temperature, a higher air velocity, a smaller fin spacing and a lower refrigerant temperature lead to more frost growth. The trends as predicted by the model are similar.

It is difficult to get an estimate of frost height from the experimental results because the breakup of the mass into the density and growth components is not known. In addition, the heat exchanger fin geometry adds to the complexity of the problem. Therefore, any quantitative comparisons must be made in mass of frost. Figure 6.1 shows the comparison between the experiment and the model. After about an hour, the model underpredicts the experimental value by approximately 12 %, which is quite good considering the above cited reasons.

B. PRESSURE DROP ACROSS THE COILS

The presence of frost results in a reduced free flow area which leads to an increase in the pressure drop across the coil. Therefore, the variables which cause more frost growth indirectly cause a higher pressure drop. In addition, a higher air velocity and a smaller fin spacing contribute to a higher pressure drop. These trends are reflected both in the experimental results and the model. Figure 6.2 shows the comparison between the model and the experiment. It is seen that the values are within 10 % even after 1 hour.

Flat Fin, 32 F, 130 FPM, 18 FPI, 80 % RH

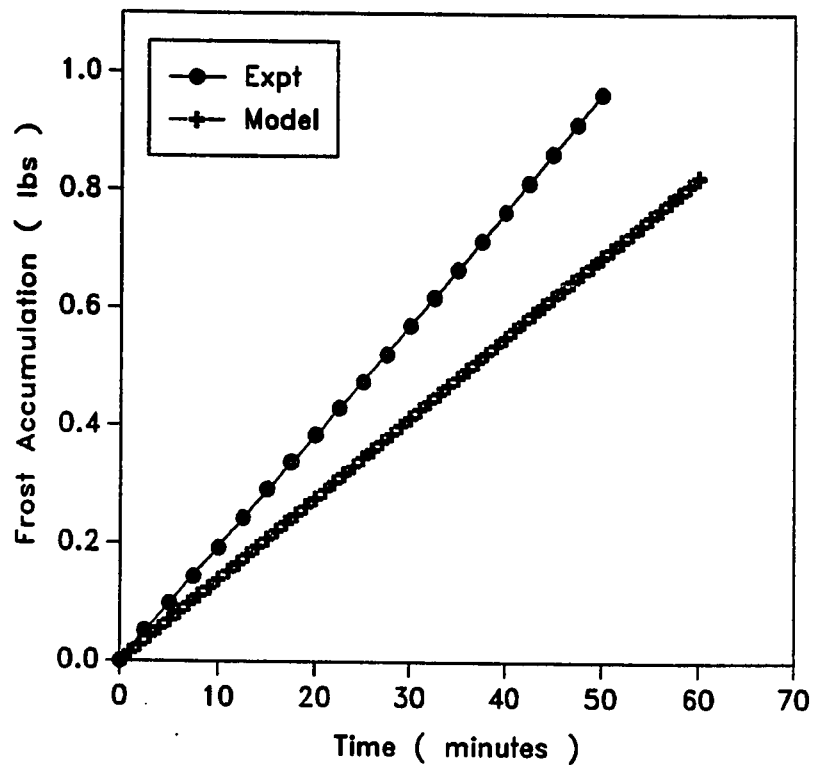


Figure 6.1 Frost Growth : Comparison between Model and Experiment

Flat Fin, 32 F, 130 FPM, 18 FPI, 80 % RH

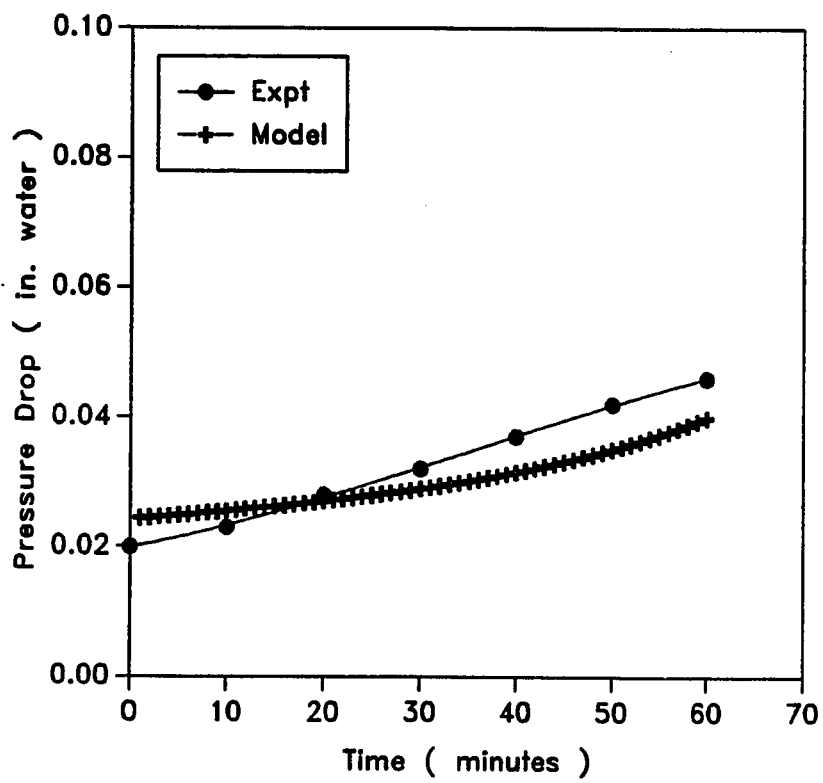


Figure 6.2 Pressure Drop : Comparison between Model and Experiment

C. ENERGY TRANSFER COEFFICIENT

The energy transfer coefficient, E_o , increases with humidity, air velocity, air temperature, lower refrigerant temperature and smaller fin spacing. The reasons for this functional relationship has already been discussed in earlier chapters. Both the model and the experimental work reflect the above trends except for humidity.

A major limitation of the model is the inability to predict the rise in the energy transfer coefficient which is seen in the experimental results. Possible modifications to that have been suggested in Chapter IV, which would allow for that rise to be predicted. Therefore, the model only shows a monotonically decreasing trend due to the presence of more and more frost. A better handle on the air side heat transfer in the presence of frost in laminar flow would dramatically improve the quality of the model.

The experimental work has shown that increasing humidity leads to a higher energy transfer coefficient. The coefficient initially increases with humidity and then drops as the frost insulates the surface of the heat exchanger from the warmer air. However, the model predicts that a higher humidity leads to a lower energy transfer coefficient which monotonically decreases with frost growth.

The air side heat transfer coefficient is a strong function of how wet the surface of the coil. Mcquiston and Parker [27] have reported that the air side heat transfer increases by 20 to 30 % as a result of wetting the coil. Therefore, if the air side heat transfer coefficient increases for a wet coil, the overall energy transfer coefficient will also increase.

The correlation for the air side heat transfer used in the model is that for a dry coil undergoing only sensible (dry) heat transfer. Since a wet coil typically has a higher h_a than a dry coil, it is easy to see that if the value of h_a in the model was multiplied by some correction factor to account for the wetness of the coil surface, the model will be able to obtain trends similar to that found from the experiments. Therefore, an appropriate modification to the correlation for the air side heat transfer coefficient would be to incorporate the effect of moisture and possibly surface roughness.

Figure 6.3 compares the energy transfer coefficients of the model and the experimental results at the conditions mentioned earlier. The values from the model are within 15 % of the experimental results. At other humidity levels, the difference between the model and experimental values is much more.

D. OTHER RESULTS

The enthalpy drop across the coil and the heat exchanger effectiveness are two important parameters which are strong functions of the latent energy process (mass transfer / frost growth) as well as humidity, air and refrigerant temperatures and fin spacing. Even though the energy transfer coefficient does not increase with humidity in the model, the enthalpy drop across the coil increases with humidity due to the additional latent heat transfer. This is because the enthalpy is a strong function of the moisture content in the air. Figures 6.4 and 6.5 compare the total enthalpy drop per unit time and the heat exchanger effectiveness between the model and the experimental results. There is about 10 % difference between the model and the experimental values for the enthalpy drop. However, for the

Flat Fin, 32 F, 130 FPM, 18 FPI, 80 % RH

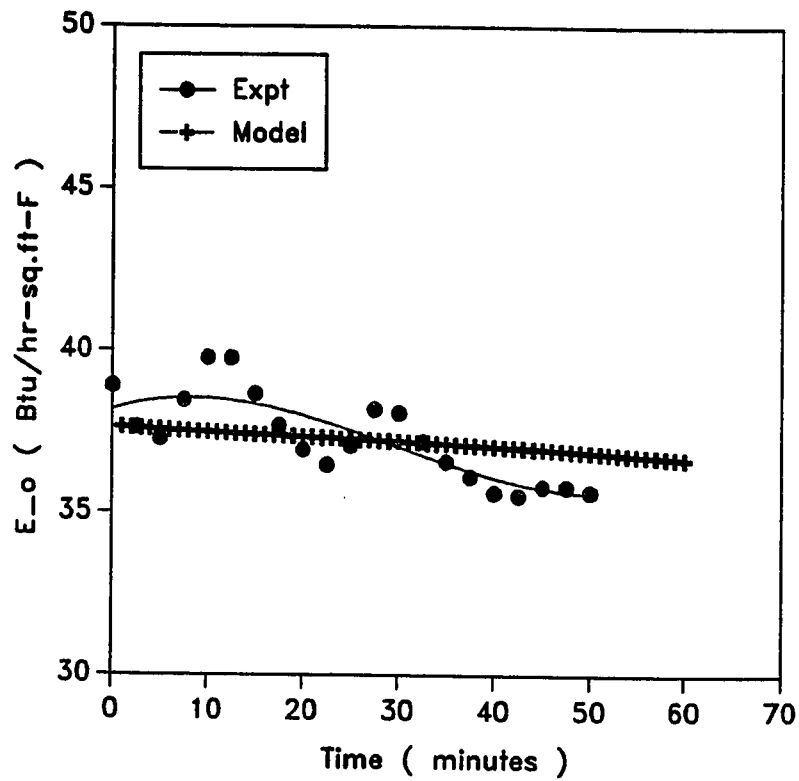


Figure 6.3 Energy Transfer Coefficient : Comparison between
Model and Experiment

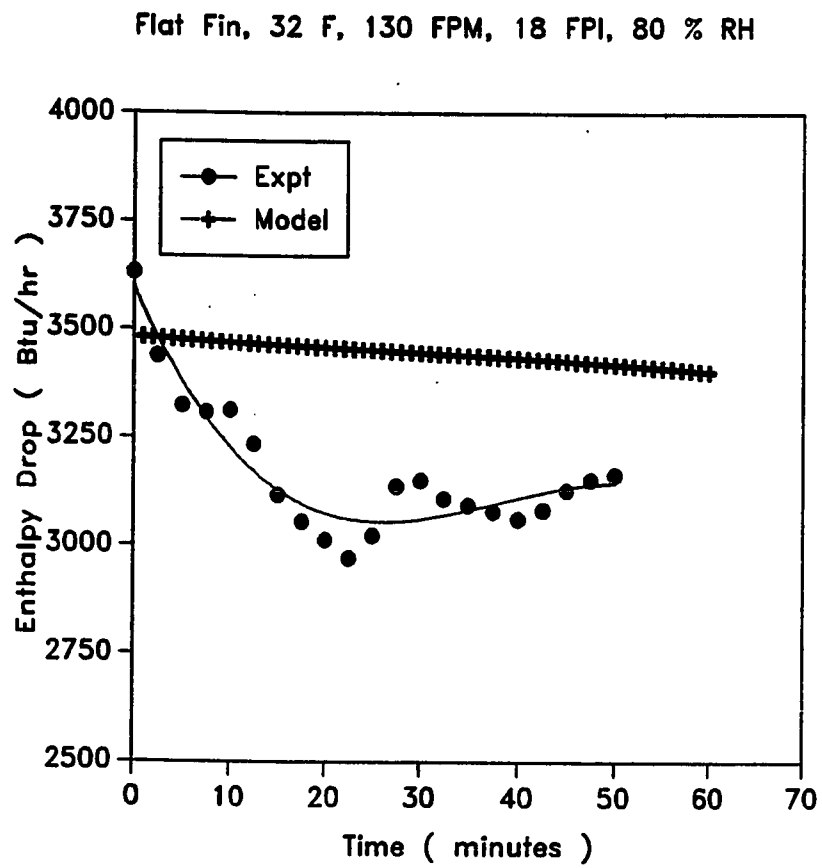


Figure 6.4 Enthalpy Drop : Comparison between Model and Experiment

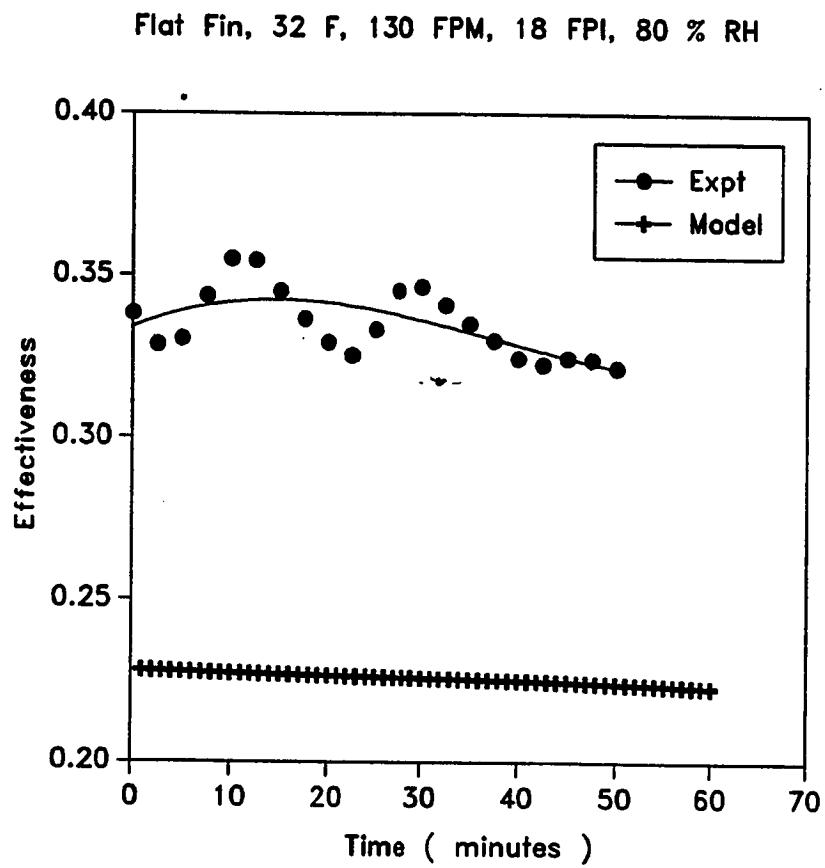


Figure 6.5 Effectiveness : Comparison between Model and Experiment

effectiveness there is a much greater (25 %) error.

E. SUGGESTED IMPROVEMENTS

Improvements in the present status of the analytical model can be made and modifications implemented. The air side heat transfer and fin geometry are the important parameters to consider.

The predictive value of the model can be improved considerably if a better air side heat transfer correlation in the presence of frost is determined. It is beyond the scope of the present study to develop such a correlation but is recommended for future work. One important aspect which must be addressed is the transient nature of the heat transfer process. The air side heat transfer is not only a function of the geometry, ambient conditions and frost surface roughness, but also time, since all the conditions such as the Reynolds Number and spacing between the fins (free flow area) constantly change with time as the frost grows.

At present only flat plate fin geometries can be modelled. If other fin types such as corrugated, wavy, louvered or spine fins could be included, the utility of the model would be greatly enhanced. Part of the problem is the complexity of the geometry but the primary problem will again be to develop a good air side heat transfer correlation for the various geometries in the presence of the frost under laminar flow.

In general, the model correlates well with the experimental results. The general trends are similar except for a few such as the effect of humidity on the energy transfer coefficient. The reasons for the differences in the

trends have been discussed and explained. It appears that a better quantification of the air side heat transfer would enable the model to be very useful in its prediction of heat exchanger performance in the presence of frost.

CHAPTER VII

CONCLUSIONS AND RECOMMENDATIONS

The effects of frost formation on the performance of finned tube heat exchangers under laminar flow conditions have been studied both experimentally and analytically. The conclusions drawn from this study are presented and discussed in this chapter. The limitations and drawbacks of the investigation as well as recommendations for future work are also presented.

A. CONCLUSIONS

Frost formation on finned heat exchangers is a very complex process with many variables. These include the environmental parameters such as air humidity, air flow velocity, air temperature, refrigerant temperature and heat exchanger geometry such as fin type and spacing. The parameters studied include frost growth, pressure drop across the coils, energy transfer coefficient (dimensional and non-dimensional) and heat exchanger effectiveness.

Frost degrades the performance of finned tube heat exchangers over a period of time. Initially, the presence of frost actually enhances the thermal performance of the heat exchangers leading to the conclusion that some frost is not altogether undesirable. However, with time, it degrades performance because of its insulating layer.

Experimental Results

The following generalized conclusions may be drawn from the experimental

work :

1. Frost growth is a strong function of the fin geometry and environmental conditions. The important factors include the humidity of the air, the air temperature, the refrigerant temperature, the air flow rate, the fin type and spacing.

Humidity is one of the dominant factors governing frost growth. Increasing the humidity increases the frost growth for the temperatures studied. Lowering the refrigerant temperatures and increasing the air flow rates also increases frost growth. The increased growth results from an increased mass transfer potential between the heat exchanger surface and the air.

The louvered fin has the maximum frost accumulation under similar conditions when compared to the other fins. The wavy, corrugated and flat fins have a lower frost growth. The flat fin type has the lowest frost growth. The total surface area for heat and mass transfer appears to be the single biggest factor affecting the frost growth. The louvered fin has the maximum surface area and the flat fin the least. Increasing the surface area to enhance heat transfer also increases the mass transfer and hence more frost growth. Such a conclusion is further supported by the fact that an increasing fin density increases frost growth.

The spine fin exhibits the same trends as the other fins in terms of a higher frost growth for a higher humidity and a higher fin density.

2. Pressure Drop across the heat exchanger coils is an indication of the blockage effect. The pressure drop is not only a function of the frost growth

but is also a function of the heat exchanger geometry.

Increased frost growth produces higher pressure drops across the coils because the frost blocks air flow through the coils. Therefore, the variables which lead to an increased frost growth lead to an increased pressure drop.

Heat exchangers with a higher fin density have a higher pressure drop across them. The effect is compounded further since the amount of frost accumulating on the coils with a higher fin density is also higher. The louvered fin coil has the highest pressure drop when compared to the other plate fins.

3. An Energy Transfer Coefficient based on a logarithmic mean enthalpy difference, (LMED), has been defined to incorporate the latent energy transfer occurring during the frosting process. Increasing the fin density leads to a higher energy transfer coefficient because of a higher latent and sensible contribution. Higher air flow rates also led to a higher coefficient. Since a larger frost accumulation results in a higher latent energy transfer, the overall energy transfer coefficient increases with frost.

It was found that the long term effect of frost growth on the energy transfer coefficient is detrimental. Initially, the energy transfer coefficient increases slightly due to an increased surface area resulting from a rough frost surface, and then decreases. This decrease is attributed to the insulating effect of the frost layer which begins to control the heat transfer in the coil.

The louvered fin accumulates the maximum frost and has the largest latent energy transfer when compared to the other fins. In addition, the larger heat

transfer surface area also contributes to a higher sensible energy transfer. On an absolute scale, the louvered fin type has the highest energy transfer coefficient followed by the wavy, corrugated and flat fin types.

However, when the above information was normalized with respect to dry (no frost) conditions, the trends were exactly reversed. The flat fin type has the highest normalized (dimensionless) energy transfer coefficient and the louvered fin type the least. It would therefore appear that the louvered fin type has the maximum adverse impact on performance when compared with other fin types.

The spine fins exhibit typical behavior in energy transfer. A higher humidity and fin density leads to a higher energy transfer coefficient. The distinctive rise in E_o which occurs in the initial stages of the frost formation process is observed very clearly for this fin type.

4. A Sensible Energy Transfer Coefficient in a dimensionless form has also been calculated based on the sensible (dry) heat transfer across the heat exchanger coil and the logarithmic mean temperature difference. The coefficient as defined is dimensionless since it is normalized with respect to dry conditions.

The sensible heat transfer coefficient remains approximately constant followed by a drop due to the insulating nature of the frost. It was found that a larger thermal potential between the air and refrigerant leads to a higher heat transfer coefficient. However, this also leads to more frost accumulation and hence a steeper fall in the heat transfer coefficient.

The flat fin type has a relatively better performance on a normalized scale than the louvered fin type despite the smaller heat transfer surface area; however, the data are very close together.

5. The Effectiveness of the various heat exchangers has been determined and it was found that the effectiveness of the heat exchangers have similar trends to that of the overall energy transfer coefficient, E_o . The factors which have a strong influence on the effectiveness are the amount of frost accumulation, fin type, fin spacing, humidity and the thermal driving potential.

A higher thermal and mass transfer potential between the refrigerant and the air results in a higher effectiveness. However, an increased mass flow rate results in a lower effectiveness since the corresponding increase in energy transfer coefficient is not in the same proportion as the increase in flow rate.

A higher fin density leads to an increase in effectiveness due to the increased surface area. The louvered fin type has the highest efficiency when compared to the other fin types. It is followed by the wavy, corrugated and flat fin types. This is ostensibly because of the increased surface area possessed by the louvered fin type in relation to the other fin types.

Mathematical Model

An analytical model to simulate the performance of finned tube heat exchangers under frosting conditions has been developed from fundamental heat and mass transfer principles. The model predicts the effects of humidity, air flow, fin geometry, air and refrigerant temperatures on frost growth, energy transfer and pressure drop.

Almost all the general trends of a higher frost growth for higher humidity, air flow, fin density and lower refrigerant temperature were consistent with the experimental results. The trends for the pressure drops across the frosted coil were similar to that found in the experiments. A higher fin density and air flow rate led to a higher energy transfer coefficient in the model. However, a higher humidity did not lead to a higher energy transfer coefficient. This is in contradiction to what has been found experimentally. The coefficient as predicted by the model has a monotonically decreasing trend due to the insulating nature of the frost unlike what is observed experimentally. The reason for the above differences is the lack of a good correlation for the air side heat transfer in the presence of frost. The results from the experimental work were compared to that of the model and it was found that the predictions were within 20 % of the experimental data.

In addition to the results for frost accumulation, pressure drop and energy transfer coefficient, the model also provides a variety of other results including non-dimensional fin analysis, Effectiveness – NTU charts, the variation of the frost height along the length of the heat exchanger in the direction of air flow, and frost properties such as surface temperature, density and thermal conductivity.

A major limitation to the mathematical model is the lack of a proper correlation for the air side heat transfer coefficient in the presence of frost under laminar conditions.

B. RECOMMENDATIONS FOR FUTURE WORK

There are quite a few recommendations for future work which can be made

based on the limitations of the work performed in the present investigations.

1. The driving force behind this investigation has been the frost formation on heat pump evaporator coils. In true practice, these coils have two phase flow (refrigerant) flowing through them and not single phase flow such as the present study. A set of tests using refrigerants such as R-22 or R-502 to confirm some of the results obtained from the present study would be useful.
2. The tests which have been conducted have been only with respect to the heat exchanger itself, and not as a true evaporator coil as a component of a heat pump. Therefore, if an actual outdoor heat pump unit were to be tested with evaporator coils of different fin geometries, the results would be of much more practical use. In addition, the entire system performance in terms of the compressor, the blower and Coefficient of Performance (COP) of the unit monitored as a function of the frost accumulation and different fin geometries.
3. The coils tested were all single tube row coils and in actual practice, multi-row coils are used. The effect of multi-rows on the performance of heat exchangers under frosting is another important aspect to be considered. There has also been considerable interest in the effects of frost growth on multi-row coils with variable fin spacing.
4. The mathematical model in its present form is designed only for flat plate fin geometries. Modifications for other geometries such as louvered, corrugated, or spine fins would be very useful.

5. A major limitation of the model is the lack of air side heat transfer data in the presence of frost for these complex geometries. A better handle on this would enhance the usefulness of the model dramatically.

REFERENCES

- [1] Chen M.M. and Rosenhow W., "Heat, Mass and Momentum Transfer inside Frosted Tubes : Experiments and Theory," *Journal of Heat Transfer*, pp. 330 - 334, August 1964.
- [2] Beatty K.O. et al, "Heat Transfer from Humid Air to Metal Under Frosting Conditions," *Journal of the ASRE*, pp. 1203-1207, December 1951.
- [3] Chung P.M. and Algren A.B., "Frost Formation and Heat Transfer on a Cylinder Surface in Humid Air Cross Flow - Pt. 1," *Heating, Piping and Air-Conditioning*, pp. 21-31, September 1958.
- [4] Chung P.M. and Algren A.B., "Frost Formation and Heat Transfer on a Cylinder Surface in Humid Air Cross Flow - Pt. 2," *Heating, Piping and Air-Conditioning*, pp. 51-62, October 1958.
- [5] Kamei S. et al, "Research on the Frost Formation in a Low Temperature Cooler Condenser," *Japanese Science Review*, vol. 2, # 3, 1952.
- [6] Yamakawa N. et al, "Forced Convection Heat and Mass Transfer under Frost Conditions," *Heat Transfer Japanese Research*, vol. 1, # 2, 1972.
- [7] Yonko J.D. and Sepsy C.F., "An Investigation of the Thermal Conductivity of Frost while forming on a Flat Horizontal Plate," *ASHRAE Transactions*, vol. 73, Pt.2, 1967.
- [8] Sanders C.T., "Some Physical Aspects of Frost Formation on Cooled Surfaces," presented at the XV International Congress of Refrigeration, International Institute of Refrigeration Commissions, B2-71, 1971.
- [9] O'Neal D.L. and Tree D.R., "A Review of Frost Formation in Simple Geometries," *ASHRAE Transactions*, vol. 91, Pt. 2, 1985.
- [10] Biguria G. and Wenzel L.A., "Measurement and Correlation of Water Frost Thermal Conductivity and Density," *I & EC Fundamentals*, vol. 9, # 1, 1970.

- [11] Seki N. et al, "An Analysis of Incipient Frost Formation," *Warme- und Stoffübertragung*, pp. 19-18, # 19, 1985.
- [12] Brian P.L.T. et al, "Cryogenic Frost Properties," *Cryogenic Technology*, pp. 205 - 212, September 1969.
- [13] Brian P.L.T. et al, "Frost Deposition on Cold Surfaces," *AI&EC Fundamentals*, vol. 9, # 3, 1970.
- [14] Dietenberger M.A., "A Generalized Correlation of the Water Frost Thermal Conductivity," *International Journal of Heat and Mass Transfer*, vol. 26, # 4, 1983.
- [15] Hayashi Y. et al, "A Study of Frost Properties Correlating with Frost Formation Types," *Journal of Heat Transfer*, pp. 239 - 245, May 1977.
- [16] Schneider, H.W., "Equation of the Growth Rate of Frost Forming on Cooled Surfaces," *International Journal of Heat and Mass Transfer*, vol. 21, # 3, 1978.
- [17] O'Neal D.L., "The Effects of Frost Formation on the Performance of a Parallel Plate Heat Exchanger," *Ph.D. Dissertation*, Mechanical Engineering, Purdue University, 1983.
- [18] White J.E. and Cremers C.J., "Prediction of Growth Parameters of Frost Deposits in Forced Convection," *Journal of Heat Transfer*, pp. 3 - 6, February 1981.
- [19] Jones B.W. and Parker J.D., "Frost Formation with Varying Environmental Parameters," *Journal of Heat Transfer*, pp. 255-259, May 1975.
- [20] Parish H.C. and Sepsy C.F., "A Numerical Analysis of Frost Formation under Forced Convection," *ASHRAE Transactions*, vol. 79, Pt.2, 1972.

- [21] Chuang M.C., "Frost Formation on Parallel Plates at Very Low Temperatures in a Humid Stream," *ASME Paper* , vol. 76-WA/HT-60, 1976.
- [22] Loper J.L., "Frost Formation upon a Thin Aluminium Tank Containing Liquid Oxygen," *ASHRAE Transactions*, vol. 69, 1960.
- [23] Hayashi Y. *et al*, "A Study of Frost Formation based on a Theoretical Model of the Frost Layer," *Heat Transfer Japanese Research*, vol. 6, # 3, 1977.
- [24] O'Neal D.L. and Tree D.R., "Frost Growth and Heat Transfer in a Parallel Plate Geometry," *ASME Paper*, vol. 84-WA/HT-107, 1984.
- [25] O'Neal D.L. and Tree D.R., "Measurement of Frost Growth and Density in a Parallel Plate Geometry," *ASHRAE Transactions*, vol. 90, Pt. 2, 1984.
- [26] Kays, W.M. and London A.L, *Compact Heat Exchangers*. McGraw-Hill Company, New York, 1964.
- [27] McQuiston F.C. and Parker J.D., *Heating, Ventilation and Air-Conditioning - Analysis and Design*. John Wiley and Sons, New York, 1982.
- [28] Kern D.Q. and Kraus A.D., *Extended Surface Heat Transfer*. McGraw Hill Company, New York, 1972.
- [29] Sanders C. Th., "The Influence of Frost Formation and Defrosting on the Performance of Air Coolers," *Ph.D. Dissertation*, Technische Hogeschool, Delft University - Netherlands, 1974.
- [30] Barrow H., "A Note on the Frosting of Heat Pump Evaporator Surfaces," *Journal of Heat Recovery Systems*, vol. 5, #3, 1985.

- [31] Stoecker W.F., "How Frost Formation on Coils affects Refrigeration Systems," *Refrigeration Engineering*, pp. 42-46, Feb. 1957..
- [32] Stoecker W.F., "Frost Formation on Refrigeration Coils," *ASHRAE Transactions*, vol. 66, 1960.
- [33] Hosoda T. and Uzahashi H., "Effects of Frost on the Heat Transfer Coefficient," *Hitachi Review*, vol. 16, # 6, 1967.
- [34] Niederer D.H., "Frosting and Defrosting Effects on Coil Heat Transfer," *ASHRAE Transactions*, vol. 82, Pt. 1, 1976.
- [35] Gatchilov T.S. and Ivanova V.S., "Characteristics of the Frost Formed on the Surface of Finned Air Coolers," presented at the XV International Congress of Refrigeration, B2-71, 1971.
- [36] Gates R.R., Huffman G.D. and Sepsy C.F., "Heat Transfer and Pressure Loss in Extended Surface Heat Exchangers Operating under Frosting Conditions - Pt. 1," *ASHRAE Transactions*, vol. 73, Pt. 2, 1967.
- [37] Huffman G.D. and Sepsy C.F., "Heat Transfer and Pressure Loss in Extended Surface Heat Exchangers Operating under Frosting Conditions - Pt. 2," *ASHRAE Transactions*, vol. 73, Pt. 2, 1967.
- [38] Tantakitti C. and Howell R.H., "Air to Air Heat Pumps Operating under Frosting Conditions on the Outdoor Coil," *ASHRAE Transactions*, vol. 92, Pt. 1, 1986.
- [39] E.R.G. Eckert and R.M. Drake, *An Analysis of Heat and Mass Transfer*. McGraw Hill Company, New York, 1972.
- [40] Gray D.L. and Webb R.L., "Heat Transfer and Friction Correlation for Finned Tube Heat Exchangers Having Plain Fins," presented at the 8th ASME International Heat Transfer Conference, pp. 2745 - 2750, San Francisco, 1986.

- [41] F.P. Incropera and D.P. Dewitt, *Fundamentals of Heat Transfer*. John Wiley and Sons, New York, 1981.
- [42] Schulte D.W. and Howell R.H., "The Effects of Air Turbulence on the Rate of Frost Growth on a Horizontal Flat Plate," *ASHRAE Transactions*, vol. 88, Pt.2, 1982.
- [43] Mitalas G. and Almahedy L., "A Fortran IV Computer Program to Evaluate the Performance of a Multi Rowed Dehumidifying Coil," *Research Report, Computer Program # 43*, Division Of Building Research, Ottawa, Canada , 1977.

NOMENCLATURE

A	Area
Bi	Biot Number
C_p	Specific Heat Capacity
d	Diameter
D_s	Diffusion Coefficient
E	Fin Efficiency Ratio
E_o	Overall Energy Transfer Coefficient
\dot{G}	Mass Velocity
h	Localized Heat Transfer Coefficient
i	Specific Enthalpy
k	Thermal Conductivity
L	Length; Equivalent Length
Le	Lewis Number
\dot{m}	Mass Flow/Deposition Rate
Nu	Nusselt Number
P	Pressure
ΔP	Pressure Drop
P	Perimeter
Pr	Prandtl Number
Q	Energy Transfer
R	Universal Gas Constant
Re	Reynolds Number
Sc	Schmidt Number
St	Stanton Number
t	Time
T	Temperature
ΔT	Temperature Difference
U_o	Overall Heat Transfer Coefficient
v	Specific Volume
V	Velocity
v	Volume

Indices

a	Air; Airside
b	Base
c	Cold; Cross-Sectional
dn	Downstream
e	Exit

f	Frost
F	Fin
h	Hot; Heat
i	Inlet; Ice
m	Mass
r	Refrigerant
s	Surface; Solid
sat	Saturated
T	Total
up	Upstream
v	Vapor

Greek Symbols

δ	Height
ρ	Density
ω	Specific Humidity
η	Efficiency
ϵ	Effectiveness
τ	Tortuosity

APPENDIX A

CALCULATION OF AIR CONDITIONS THROUGH HEAT EXCHANGER

In order to determine the different conditions of the humid air as it flows across the coil, the refrigerant and also the resulting frost deposition, it will be assumed that the heat exchanger is of a counterflow type, although in reality pure cross flow exists. Similar relations could be derived for other flow arrangements.

Equations will be presented and derived for the calculation of the exit air enthalpy, temperature, humidity and effective surface conditions for the limiting case when the refrigerant temperature and internal heat transfer coefficient remain constant. The driving potential is the difference between the free stream air enthalpy and the enthalpy at the heat exchanger surface. The enthalpy at the surface of the heat exchanger tubes can be approximated by the saturated air enthalpy at the temperature of the refrigerant. In this case, the situation in typical evaporator coils is approximated.

Consider the following energy balance for a differential element of the counterflow heat exchanger :

For the air side :

$$d\dot{Q}_{total} = \dot{G}_a di_a \quad (A.1)$$

For the refrigerant side :

$$d\dot{Q}_{total} = \dot{G}_r di_r \quad (A.2)$$

where,

\dot{G} is the mass flow rate per unit area

i_r is the enthalpy of saturated air at the surface of the heat exchanger

In addition, from the enthalpy potential :

$$d\dot{Q}_{total} = \frac{E_o}{c_{p_a}} (i_a - i_r) dA_F \quad (A.3)$$

where, E_o has been defined in Chapter IV.

Combining the above equations leads to :

$$d(i_a - i_r) = \frac{NE_o}{c_{p_a}}(i_a - i_r)dA_F \quad (A.4)$$

where

$$N = \frac{1}{G_a} - \frac{1}{G_r} \quad (A.5)$$

Integrating this expression over the length of the heat exchanger element leads to :

$$i_{a_c} = i_{a_i} - (i_{a_i} - i_r) \left[1 - e^{-\frac{NE_o A_F}{c_{p_a}}} \right] \quad (A.6)$$

APPENDIX B
NON-DIMENSIONAL FIN ANALYSIS

A more useful method of representing fin performance would be to do so in non-dimensional heat transfer and geometric parameters. Such expressions allow for a better understanding of the heat transfer mechanisms.

A general form of the energy equation for a fin with the frost layer can be derived by applying the conservation of energy to an elemental volume in a general extended surface.

The following assumptions are made :

1. There is only one-dimensional conduction in the longitudinal (x) direction. This is so since the fin is very thin and long.
2. There is no heat transfer in the frost layer along the fin length in the direction of the primary surface.
3. Steady state conditions exist.
4. Thermal conductivities of the fin material and the frost are constant.
5. The convective heat transfer coefficient h , is uniform all along the length of the fin.
6. The frost layer has a uniform thickness along the fin length.
7. Radiation effects are negligible and there is no internal heat generation.
8. The mass transfer effects are absorbed into h .
9. The fin tip is well insulated.
10. The base temperature of the fin is that of the primary surface : T_b

From an energy balance :

$$\frac{d^2T}{dx^2} + \frac{1}{A_c} \frac{dA_c}{dx} \frac{dT}{dx} - \left[\frac{1}{k_F A_c} \frac{1}{\left(\frac{1}{h} + R_F\right)} \frac{dA_s}{dx} \right] (T - T_\infty) = 0 \quad (B.1)$$

subject to the boundary conditions :

$$\begin{aligned} T &= T_b & @ & x = 0 \\ -k_F \frac{dT}{dx} &= 0 & @ & x = L \end{aligned}$$

where,

dA_s is the surface area of the differential element.

R_F is the combined thermal resistance of the air and frost layer.

Detailed Thermal Analysis of Rectangular Fin

The cross sectional area, A_c , is constant and $A_s = Px$, where A_s is the surface area measured from the base to x and P is the fin perimeter, both of which essentially remain constant even with the frost.

The thermal resistance of the frost layer can be represented by :

$$R_F = \frac{\delta_f}{k_f} \quad (B.2)$$

Therefore, Equation (B.1) simplifies to :

$$\frac{d^2T}{dx^2} - \left[\frac{P}{kA_c} \frac{1}{\left(\frac{1}{h} + \frac{\delta_f}{k_f}\right)} \right] (T - T_\infty) = 0 \quad (B.3)$$

From practical geometrical considerations, the following approximations are valid:

$$P \approx 2W$$

$$W \gg (\delta_f \text{ and } \delta_F)$$

Therefore, Equation (B.3) can be further reduced to :

$$\frac{d^2T}{dx^2} - \left[\frac{2}{k\delta_F} \frac{1}{\left(\frac{1}{h} + \frac{\delta_f}{k_f}\right)} \right] (T - T_\infty) = 0 \quad (B.4)$$

Applying a transformation to dimensionless parameters and rearranging terms, Equation (B.4) simplifies to the familiar differential equation representing the energy balance for a fin :

$$\frac{d^2\theta}{dx^2} - m_f^2\theta = 0 \quad (B.5)$$

where, m_f is the frosted fin parameter :

$$m_f^2 = H_F \times H_f \quad (B.6)$$

where the dimensionless heat transfer coefficient for the frost, H_f :

$$H_f = \left[\frac{2k^*}{\left(2k^* + Bi_F\delta_f^*\right)} \right] \quad (B.7)$$

and the dimensionless fin heat transfer parameter H_F

$$H_F = \frac{Bi}{\delta_F} \quad (B.8)$$

For no frost, $\delta_f = 0$ and H_f reduces to unity.

Equation (B.5) can be solved subject to the boundary conditions mentioned previously to result in the familiar solution :

$$\theta(x^*) = \frac{\text{Cosh}[m_f(1-x^*)]}{\text{Cosh}(m_f)} \quad (B.9)$$

The *dimensionless heat transfer rate* at the base of the fin can be expressed as a ratio of the heat transfer with frost as to that without :

$$q^* = \frac{m_f \text{Tanh}(m_f)}{m_o \text{Tanh}(m_o)} \quad (B.10)$$

where,

$$m_o = m_f \quad \text{when} \quad \delta_f = 0 \quad (B.11)$$

Applying the definition of fin efficiency, η_F :

$$\eta_F = \frac{\text{Tanh}(m_f)}{m_f} \quad (B.12)$$

We can define a *Fin Efficiency Ratio*, E , to be the ratio of the fin efficiency of the frosted fin to that of the unfrosted fin :

$$E = \frac{\eta_F}{\eta_o} \quad (B.13)$$

APPENDIX C

HEAT EXCHANGER TEST COILS

This appendix discusses the geometrical details of the test heat exchangers in terms of fin type, overall dimensions and construction.

Five finned tube heat exchangers were tested of which the first four have plate type fins :

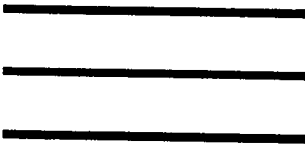
1. Louvered
2. Corrugated
3. Wavy
4. Flat
5. Spine

These fin types are sketched in Figure C.1. It can be easily seen that the louvered has the maximum surface area and the flat fin type the least area.

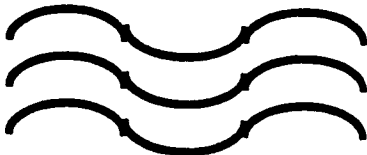
The plate fin type heat exchangers all had identical dimensions. The geometrical details are presented in Figure C.2. There were 18 tubes all manifolded together in order to ensure an even temperature distribution across the heat exchanger. A complete list of the fin type and densities is given in Table C.1. The spine fins were of the same dimensions and construction except that the number of tubes was 20.

In the case of the plate fin heat exchangers, the fins were all aluminum (0.0055 inches thick) with copper tubes with a wall thickness of 0.016 inches. However, for the spine fin heat exchangers, the tubes and the fins were both aluminum. The fins are 1.32 inches in height and the tube thickness 0.031 inches. All the coils were single row coils with an equal spacing between them.

The plate fin heat exchangers have fin densities defined in terms of fins per inch in a direction perpendicular to the length of the fins. In the case of the spine fins, the fin density is defined in terms of number of fins per lineal inch of the circumference when rolled out flat.



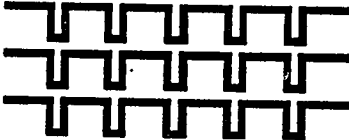
FLAT FIN



WAVY FIN



CORRUGATED FIN



LOUVERED/PERFORATED FIN

Figure C.1 Fin Types

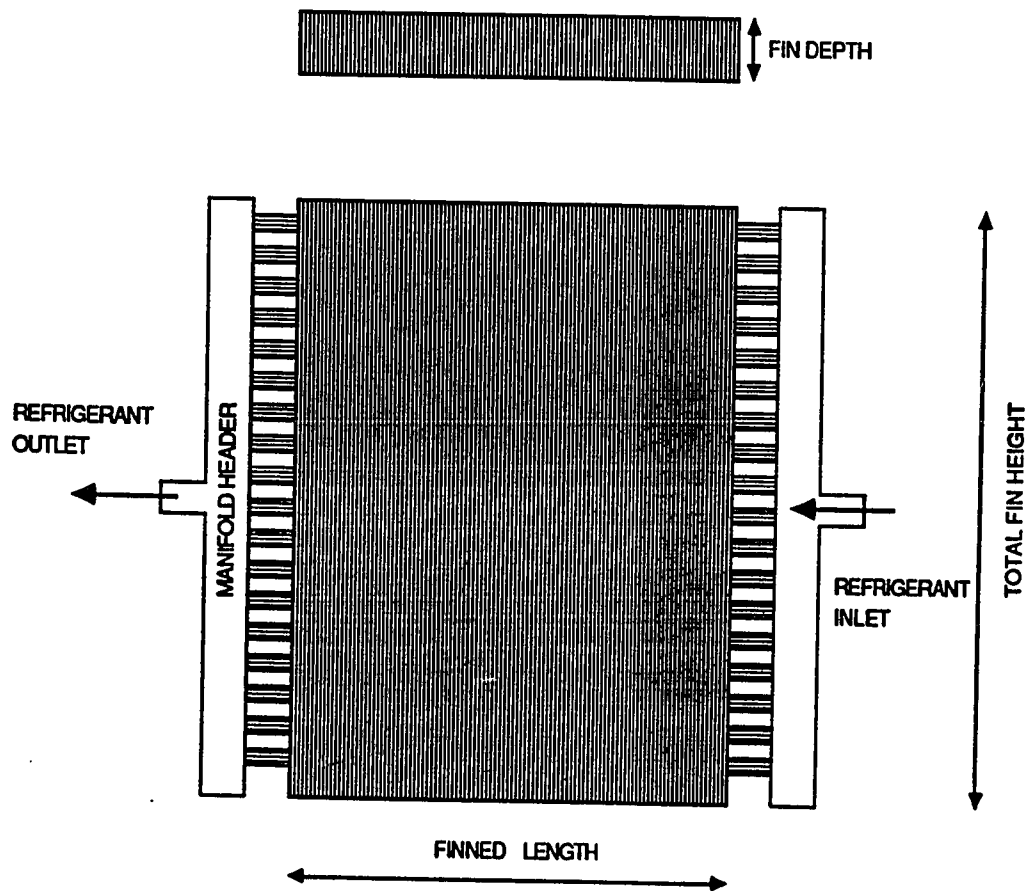


Figure C.2 Test Heat Exchanger Coil

Table C.1 Fin Geometry Details

		FINS PER INCH (FPI)				
		10	14	18	20	24
FIN GEOMETRY	FLAT			•		
	WAVY	•		•		
	CORRUGATED			•		
	LOUVERED		•	•	•	
	SPINE				•	•

APPENDIX D
ENERGY TRANSFER COEFFICIENT, E_o

In this appendix, the energy transfer coefficient, E_o , is derived in terms of the Logarithmic Mean Enthalpy Difference (LMED).

Consider the following equation representing the sensible (dry) heat transfer in a heat exchanger for an elemental section of the heat exchanger :

$$d\dot{Q}_s = U_o \, dA \, \Delta T \quad (D.1)$$

where :

$$\Delta T = (T_h - T_c)$$

Now consider a case where there is simultaneous heat and mass transfer occurring (i.e. humid air where there is also a latent component in addition to the sensible component). McQuiston and Parker [27] have shown that with appropriate assumptions the following expression for an elemental section of a heat exchanger is valid : (refer Figure D.1)

$$d\dot{Q}_t = H_t \, dA \, \Delta i \quad (D.2)$$

where :

$$\Delta i = (i_h - i_c)$$

This elemental energy transfer , $d\dot{Q}$ is equal to the energy given up by the hot fluid or gained by the cold fluid flowing from position A to A + dA :

$$d\dot{Q}_t = -\dot{m}_h \, di_h \text{ (hot)} = \dot{m}_c \, di_c \text{ (cold)} \quad (D.3)$$

where :

$$\begin{aligned} di_h &= \text{changes in the enthalpy of the hot fluid} \\ di_c &= \text{changes in the enthalpy of the cold fluid} \end{aligned}$$

We note that :

$$d(\Delta i) = di_h - di_c \quad (D.4)$$

Substituting Equation (D.4) into Equation (D.3) we get the following expression :

$$d(\Delta i) = -B \, d\dot{Q} \quad (D.5)$$

where :

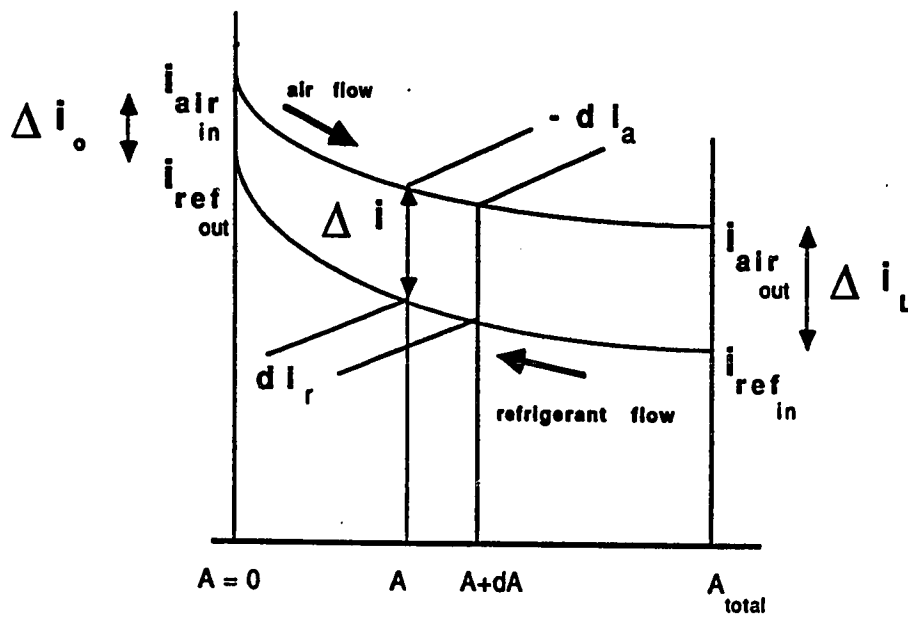


Figure D.1 Nomenclature for the derivation of the LMED

$$B = \left[\frac{1}{\dot{m}_h} + \frac{1}{\dot{m}_c} \right]$$

Eliminate $d\dot{Q}_t$ from Equations (D.5) and (D.2) to obtain :

$$\frac{d(\Delta i)}{\Delta i} = -H_t B dA \quad (D.6)$$

Integrate this over the entire heat exchanger surface area and perform some simple algebraic manipulations to obtain the following expression :

$$B H_m A_t = \ln \frac{\Delta i_o}{\Delta i_L} \quad (D.7)$$

where :

$$H_m = \frac{1}{A_t} \int_0^{A_t} H_t dA \quad (D.8)$$

and

$$\begin{aligned} \Delta i_o &= i_{h_{in}} - i_{c_{out}} \\ \Delta i_L &= i_{h_{out}} - i_{c_{in}} \end{aligned}$$

Integrating Equation (D.5) and eliminating B from it and Equation (D.7) results in the following expression :

$$\dot{Q}_t = A_t H_m \left[\frac{\Delta i_o - \Delta i_L}{\ln \left(\frac{\Delta i_o}{\Delta i_L} \right)} \right] \quad (D.9)$$

This can be rewritten as :

$$\dot{Q}_t = \frac{A_t E_o \Delta i_m}{c_{p_h}} \quad (D.10)$$

where the energy transfer coefficient, E_o is defined as† :

$$E_o = H_m \times c_{p_h} \quad (D.11)$$

and the Logarithmic Mean Enthalpy Difference, Δi_m , (LMED) is defined as :

† The choice of the specific heat of the hot fluid is arbitrary – it could just as well be that of the cold fluid.

$$\Delta i_m = \left[\frac{\Delta i_o - \Delta i_i}{\ln \left(\frac{\Delta i_o}{\Delta i_i} \right)} \right] \quad (D.12)$$

The above manner in which a logarithmic mean has been used for enthalpy instead of the more common temperature has been used by other investigators such as Sanders [29] and Mitalas [42]. The derivation is along similar lines as the LMTD with appropriate modifications.

Note that the manner in which E_o is defined is such that it is a direct analog of the sensible heat transfer coefficient. The introduction of the specific heat term, allows for it to have the same units as the heat transfer coefficient. This gives it a more physical meaning. Since it is an energy related term, has been defined as an energy transfer coefficient.

The above analysis has derived the enthalpy analog of the logarithmic mean temperature difference. It has also defined an energy transfer coefficient which is the combined latent and sensible energy analog of the sensible heat transfer coefficient. Since the frosting mechanism is a combined heat and mass transfer process and the above methodology is in a familiar format, it is convenient to use.

APPENDIX E

EXPERIMENTAL UNCERTAINTY

An uncertainty analysis was performed on the frost accumulation, m_f , the dimensionless sensible heat transfer coefficient, U^* , and the energy transfer coefficient, E_o . This appendix summarizes the calculation of uncertainty for each of the above variables. Because of the large quantity of the data, the uncertainty analysis presented here is restricted to the conditions for the case of the louvered fin coil at a high relative humidity, 10 minutes into the test. This case was representative of those conducted during the study.

The average values of the various variables at that particular state are listed below :

T_r	=	7.8 ° F
T_{ai}	=	32.8 ° F
T_{ae}	=	25.8 ° F
ΔP_{sys}	=	0.37 in. water
ϕ_{ai}	=	85 %
ϕ_{ae}	=	89 %
ω_{ai}	=	0.0034 lb/lb
ω_{ae}	=	0.0023 lb/lb
i_r	=	2.9 Btu/lb
i_{ai}	=	11.6 Btu/lb
i_{ae}	=	8.6 Btu/lb

The uncertainty of the variables used in this appendix is always denoted by a "δ" in front of the variable. The uncertainty of the above variables is listed below :

δT_r	=	± 0.1 ° F
δT_{ai}	=	± 0.1 ° F
δT_{ae}	=	± 0.1 ° F
$\delta \Delta P_{sys}$	=	± 0.04 in. water
δi_{ai}	=	± 0.2 Btu/lb
δi_{ae}	=	± 0.2 Btu/lb
δi_r	=	± 0.2 Btu/lb
$\delta \phi_{ai}$	=	± 3 % RH
$\delta \phi_{ae}$	=	± 3 % RH

The calculation for the uncertainty is based on the following formulation. If a calculated quantity, N , is a function of n measured variables $u_1, u_2, u_3, \dots, u_n$ such that :

$$N = f(u_1, u_2, u_3, \dots, u_n) \quad (E.1)$$

If the uncertainty in each variable $u_1, u_2, u_3, \dots, u_n$ were denoted as ${}_{-}\delta u_1, {}_{+}\delta u_2, {}_{-}\delta u_3, \dots, {}_{+}\delta u_n$, respectively, then the uncertainty would be given as :

$$u_N = \pm \sqrt{\sum_{i=1}^n \left(\delta u_i \frac{\partial f}{\partial u_i} \right)^2} \quad (E.2)$$

Equation (E.2) was used to calculate the uncertainties.

FROST ACCUMULATION

The frost accumulation was calculated from the difference in moisture levels before and after the test coil. This moisture difference is a function of the air flow rate, \dot{m}_a and the specific humidities upstream and downstream of the coil. Hence the uncertainty in the frost accumulation is actually a function of the uncertainty in the mass flow rate of the air and the uncertainty in the humidities.

First consider the uncertainty in the air flow rate. The air flow rate across the coil was measured via the use of a standard ASME nozzle and hence the uncertainty in the air flow is actually a function of the uncertainty in the pressure drop across the nozzle alone. All other parameters have been assumed constant.

$$u_{\dot{m}_a} = u_{\Delta P, v} = \sqrt{\left(\frac{\delta \Delta P}{2\Delta P} \right)^2} \quad (E.3)$$

Now consider the uncertainty in the humidity : The specific humidity was not measured directly but is actually a function of the relative humidity and the dry bulb temperature. Hence the uncertainty in the specific humidity is :

$$u_w = \sqrt{(u_\phi)^2 + (u_{T_a})^2} \quad (E.4)$$

This uncertainty is calculated upstream as well as downstream of the coil.

The total uncertainty in the frost accumulation is :

$$u_{m_f} = \sqrt{(u_w)^2 + (u_{m_a})^2} \quad (E.5)$$

Upon substituting the appropriate values the overall uncertainty in the frost accumulation is $\pm 6.43\%$.

DIMENSIONLESS SENSIBLE HEAT TRANSFER COEFFICIENT

The uncertainty in U^* is the same as the uncertainty in the actual heat transfer coefficient, U_o . The uncertainty of U_o is a function of the uncertainty in the sensible heat transfer, Q_s , and the uncertainty in the Logarithmic Mean Temperature Difference (LMTD).

Consider the uncertainty in the sensible heat transfer. The sensible heat transfer is a function of the air flow rate and the air temperatures, upstream and downstream of the coil. Therefore, the uncertainty in the sensible heat transfer is :

$$u_{Q_s} = \sqrt{(u_{\dot{m}_a})^2 + \left(\frac{\delta T_{ae}}{T_{ae}}\right)^2 + \left(\frac{\delta T_{ai}}{T_{ai}}\right)^2} \quad (E.6)$$

Now consider the uncertainty in the LMTD. This is given by the following expression :

$$u_{LMTD} = \sqrt{\left(\frac{\delta T_{ae}}{T_{ae} - T_r}\right)^2 + \left(\frac{\delta T_{ai}}{T_{ai} - T_r}\right)^2 + \left(\frac{\delta T_r}{T_{ae} - T_r} + \frac{\delta T_r}{T_{ai} - T_r}\right)^2} \quad (E.7)$$

Therefore the total uncertainty in U^* is :

$$u_{U^*} = \sqrt{(u_{Q_s})^2 + (u_{LMTD})^2} \quad (E.8)$$

Upon substituting the relevant values, the uncertainty is : $\pm 7.12\%$.

ENERGY TRANSFER COEFFICIENT

The uncertainty calculation for the energy transfer coefficient, E_o , is similar

to the above calculation except that enthalpies are used instead of temperatures to account for the latent contributions.

. The uncertainty in the total heat transfer, Q , is :

$$u_Q = \sqrt{\left(u_{m_a}\right)^2 + \left(\frac{\delta i_{ae}}{i_{ae}}\right)^2 + \left(\frac{\delta i_{ai}}{i_{ai}}\right)^2} \quad (E.9)$$

Now consider the uncertainty in the Logarithmic Mean Enthalpy Difference, LMED. This is given by the following expression :

$$u_{LMED} = \sqrt{\left(\frac{\delta i_{ae}}{i_{ae} - i_r}\right)^2 + \left(\frac{\delta i_{ai}}{i_{ai} - i_r}\right)^2 + \left(\frac{\delta i_r}{i_{ae} - i_r} + \frac{\delta i_r}{i_{ai} - i_r}\right)^2} \quad (E.10)$$

Therefore the total uncertainty in E_o is :

$$u_{E_o} = \sqrt{(u_Q)^2 + (u_{LMED})^2} \quad (E.11)$$

Upon substituting the relevant values, the uncertainty is : ± 8.71 %.

VITA

Sekhar Narayana Kondepudi was born on October 30, 1961 in the town of Bhimavaram, Andhra Pradesh, India. His parents are Professor Kondepudi Ramamohan Rao and Mrs. Kondepudi Hymavathi. He has been married to Anupama Kondepudi since May 1986.

He went to high school at St. Josephs Institution, Singapore from 1974 to 1978. He graduated with honors from the Indian Institute of Technology, Powai, Bombay, India in May 1983 with a Bachelor's in Mechanical Engineering. He then came to Colorado State University, Fort Collins, Colorado, for his Master's in Mechanical Engineering and completed it in 1985. Following this, he came to Texas A & M University for his doctoral work. At present, he is employed as a Design Engineer with the TRANE Company in Tyler, Texas.

His interests are varied, including Heating, Ventilating and Air-Conditioning and Refrigeration, (HVAC & R), Heat and Mass Transfer, Fluid Mechanics, Energy Conservation, Computer Modeling and Simulation. He has coauthored nine publications (not including his doctoral and masters theses), of which seven are refereed journal publications, one conference proceeding and a popular article in a quasi-technical magazine.

His permanent mailing address is in India :

Sekhar Narayana Kondepudi

33, Arvind Nagar

Hyderabad

INDIA 500 029